



**Politecnico
di Torino**

Politecnico di Torino

Corso di Laurea Magistrale in ingegneria Energetica e Nucleare

A.a. 2022/2023

Sessione di Laurea Marzo 2023

Torino Green Airport

Assessment of the integration of a Molten Carbonate
Fuel Cell with a variable hydrogen-natural gas feeding.

Relatori:

Marta Gandiglio

Paolo Marocco

Candidati:

Paolo Torta

Nomenclature

AFC	Alkaline fuel cell	KPI	Key Performance Indicator
BOP	Balance of Plant	LTFC	Low Temperature Fuel Cell
BOS	Balance of System	MCFC	Molten Carbonate Fuel Cell
CC	Carbon Capture	MW	Molecular Weight
CCHP	Combined Cooling, Heating and Power	NG	Natural Gas
CCS	Carbon Capture and Storage	NU	United Nations
CHP	Combined Heat and Power	OCV	Open Circuit Voltage
CTOT	Total Current	ONU	Organization of United Nations
DMFC	Direct methanol fuel cell	PAFC	Phosphoric acid fuel cell
F	Faraday Constant	PEMFC	Proton exchange membrane fuel cell
FCE	Fuel Cell Energy	PES	Primary Energy Savings
FU	Fuel utilization	S/C	Steam to Carbon ratio
GT	Gas Turbine	SMR	Steam Methane Reforming
GWP	Global Warming Potential	SOFC	Solid oxide fuel cell
HRU	Heat Recovery Unit	UNEP	United Nations Environment Program
HTFC	High Temperature Fuel Cell		

Summary

Nomenclature	2
Summary	3
1. Introduction to the project - Torino Green Airport	5
2. The climate problem	6
3. Trigeneration	9
4. Fuel cell technologies – An overview	9
5. Molten Carbonate Fuel Cell – MCFC	11
5.1 Anode	16
5.2 Cathode	17
5.3 Electrolyte	18
5.4 Generals needs and problems	20
5.5 Reforming of the methane	24
6. Absorption heat pump	25
7. Molten Carbonate Fuel Cell - Plant model	27
7.1 Context	27
7.2 Airport buildings served	35
7.3 Energetic Model and Energy needs of the airport	39
7.3.1 Results of the simulations for 10 months operation	45
7.4 Storage	54
7.5 Fuel cell stack datasheet	55
7.6 PV plant	58
7.7 PV plant and electrolyze for the production of green hydrogen	59
7.8 Problems regarding the adoption of a fuel cell	59
8. Plant model in Aspen Plus	60
8.1 Model equations	62
8.2 Aspen Plus model assumptions and results	65
8.3 Validation of the model	67
8.4 Molten Carbonate Fuel Cell Model Balance of Plant	71
8.5 Design Specifications	74
8.6 Fuel Inlet Composition	75
8.7 Determination of numbers of cells	75
8.8 Pressure drops in the components	76
8.1 Parametric and Sensitivity analysis	79

8.1.1	Variation of current density	79
8.1.2	Variation of steam-to-carbon (S/C) ratio.....	80
8.1.3	Variation of temperature of the stack.....	80
8.1.4	Variation of pressure.....	81
8.1.5	Variation of the fuel utilization factor <i>UF</i>	82
9.	Partially direct and indirect reforming	82
10.	Fuel cell hydrogen fuel capabilities	85
10.1	Fuel cell hydrogen capabilities at constant volume flow rate.....	87
10.2	Blending mixture	90
11.	Economical evaluation	92
11.1	High Efficiency cogenerator certificate (CAR).....	94
1.1	Economical evaluation	98
1.2	Cash flow analysis.....	103
12.	Conclusions	111
13.	Figures.....	112
14.	Tables	114
	Bibliography.....	115

1. Introduction to the project - Torino Green Airpot

Snam, SAGAT and the subsidiary company Renovit, together for the realization of a fuel cell plant in the airport of Turin. Snam is one of the most important energy companies for the transmission of natural gas. SAGAT is the society that manage Caselle's airport. The project foresees the construction of a 1.2 MW cogenerative plant. Through the installation of three fuel cells able to produce electricity for 1.2 MWh and heat for 840 kWh each hour [1]. The fuel cells have been studied in collaboration with Fuel Cell Energy. If completed this will be the first cogenerative plant in Italy in terms of size and typology. The chosen Molten Carbonate Fuel Cells, MCFC, can works with a variable percent of hydrogen and natural gas. Initially, at least for the first years the installation, the fuel cells will be fed with natural gas taken from the grid. In future, expecting a higher penetration of hydrogen in the market, the fuel cells can accept different fuel compositions in different blend ratio. This installation could be a practical contribution in the huge campaign of decarbonization currently in acts [2]. All the produced electrical, thermal and cooling energy from the fuel cells will be auto-consumed from SAGAT. Actually, the consumptions are 17.000 MWh for electrical energy, 8.714 MWh for the thermal energy. Nowadays 100% of the electrical energy comes from certified renewable sources [3]. The mission of Torino Airport is managing the airport infrastructure and operations in an energy-efficient way, consuming less energy, avoiding the waste of resources and promote the respect towards the environment, reduce water consumption and reuse it, reduce noise emissions, reduce greenhouse gas emissions and pollutants in the atmosphere. Turin Airport joined the ACI Europe NetZero 2050 protocol in 2019 and in 2021 obtained the Level 2 'Reduction' accreditation of the ACA Airport Carbon Accreditation program. In 2022 it signed the Toulouse Declaration, confirming its commitment to environmental sustainability. The airport of Turin in the decade 2009-2019 saw significant results in favor of a better management of the energy and of emissions reduction. Electricity, fuels heating and CO_2 emissions were reduced over the years [4].

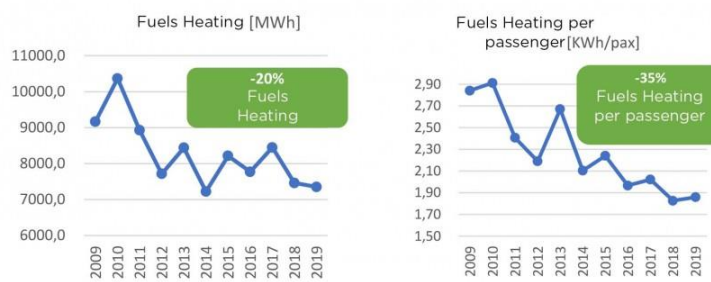


Figure 1 Electrical energy during the years

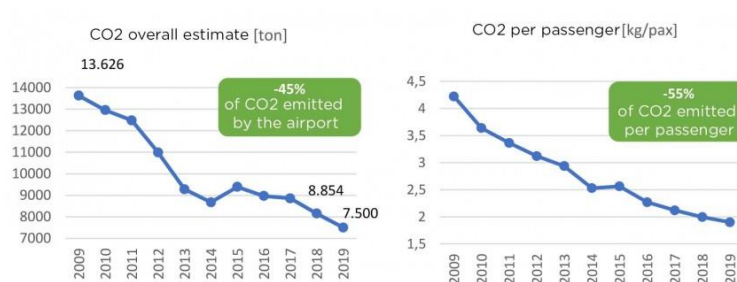


Figure 2 CO2 emissions during the years

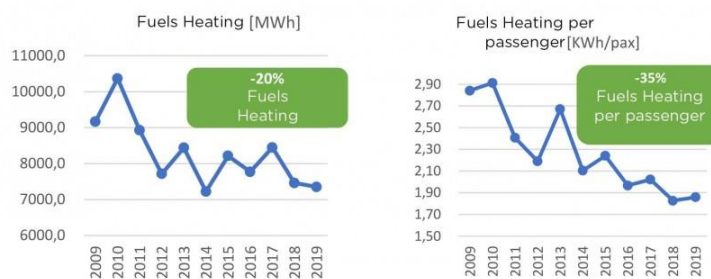


Figure 3 Fuel consumptions during the years

2. The climate problem

The aim of the work it is to develop a model for a fuel cell. These devices are one of the possible solutions to limit and counteract the climate problem. A lot of efforts have been done and will be made to mitigate the current effect of the global warming. As an introductory part, the author of this work, summaries in three categories the big problems of our times.

Since the seventies many documents have been signed in view of a sustainable development. The first conference ONU on the Human Environment in 1972 was held in Stockholm where born UNEP, United Nations Environment Program, have been defined helps for developing countries and the commitment to safeguarding the environment. In

1987 has been defined the concepts of sustainable developments, with the Brundtland report also known as “our common future”:

Sustainable development is **development that meets the needs of the present without compromising the ability of future generations to meet their own needs.**

In 1992 with the second summit of the NU held in Rio was defined the Agenda 21, with more than 2500 recommendations for action. A main turning point was in 1992 with the Conference CPO3 on the climate change, with the birth of the Kyoto protocol. It is one of the most important legal instruments with international validity for the reduction of the emission in atmosphere of greenhouse gases. Another steps was the Universal Declaration on Cultural Diversity 2001 where the three cornerstone of the sustainable development were strengthened: Economic, social, and environmental development. The more recent agreement of Paris 2015 establishes the collaboration between 195 countries to keep the continuous increase of the average temperature beyond 2°C. The Agenda 2030 was approved in the summit of UN for the sustainable development, introducing 17 points for the poverty eradication and an easy access to the energy for each individual.

- Population growth

The population grown significantly during these last decades. In thousands of years the population reach one billion while two hundred years from one billion to eight billion.

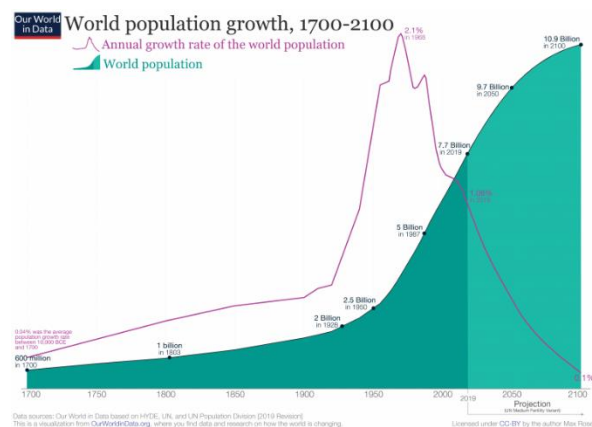


Figure 4 World population growth

- End of fossil resource
- Increase of CO_2 in atmosphere and higher temperature

The Global Warming Potential (GWP) was developed to allow comparisons of the global warming impacts of different gases. Specifically, it is a measure of how much energy the emissions of 1 ton of a gas will absorb over a given period of time, relative to the emissions of 1 ton of carbon dioxide (CO₂). The larger the GWP, the more that a given gas warms the Earth compared to CO₂ over that time period. The time period usually used for GWPs is 100 years. GWPs provide a common unit of measure, which allows analysts to add up emissions estimates of different gases and allows policymakers to compare emissions reduction opportunities across sectors and gases. The GWP depends from the capacity of the substance of absorbs heat and the time spent in the atmosphere. Another molecule that worries the scientist is the CH₄. The methane has a GWP 23 times bigger than the CO₂ potential. Possible future leakages of methane from the permafrost, that acts as a natural barrier, should be taken seriously into account. Regarding the CO₂ the big problem is that can stay in the atmosphere for more than 100 years, whereases the methane only 10. In the book “A Farewell to Ice: A Report from the Arctic” of Peter Wadham it is underline that the potential heat of the CO₂ has not been reached yet. In the past, from the observatory in Mauna Loa, the concentration of CO₂ in the atmosphere was on 280 ppm instead today the concentration is higher than 420 ppm. If today, we could stop the emissions of CO₂ into the atmosphere the earth system would take about 45 years to return at 350 ppm, that is an acceptable safety threshold for many scientists . To respect the limit imposed from the Paris agreement, a possibility is to capture from the atmosphere 600 Gt of carbon dioxide within the end of the century. The actual world annual emissions are near 40 Gt.

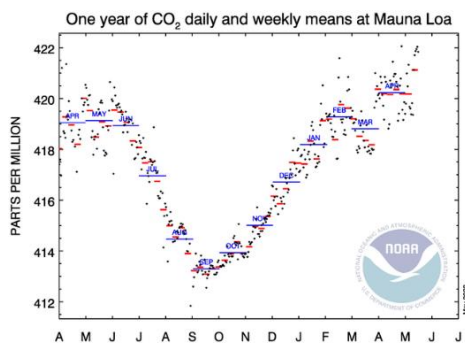


Figure 5 CO₂ daily and weekly means at Mauna Loa

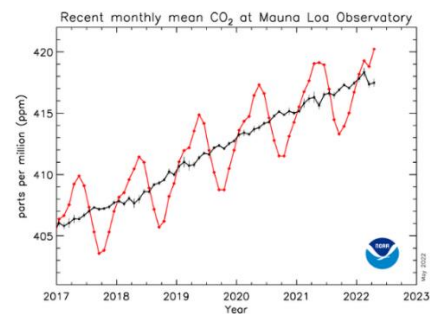


Figure 6 CO₂ value at Mauna Loa Observatory

3. Trigeneration

The trigeneration it is conceptually an extension of the cogeneration. In the trigeneration plants there is the simultaneous production, starting from the same source, of heat, electricity and cooling energy (with the production of air or cold water). Typical trigeneration plants are a coupling between a cogenerator plant and an absorber. The trigeneration it is also indicated as CCHP (Combined Cooling, Heating and Power). The trigeneration plants are composed by a prime mover that is fed with a fuel, an electric generator for the transformation of the mechanical energy in electricity, heat exchangers used to exploit the heat produced and deliver it at disposal to the final users, the absorption chiller that using a part of the recovered heat generate cooling energy. With respect a cogenerator plant, the global efficiency for a trigeneration plant it is higher because the better exploitation of the heating value of the fuel.

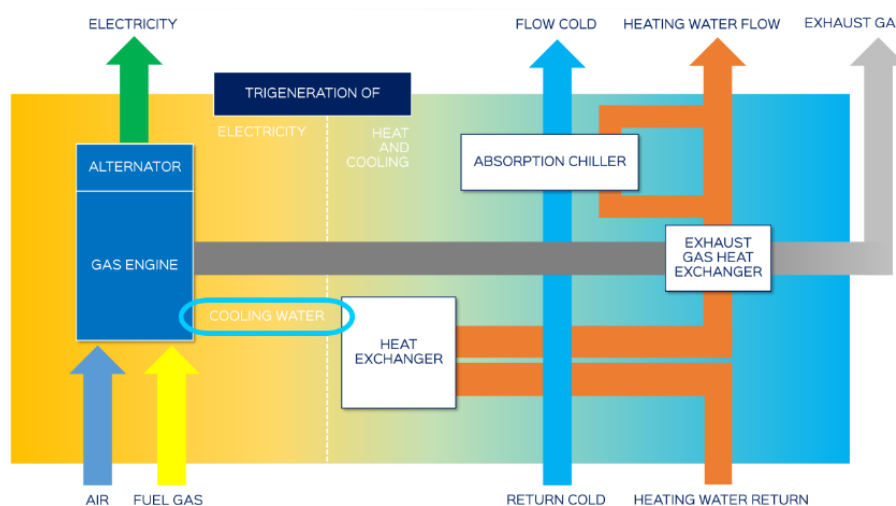


Figure 7 Trigeneration Scheme[5]

4. Fuel cell technologies – An overview

The electrochemical cells are structures that exploiting the classical redox reactions are able to generate, or even store, electrical power. The fuel cell, that are a type off electrochemical cells, are open thermodynamic systems since the reactants are not stored inside the cell but are taken outside as fuels. More in general, the reaction between hydrogen and oxygen it is arranged in a way that the device is able to produce electricity

and heat. The big differences between fuel cells are in the chemical and physical characteristics of the electrolyte and in the working temperature. The value of temperature changes the kinetic and so the conduction of the species. In the fuel cells, there is no combustion and there are only chemical reactions. For these reasons the FC can produce energy with minimum emission of pollutants with respect the traditional internal combustion engine. However, the reducing agent and oxidant must be continuously replenished in cells. Most of the fuel cells systems present the single cell, the stack, the balance of plant (BOP). Hydrogen and hydrocarbon fuels contain significant chemical energy hence are used for different applications.

In the market there are different types of fuel cell technologies [6]:

- Proton exchange membrane fuel cell (PEMFC)
- Alkaline fuel cell (AFC)
- Solide oxide fuel cell (SOFC)
- Molten carbonate fuel cell (MCFC)
- Phosphoric acid fuel cell (PAFC)
- Direct methanol fuel cell (DMFC)

Each of these technologies have a certain tendency to accept or not different fuels, this is known as the fuel flexibility. Different fuels can affect and pollute the device, also in an irreversible way. For instance, the PEM-FC are really sensible to other fuels different from hydrogen, instead the MC-FC can accept other fuels like methane or also mixture of hydrogen and methane.

Liquid electrolyte is limited from temperate, that cannot generally exceed $200\text{ }^{\circ}\text{C}$ due to too high vapor pressure and degradation. The working temperature change also the way the fuel is treat. In the LT-FC all the fuels must be converted in hydrogen before entering the cell. Another requirement in the LT-FC application it is the catalyst, generally platinum, that is strongly affected by the CO. Instead, for the HT-FC, the catalyst It is not require and no Nobel metals are use. In the HT-FC the methane can be entirely converted in hydrogen or can also be directly oxidated electrochemically inside the anode of the cell.

Fuel cell type	AFC	PAFC	SOFC	MCFC	PEMFC	DMFC
Common electrolyte	Aqueous solution of potassium hydroxide soaked in a matrix	Liquid phosphoric acid soaked in a matrix	Yittria stabilized zirconie	Liquid solution of lithium, sodium, and/or potassium carbonates, soaked in a matrix	Solid organic polymer poly-perfluoro sulfonic acid	Solid polymer membrane
anode reaction				$H_2O + CO_3^{2-} \rightarrow H_2O + CO_2 + 2e^-$		
Cathode reaction				$\frac{1}{2}O_2 + CO_2 + 2e^- \rightarrow CO_3^{2-}$		
Charge carrier	OH^-	H^+	O-	CO_3^-	H^+	H^+
Fuel	Pure H2	Pure H3	H2, CO, CH4, other	H2, CO, CH4, other	Pure H2	CH3OH
Oxidant	O2 in air	O2 in air	O2 in air	O2 in air	O2 in air	O2 in air
Cogeneration	No	Yes	Yes	Yes	No	No
Reformer is required	Yes	Yes			Yes	
Cell voltage	1	1,1	0,8-1,0	0,7-1,0	1,1	0,2-0,4

Table 1 Fuel cells types[7]

The fuel cells generally have higher efficiencies compared to traditional devices for the energy production. The FC are also reliable for their simple design and operation. Another advantage is that when hydrogen is used as reactance makes the fuel cell the most environmentally clean and noiseless energy system. An important aspect, especially true for the PEMFC, it is that hydrogen is a necessity and not an ecological choice. The cons of fuel cells are that they cannot produce big amount of current due to diminutive contact area between electrodes, electrolyte and the gas. Another limiting factor is the distance between electrodes. To improve the performances of the cell the contact area should be maximize. A thin layer of electrolyte with flat porous electrodes is considered for electrolyte to allow an easier gas penetration. Alkaline fuel cells are the most efficient, followed by PEMFC and MCFC. Generally, SOFC and MCFC have higher CHP efficiency.

5. Molten Carbonate Fuel Cell – MCFC

The MCFC are cells that works at high temperature. For this reason, are high temperature fuel cells. The typical operating temperature is about 650 °C. The electrolyte is a dense liquid, quite solid, originated by a mixture of carbonates (molten salts). Nowadays the

more used electrolyte is a mixture of Potassium and Lithium carbonates ($K_2CO_3 - LiCO_3$). As common for all the fuel cells, the main components are anode, cathode, electrolyte and an external circuit for the electrons flow [8].

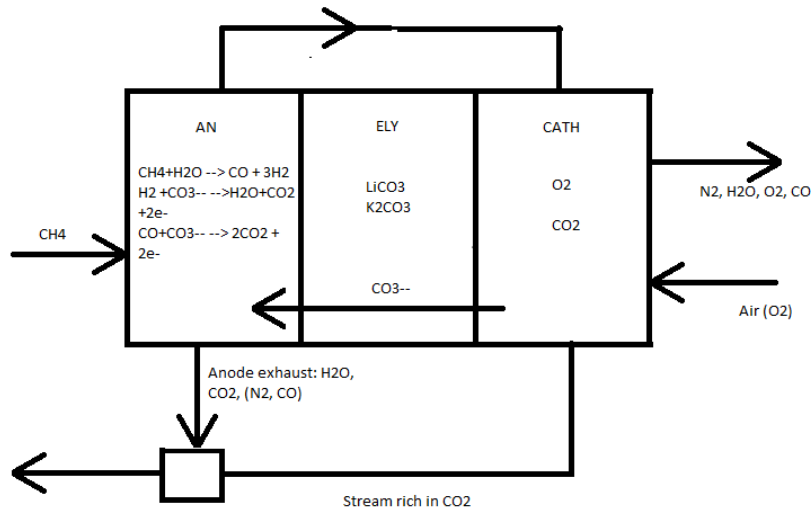
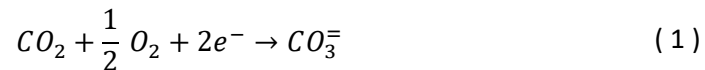


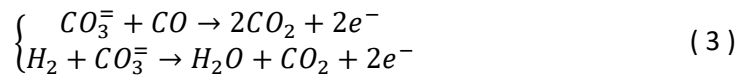
Figure 8. MCFC general design

The ions inside the electrolyte are CO_3^- . The reduction, at the cathode, generate the carbonic group in accordance to the following reaction:



To complete the reaction requires the presence in the cathode of CO_2 , O_2 and the electrons coming from the external circuit. The required CO_2 is used as reactant in the cathode and so it is for this reason that there are nowadays many applications of MCFC technology used to capture the CO_2 . The cells are inserted downstream the exhaust stream of a combustion process, where the CO_2 concentration is still high. The carbon dioxide in the exhaust is used as a reactant in the cathode, in a logic of *carbon sequestration*. To summarize the carbon dioxide can be taken from two main sources:

1. From the exhaust of a plant rich in CO_2 of whatever stream after a combustion process. If all the CO_2 is consumed, in theory there is the possibility to have only water at the anode outlet. And no CO_2 emissions in the atmosphere.
2. Directly from the anode of the same MCFC making a recirculation loop. In fact, at the anode the reactions that occurs are the following:



The first reaction is the steam methane reforming while the other two are the oxidations reactions in the anode of CO and H_2 . The SMR reaction is favorite, and it is sustained at high temperature. The hydrogen oxidation is an exothermic reaction, an accurate thermal management of the MCFC it is needed. The airflow on the cathode side is therefore used as coolant, it means that air in excess with respect the stoichiometric is sent to the cathode.

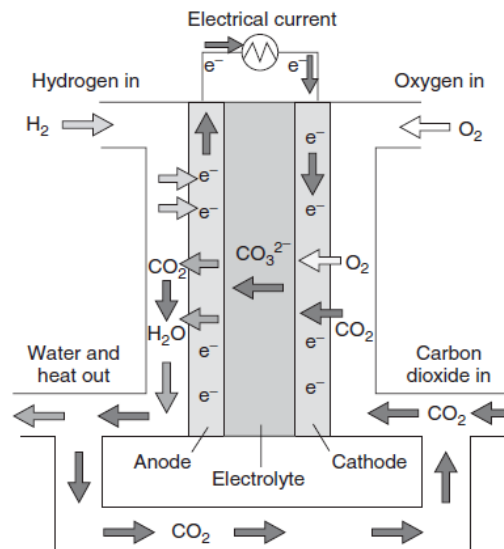


Figure 9 MCFC operating principle with partial recirculation

In the application of the study at the airport, there are no available exhaust streams that can be used as source of CO_2 to feed the cathode. A partial recirculation of CO_2 from anode to cathode is designed. In Torino Green Airport project, the MCFC is directly fed with natural gas taken from the grid. In comparison to other fuel cells, the MCFC has a lower power density due to the limited zones of effective electrode reactions and also has low solubilities of oxygen and hydrogen in molten carbonates. In addition, it has the thickest electrodes-electrolyte distance assembly. For these reasons the MCFC are suitable, like for the Torino Green Airport, for stationary power applications. The water produced into the anode electrode, makes in the outlet anodic gas content more water than the inlet. The higher partial pressure, due to water, leads to a decrease of the cell voltage and cell efficiency. This loss is evident from the Nerst equation, due to a change of gas composition.

A characteristic of the MCFC with respect to the other cells, it is observed in the polarization curve. The MCFC has a linear behavior, and the steepness is the highest among the others hydrogen-oxygen fuel cells [9].

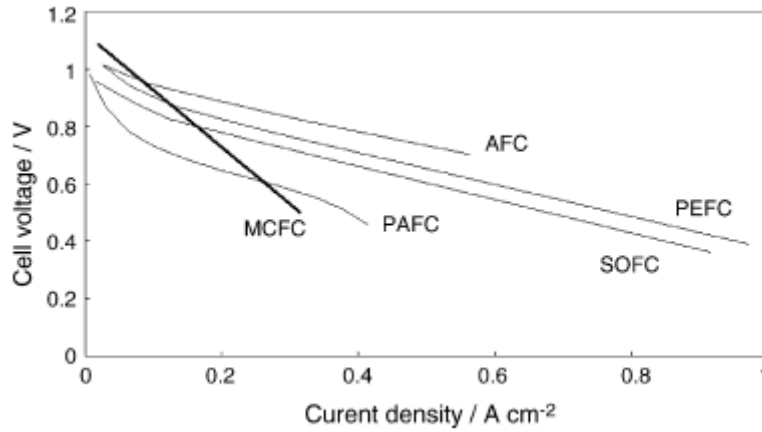


Figure 10. Polarization curves for various fuel cells.

The MCFC has the lowest current density at high power, and can reach high efficiency only in a narrow range of current density, up to ca. 150 mA cm^{-2} . The molten carbonate fuel cell has one of the thickest electrodes-electrolyte assembly (order of magnitude 1-3 mm), and also the thickest electrolyte (order of magnitude 0.5-1.5 mm). The advantages of thick electrolyte is the neutralization of the NiO cathode dissolution, which otherwise may lead to the formation of Ni dendrites and consequently the creation of a short circuit inside the cell. The ohmic drop, responsible for the linear trend in the polarization curve, remains acceptable even when the matrix electrolyte is relatively thick. In the cathode of MCFC, the overpotentials are lower with respect to the PEMFC or PAFC.

At the interface, the balance of the gas in the porous electrodes and the electrolyte, is established exploiting a balance of capillary pressure. In literature a relationship between the surface tension and the diameters of the pores has been found :

$$\frac{\gamma_a \cos \theta_a}{D_a} = \frac{\gamma_c \cos \theta_c}{D_c} = \frac{\gamma_e \cos \theta_e}{D_e} \quad (4)$$

Where γ indicate the interfacial surface tension, θ the contact angle of the electrolyte and D the pores diameter. The subscripts a, c and e refer to the anode, cathode and electrolyte matrix.

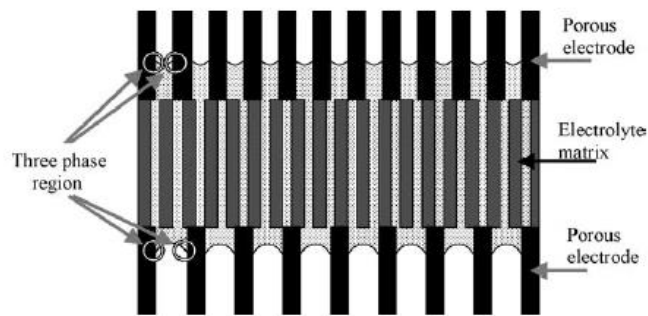


Figure 11 Distribution of molten carbonate electrolyte in porous electrodes of MCFC as a result of balance in capillary pressure [9].

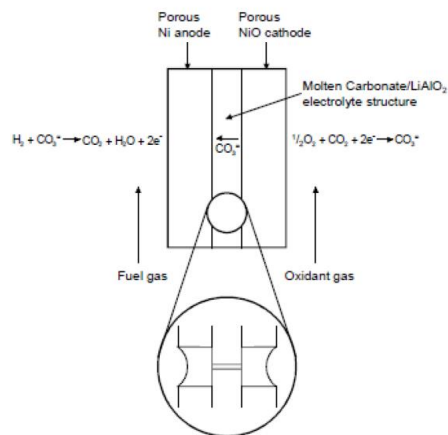


Figure 12 Connections between anode, cathode, electrolyte

With the configuration presented, the electrolyte absorbs many carbonates, whereas the electrodes are partially filled, this is a function of the distribution and dimension [10]. A no correct proportion between pores and quantity of electrolyte, can cause an inhibition of the reaction, or also put in contact the anodic and cathodic gas. This phenomenon is known as *cross-over*. The pores of the matrix are smaller and filled with the electrolyte, whereas the electrodes are partially filled with the electrolyte, proportionally to the distribution of the diameters due to the pores [10].

The main competitors in the market against the MCFC are SOFC and PEMFC. However, there are some differences between them and the MCFC has some advantages.

- The operating temperature is 650°C that is optimal for an internal reforming and to exploit the useable heat. The operating temperature of the other devices are generally too low for an internal reforming.
- The MCFC can accept a wider range of fuels, for example the CO is a useable fuel for the MCFC, but it is a poison in the PEMFC for the presence of Pt catalyst.

- The efficiency of the MCFC is higher than PEMFC.
- The liquid electrolyte in the MCFC permits an easier gas seal and the device presents a low contact resistance, for the SOFC it is more complicated.
- MCFC can accept CO_2 that is an asset if the cells are coupled in a stream of exhaust rich in CO_2 . This can be seen as a form of carbon capture. Also the SOFC can accept CO_2 .
- MCFC can directly accept hydrogen, carbon monoxide, natural gas and propane.
- MCFC don't require noble metal catalyst for the electrochemical reactions of oxidation and reduction, this is an advantage due to the high temperature

The reversible potential for the MCFC, by taking into account the transfers of CO_2 , is described:

$$E = E^\circ + \frac{RT}{2F} \cdot \ln \frac{P_{H_2} \cdot P_{O_2}^{\frac{1}{2}}}{P_{H_2O}} + \frac{RT}{2F} \cdot \ln \frac{P_{CO_2c}}{P_{CO_2a}} \quad (5)$$

Where "a" is for the anode and "c" for cathode. When the two partial pressures for the CO_2 are equal, the potential of the cell depends only by P_{H_2} , P_{O_2} , P_{H_2O} . In general the two partial pressures are different. The CO_2 that is required at the cathode, makes it necessary a dedicated circuit where the CO_2 at the anode outlet can reach the cathode inlet. This is particularly true in the application that will be analyzed, since at the airport it is not foreseen a stream of exhaust that can feed the cell.

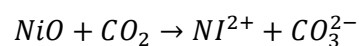
5.1 Anode

At the state of art, are generally alloy of Ni-Cr/Ni-Al. The porosity is typically higher than 55% and it is produced with the tape-casting technique. One main problem for Ni-Cr is the creep, but the contact resistance between the components is minimized. Cr was added to eliminate the problem of sintering of the anode during the operation of the cell, it also reacts with the Li of the electrolyte and consumes the carbonate. The addition of Cr can lead to the formation of dispersed Cr_2O_3 particles during sintering, that may reduce creep resistance. Cr in the anode can also be easily lithiated by the electrolyte to produce $LiCrO_2$, this should be avoided because consumes electrolyte and creates micropores that affects the performance in a negative way [11]. The second category of Ni-Al resists from creep, mainly due to the formation of $LiAlO_2$. These particles are finely dispersed in

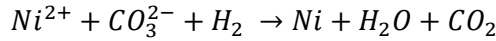
the network structure of Bi-Al, but remain electrochemically inert. However, there are problems of costs and additional research it is needed. Creep deformation is mainly related to the movement of dislocation, so by adding solute atoms, precipitates, or oxide particles the creep resistance increase. This is known as strengthening techniques. There are trials using CeO_2 , Ce , Dy , Sn as additives to Ni. During the years also some proposals were on the use of ceramic materials such as oxides of lanthanum La_2O_3 and samarium Sm_2O_3 with titanium powder to provide electronic conductivity. This also in order to reduce the sulfur tolerance [10]. The main drawback it is the low current density. In the MCFC being the temperature high, the kinetic of the reaction at the anode it is high and are not required big surfaces.

5.2 Cathode

In the oxidizing atmosphere of the cathode, only a few noble metals have adequate stability to be selected for this application. The cathode must have a good electrical conduction and mechanical resistance. Generally, are realized with NiO and Li. The NiO offers a sufficiently insolubility in the carbonate electrolyte. One of the main concerns for the MCFC is the dissolution at the cathode. Other solutions can be $LiFeO_2$ that are chemically stable and doesn't present phenomena of dissolutions and are less efficient. One of the main issues, in the MCFC, is that the nickel has a lower value of solubility, but still significant to the molten carbonate. A problem is the formation of some ions of nickel in the electrolyte, that goes to the anode. The ions of nickel reduced at the anode, and as a consequence, there is the precipitation of metallic nickel. This phenomenon can create interna short circuit in the cell, with a consequent decrease in power, or even the break of the cell. The phenomenon of the dissolution of nickel increases if the partial pressure of the CO_2 increase. The dissolution from the cathode into the carbonate electrolyte occurs according to:



To counteract the problem, a solution is to use a consistent number of carbonates, work at near ambient pressure, increasing the thickness of the matrixes in order to make the path of the Nickel ions longer. The nickel ions flow through the matrix towards the anode, where react with hydrogen according to the reaction:



When the metallic Ni precipitate inside the matrix, it acts like a bridge from anode to cathode, in which flows an undesired and dangerous short circuit current.

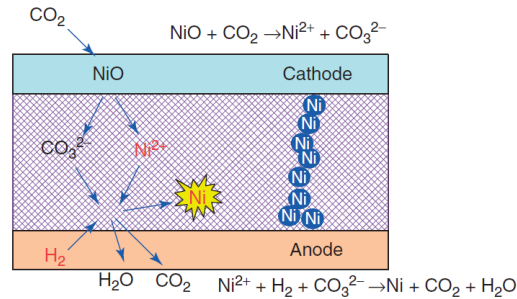


Figure 13 Schematic of Ni shorting the cell in the electrolyte matrix [11]

The partial pressure of the CO_2 at the inlet cathode it is proportional to the working pressure at the cathode and from the molar fraction of the CO_2 in the mixture:

$$p_{CO_2} = p_{cat} \cdot y_{CO_2,cat} \quad (6)$$

The solubility of the nickel oxide depends also from the carbonate composition, from the working temperature, from the partial pressure of the vapor produced inside the cell. At the state of art, to decrease the dissolution rate of NiO, NiO-composite cathode materials are the most promising. A solution is to coat or dope the NiO surface with element with low solubility or even combined with basicity-enhancing additives in the carbonate's electrolyte.

5.3 Electrolyte

The electrolyte composition in a MCFC affects the cell internal resistance, the gas solubility, the corrosion, the cathode kinetics and the electrolyte loss rate. The proper choice of the electrolyte is a key aspect to be considered also for cell performances and cell life time. The electrolyte in these devices is a liquid, quite dense. The most common used are potassium and lithium carbonates, Li_2CO_3/K_2CO_3 . Another popular configuration is $LiCO_3/NaCO_3$. The first one it is suitable for atmospheric pressure instead the second it is used at higher pressure. Advantages of Li-Na electrolyte are improved NiO cathode stability, reduced electrolyte evaporation, and decreased ohmic polarization [11]. The electrochemical activity it is directly affected by the composition. One main concern for the MCFC is the possible evaporation of the electrolyte that should

be taken carefully into account. Generally, at higher pressure the performance increases because for the same output the thickness of the electrolyte could increase. The electrolyte $LiCO_3/NaCO_3$ is more sensible to the temperature. In the device, the strongest tension losses are due to the cathode and to the electrolyte. The electrolyte it is responsible for the majority of the ohmic losses, so the structure should be changed to increase the performances. For instance, it was observed from literature, that by increasing the porosity of the electrolyte of 5% the ohmic resistance decrease by 15% and passing through a component Li/K to one L/Na the reduction is of 40% [10].

The molten carbonate is in general a very corrosive medium, therefore there is the necessity to produce cell components that ensure stability and good performance [11].

Anode	Material	Ni-Cr/Ni-Al/Ni-Al-Cr
	Thickness (mm)	0,2-0,5
	Porosity (%)	45-70 initial
	Surface area (m ² g ⁻¹)	0,1-1
Cathode	Material	Lithiated NiO
	Thickness (mm)	0,5-1
	Porosity (%)	70-80, Initial
		60-65, After lithiation and oxidation
	Surface area (m ² g ⁻¹)	0,15 (Ni pre-test), 0,5 (post-test)
Electrolyte support	Material	gamma-LiAlO ₂ , alpha-LiAlO ₂
	Thickness (mm)	0,5-1
	Surface area (m ² g ⁻¹)	0,1-12
Electrolyte	Composition (mol%)	62Li-38K
		72Li-28K
		52Li-48Na
Current collector	Anode	Ni or Ni-plated steel, 1 mm thick
	Cathode	316SS, 1 mm thick

Table 2 Fuel cells materials

The ohmic drop, that for a MCFC are around the 70% of the total are a function of the thickness of the electrolyte [10]:

$$\Delta V = 0.533 \cdot s \quad (7)$$

Where s is the thickness of the electrolyte in centimeter. A reduction in the thickness of the electrolyte reduces the losses but reduce also the maximum power of the cell. Generally, with the tape-casting the thickness is around 0.25-0.5 mm. With that thickness the losses are acceptable and not so high, but the power density remains a problem at dozens of $\left[\frac{kW}{cm^2}\right]$.

5.4 Generals needs and problems

Startup and shut down of the MCFC

The fusion temperature of the carbonate is around 450°C. When it melts the thermal stress on the stack is stronger, and a good design should be done. To be in operation at the design working temperature the MCFC require around 70 hours. For comparison, a PEM require only some seconds to be in operation. The longer start up time, as well as the shutdown, it is needed to prevent damages to the supports of the electrolyte and so undesired and problematic cross-over. Another precaution is to prevent the anode reoxidation during the shutdown, this it is solve using a flow of inert gas. For all these reasons, the MCFC, being quite stiff devices, should be preferably used for stationary application, or in application where the required power is continuous.

Dependences from pressure

Accordingly to the Nerst equation it can be observed that with an increase in pressure, there is a correspondence increase of the potential of the cell working at 650°C. This increase in the potential it is due to the increase in partial pressure of the reagents, that enhanced the gas solubility, and enhancing also the mass transport. The main problem when there is an increase in pressure is the carbonic deposition and methane formation:



The carbon deposition, can obstacle the passages of the gas to the anode. The methane formation should be avoided because for each mole produced, the system loss moles of hydrogen, so decreasing the amount of reagents inside the cells and so the efficiency. A possible solution was found by adding water and CO_2 to the gas fuel [10] Instead the

water gas shift reaction it is not affected by the increase of pressure because the number of moles in the reagents is the same in the products.

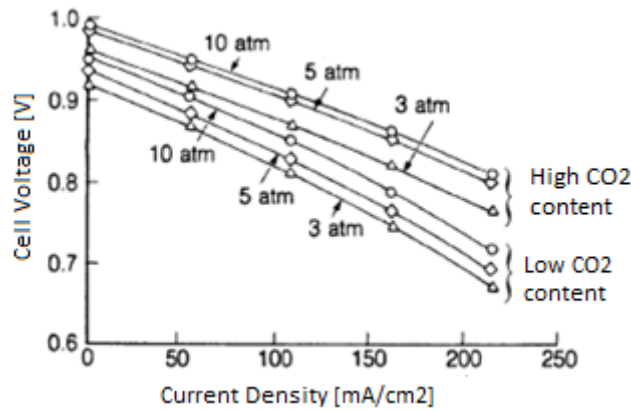


Figure 14 Dependences MCFC from pressure Cell voltage and current density

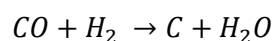
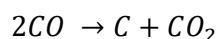
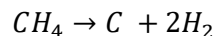
Increment of pressure in the MCFC, correspond to a higher differential in potential between the electrodes. This is due to the maximum solubility of the reagents in the gas and due to an increase of mass transport phenomena.

Recirculation of CO₂ from anode to cathode

The produced CO₂ at the anode, it is generally recirculated to the cathode, where the carbon dioxide is used as reactant. Before being recirculated, these anode gases should be previously oxidated and cooled, because they contain combustion gases that can even burn at the inlet cathode with the oxygen present in the electrode. This must be avoided, otherwise there is the formation of undesired hot spot into the cell [12].

Carbon deposition

A problem in the MCFC is the deposition of carbon on the solid matrix in the anode compart that reduce the surface available for the reaction and so limit the electrical power. The carbon deposition is due to the cracking of the methane, from Boudouard and from vapor production from CO [12]:



The reactions are in order, cracking of the methane, Boudouard reaction, production of the water vapor. The water vapor in excess with respect the stoichiometric enhance the

reforming of the methane respect the cracking and obstacle the production of new vapor. An amount of CO_2 , in small percentage, in the inlet mixture reduce the production of carbon because the equilibrium it is more shift towards left.

In this application, the MCFC is fed by natural gas, so the CO_2 it is produced mainly:

- From the water gas shift reaction, and increase for a directly internal reforming configuration because there is a direct consumption of hydrogen inside the anode and the equilibrium is shift towards right.
- From anode reactions, the amount of CO_2 increase if the working point of the cell is shifted at higher current.

Electrolyte loss

At the startup of the MCFC there is a significant loss of carbonate electrolyte because the lithiation of the cell components. During the operation there is a continuously decrease in performance because higher losses. The continuous losses are caused by different factors like direct vaporization, electrolyte creep, slow corrosion of the structural components. This cause an increase in ohmic resistance and electrode polarization, also the gas crossover and gas leaking towards the ambient should be considered. There are two main phases in which two different behaviors of the loss in voltage can be observed. The first stage shows a constant rate degradation because an increase in internal resistance is observed and polarization. The second stage it is steeper because the Ni shorting of the cell [10].

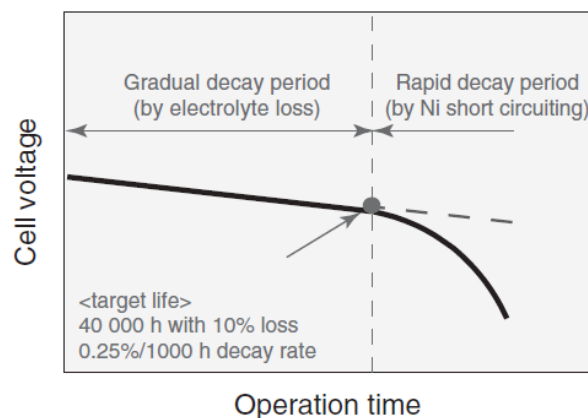


Figure 15 Schematic of MCFC degradation with time at a constant current level.

A practical solution to counteract the electrolyte loss is replacing Li-K electrolyte by the Li-Na that is a less volatile electrolyte. Also, the corrosion rate should be limited using highly corrosion-resistant alloys, but generally these compositions are really expensive.

Tolerance to contaminants

There are different advantages in using nickel, but severe drawbacks are encountered when the MCFC is fed with a fuel that is not hydrogen. There is an affinity of nickel with contaminant compounds that can poison its catalytic activity with a consequently degradation. In literature exist indication of the tolerance levels for each impurity. The test is generally destructive for the device and takes a lot of time.

Contaminant	Tolerance (ppm)	Effects
Sulfides, for example, H₂s, COS, and CS₂	0,5-1	Electrode deactivation, usurpation of electrolyte
Halides, for example, HCl and HF	0,1-1	Corrosion, usurpation of electrolyte
Siloxanes, for example, HDMS and D5	10-100	Silicate deposits
Particulates	10-100	Deposition, plugging
Tars	2000	Carbon deposition
Heavy metals, for example, As, Pb, Zn, Cd and Hg	1-20	Deposition, usurpation of electrolyte

Table 3 Contaminants and their tolerance limits for MCFCs

When the tolerance range are known, an optimization for the design and integration of the clean-up unit can be done, there is also a saving in cost. One of the main problems for the MCFC poisoning is related to sulfur compounds. The effects of H_2S on the nickel-based catalyst are dependent from many factors such bulk concentration, concentration relative to hydrogen in the fuel, humidity, electrical load, and temperature. In literature is confirmed a propensity of the Ni to react with sulfur as temperature decreases. Concentration of sulfur compound of 5-10 ppm damage the device. In the MCFC there is also the degradation of the electrolyte from the hydrogen sulfide, in facts it can react chemically with the carbonates to form either sulfide or sulfate ions. This is equivalent to a reduced cell performance. All the presented issues from contaminants are generally preferably solved with a gas clean-up unit, the sulfur cannot reach the electrodes in order to preserve the life time of the cell.

5.5 Reforming of the methane

When MCFC is fed by methane, like in the case study presented. In general, there are three ways to do the reforming for fuel cells, so also for MCFC [12]:

- Direct internally: The reforming and the anode compartment coincide, there is not a material surface that divide the two. The thermal energy needed from the reaction come directly from the cell. The hydrogen that is produced it is directly burn at the anode. This configuration it is also known as Direct Internal Reforming (DIR). The reaction doesn't work in equilibrium since the consumption of the hydrogen shift the reaction towards the right part and enhance the conversion of the methane.
- Indirect internal: There is a physical, with a material surface, separation between anodic compartment and reforming zone. The thermal energy needed from the reaction come directly from the cell. This configuration it is also known as indirect Internal Reforming (IIR). The conversion of methane reaches the equilibrium point as limit condition.
- External: There is a net distinction between the anode compartment and the reformer. The thermal energy can be also provided externally from the cell. The two temperatures of the reforming and of the anode compartment can be very different. This configuration it is also known as External Reforming (ER).

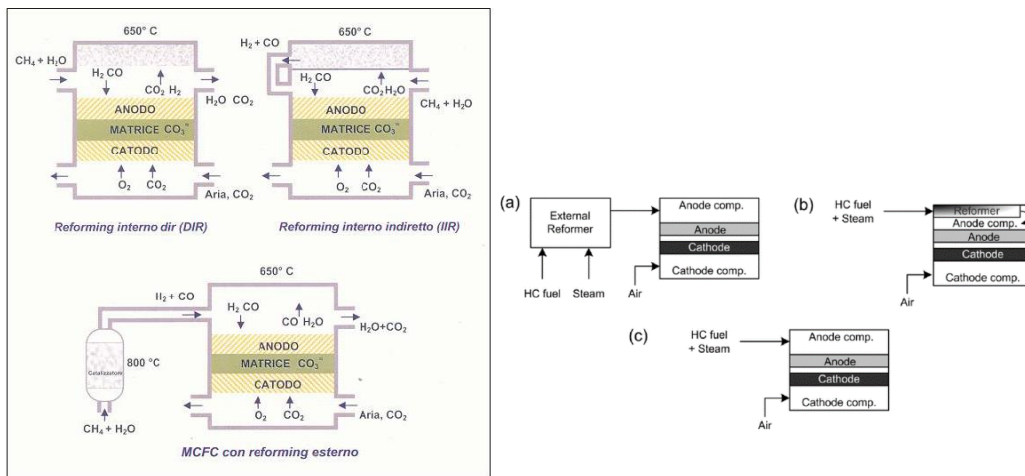


Figure 16 Strategies for the reforming of methane

The SMR is an endothermic reaction, so it acts as a sink for the heat generated by the oxidation reaction [11].

6. Absorption heat pump

The absorber is a machine that produce cooling energy starting from a heat source. The absorber which was planned to install it is a lithium bromide type. The salts have the capacity to absorb the humidity, in particular the vapor formed in the evaporator.

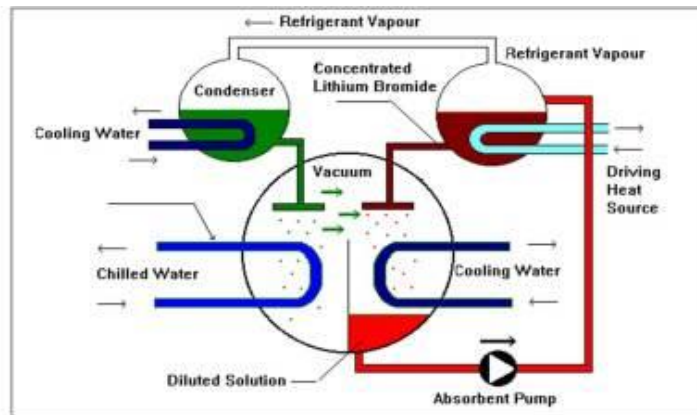


Figure 17 Scheme lithium absorber [13]

The solution of $BrLi$ it is able to absorb a certain quantity of vapor with an intrinsic capacity. When the solution is too diluted, it is no more effective. At this point, to continue the process, there is the removal of the water trapped into the salts and into the generator. By heating the solution in the generator, the water in excess evaporates, and the solution it is newly send in the absorbent section to trap the vapor coming from the evaporator. The water coming from the generator that is in the vapor phase is returned to the liquid state by using a condenser. The water in the liquid state it is send to the evaporator and the process can continue. To have an evaporation point of the water even at low temperatures the pressure in the evaporator must be sufficiently low. Atmospheric pressure water boils at $100\text{ }^{\circ}\text{C}$: to bring the boiling temperature below $7\text{ }^{\circ}\text{C}$ the pressure must be about $1/100$ of the ambient pressure: the units operate under vacuum. The degree of vacuum required by the evaporator is maintained thanks to the strong affinity between the solution and the water vapor.

There are two types of absorbers:

- Single Stage requires hot water at 90°C or overheated at 130°C, vapor at low pressure 1 bar.
- Double Stage requires vapor at high pressure 8 bar, gases, fumes.

The double stage absorber is used when the thermal energy it is at high level, the second stage it is in cascade after the first stage and no further heat is required, this allows the higher efficiency of the machine. The main drawback of the double stage is the less flexibility because the higher complexity of the machine. The COP of the machine are higher than 0.7 for the single stage and higher than 1.2 for the double stage. The absorbers need a small amount of electrical energy during working conditions, because it is used only for the pumps needed for movements of the fluids inside the machine. The refrigerant is water. Water that is mixed with ammonia or lithium bromide, the last is safer and nontoxic.

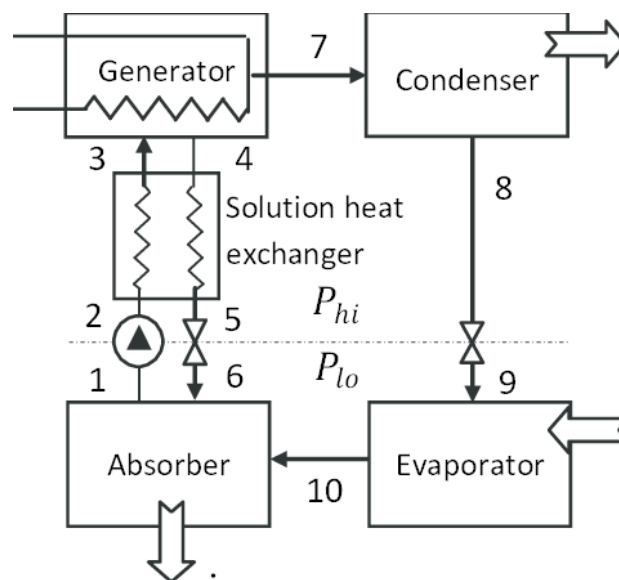


Figure 18 Absorber technical scheme

All the unwanted heat from the building is extracted thanks the chilled water loop that runs in the evaporator. The cold condensed water coming from the condenser will spray over the chilled water tubes and cover the surface of the tubes with a thin film of cold water. The thermal energy embedded in the chilled water it is the unwanted heat from the building, and it is transferred into the low temperature water film which was sprayed across the outside of the chilled water tubes. The two water never mix. Due to the low pressure of the chamber, near vacuum, the water boils, and as it evaporates it carries away all the unwanted heat from the building. After this passage the water it is at a lower

temperature and can be newly pumped inside the building again to collect more heat and bring it back to the absorption chiller. There is also a water recirculation loop needed to recirculate any water that missed the tubes and didn't boil off into steam or water vapor and this will be pumped back on the top of the evaporator and sprayed until all of it evaporates into steam [14]. The water in vapor phase is attracted by the lithium bromide solution.

7. Molten Carbonate Fuel Cell - Plant model

7.1 Context

Torino Green Airport project was born in 2021. The company STEAM did a feasibility study based on the energy data provided from SAGAT and characterized the loads and the project of the airport. Actually, the thermal needs of the airport are satisfied by common boilers, that are quite dated. The installation of the existing plant goes back on 1993, and further updates have been made during the Olympics in 2006. The future installation of the fuel cells will serve a great part of the airport. The electrical needs produced from the fuel cells will supply the electrical demand of the airport without distinction of the buildings. Caselle, known as international airport of Sandro-Pertini. It is located 16 km north from Turin, on a territory belonging three different municipalities: Caselle Torinese, San Francesco al Campo and San Maurizio Canavese.

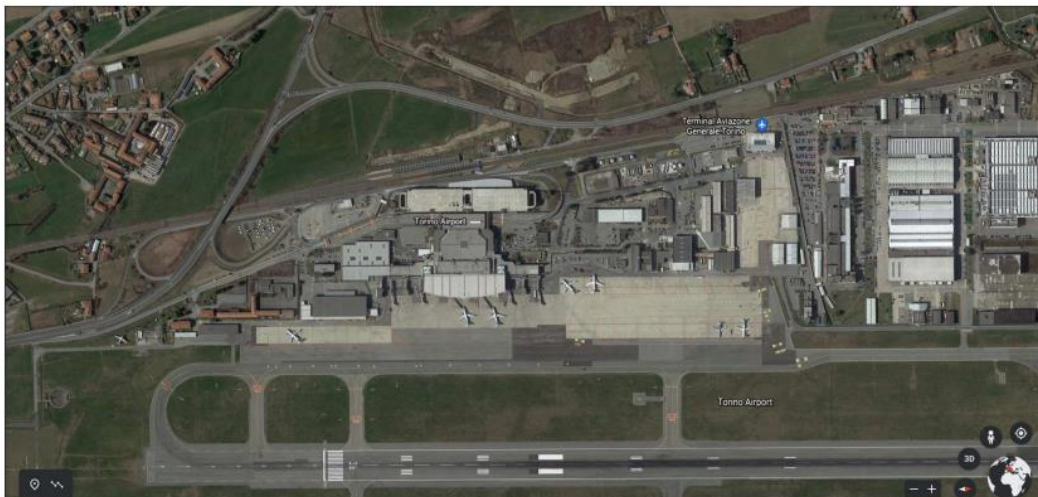


Figure 19 Torino-Caselle Airport satellite view

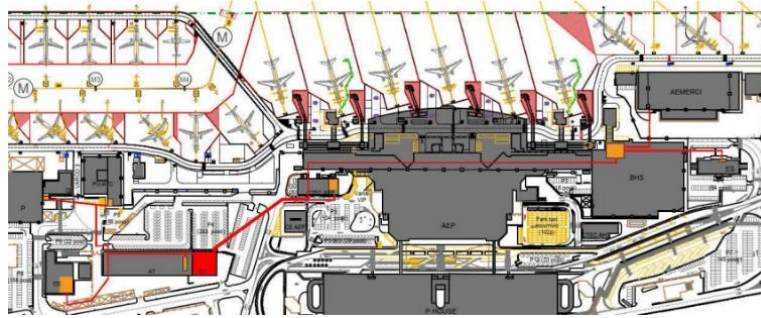


Figure 20 Thermal station (red) and connections to the substations (orange)

The will to install fuel cells technologies is interesting because several advantages have been created. High temperature fuel cells have the advantage of larger fuel flexibility with respect others types working at lower temperature.

- **Primary thermal station place for the installation of fuel cells**

In the principal substation there are four boilers feed by natural gas for the production of hot and overheated water.

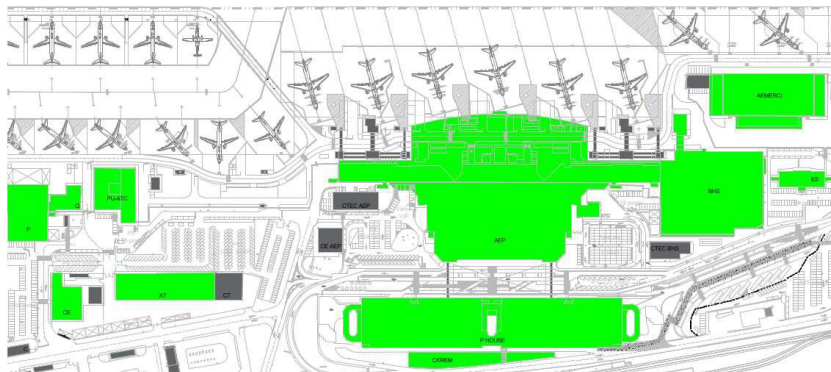


Figure 21 Airport view

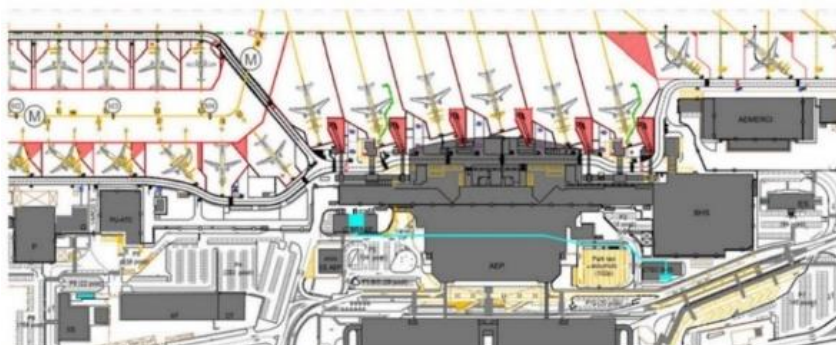


Figure 22 Cooling stations (blue) and pipes for cooling water

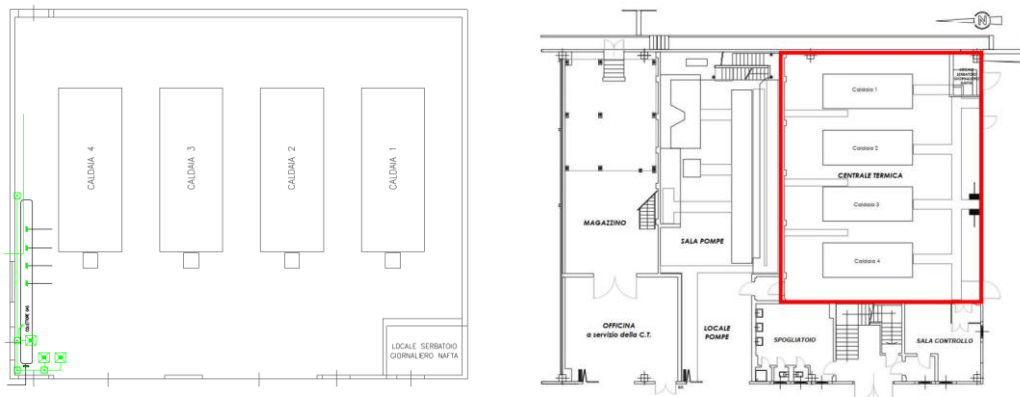


Figure 23 Thermal station

Actually the 4-th boiler it is disused, in the future a possible solution, complementary to the fuel cells, could be the installation of an internal combustion engine (ICE) in the same place. The other three boilers produce, in the winter season, hot water at 90°C. The fuel cells could be installed in place of the boilers number 4 and 2 and the third cell could be installed in the workshop. The choice to put the fuel cells inside a building it is beneficial also from an economical point of view since there will be no need to construct a containment wall around the machine. The boiler number 4 it was dismantled by SAGAT, the boiler number 2 will be dismantled during the steps for the installation of the fuel cells. All the spaces inside the rooms are naturally ventilated. The presence of asbestos in some parts of the plants push towards a massive review of the presence situation.

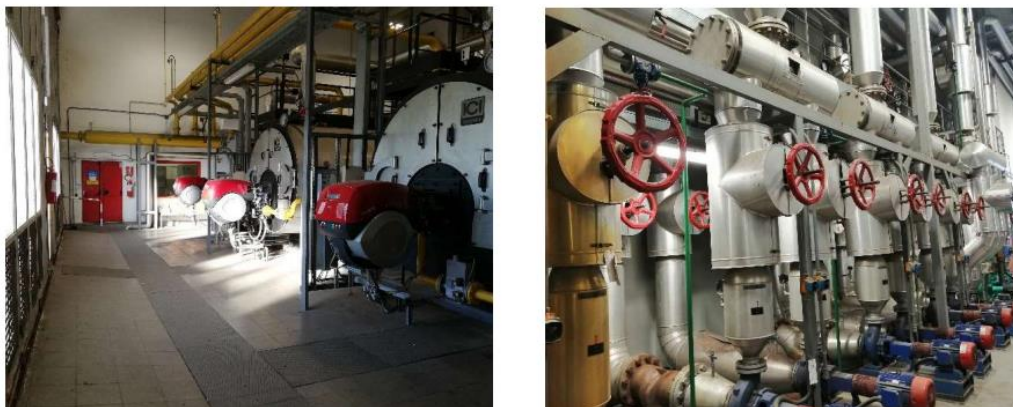


Figure 24 Photo of thermal station and pumping room

The space for the installation of the first two cells is in the actual thermal station, a proper ventilation is also mandatory. There will be a space for the cells and another for the boilers. The space for the third cell has been identified in the warehouse adjacent to the pump room in the primary thermal station. The division of the two spaces, one for the

boilers and another for the fuel cells, will be done with the construction of a wall in the middle. It will be also necessary a restoration of the façade of the building.

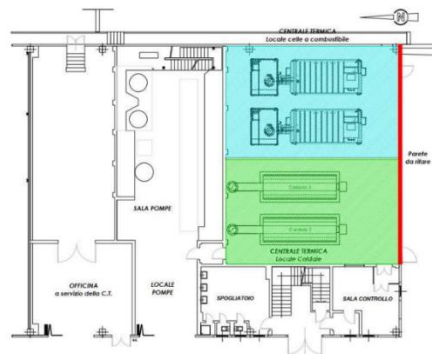


Figure 25 External façade of the thermal station

It will be needed a space for the metering section, that it is mandatory in order to obtain the high efficiency cogenerations and the title of energy efficiency (TEE). Others possible interventions is the substitution of the older economizers with a new model that preheat up to 70°C the returned water from the boilers. A second possibility it is the diminishing of the two remaining existing boilers with new models.



Figure 26 Warehouse, space for the installation of the third cell

All the space must be proper ventilated in order to avoid unwanted stagnations of gases like methane or hydrogen. A further updated is the hot water storage that will be installed in the area outside the principal thermal station. The size of the storage will be 200 cubic meter that will be used to cumulate the heat produced during night, or more in general when the thermal loads are low. In the discharging phase, part of the stored heat will be released to cover the demand. A metering section is needed to account the energy flows in charge and discharge. Four additional pumps will be needed to support the storage. Further devices needed are, a compressor, 16 stacks with 6 tanks with nitrogen and a gas cleaning system to treat the natural gas before entering the cells.



Figure 27 External space for storage installation and auxiliaries

For the Nord part of the network will be install a new intermediate heat exchanger that will be used as a separator of the new line with respect the existing.



Figure 29 Heat Hexchanger S.C.T.



Figure 28 Warehouse for the third cell (left) and existing boilers (right)

A further intervention will be the installation of the electrical panel at the service of the electro pumps with inverters.

- **Pumping station**

There will be the substitution of the existing pumping groups and two pumps will be added for the two economizers installed in the principal thermal station.

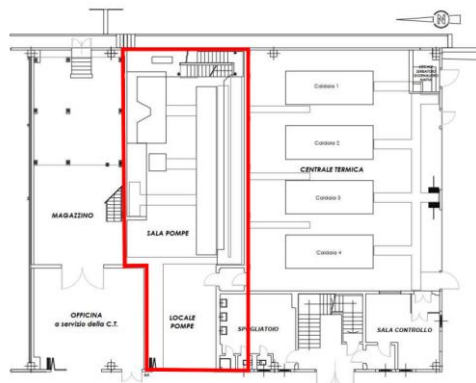


Figure 30 Pumping room

The principal collector should be modified in order to sustain the new mass flow rates. The delta of the collector will be 65/85 °C in winter and 70/90°C in summer. All the new pumps will be equipped with inverter. All the local it is natural ventilated.

- **Warehouse room–future third fuel cell room**

The storage room currently contains a loft. As for the principal thermal station there will be the necessity to have a proper ventilation in order to avoid stagnation in the room of unwanted gases like natural gas or hydrogen.

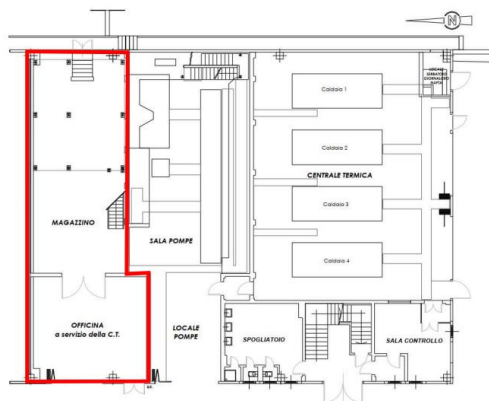


Figure 31 Warehouse for the third cell

To assist the fuel cells will be installed a compressed air storage and a system for the treatment of the water.

- **AEPAX thermal substation**

There is the water plant, refrigeration thermal plant and electrical room, outside the building there are the evaporative cooling tower to serve the refrigeration units. This

station served thermal and cooling needs of the terminal. Outside the structure, there is a cogenerator that can be used in case of emergency.

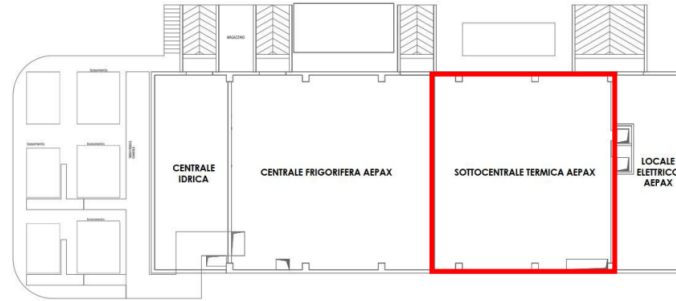


Figure 32 AEPAX thermal substation

- **AEPAX refrigerant station**

The refrigerant station has been renewed in July 2018. There are two refrigerators' groups with mechanical compression. The cooling water produced is at 7°C, the water is collected in a collector and with pumps send towards the aerostation. The water from the aerostation returns at 12°C.

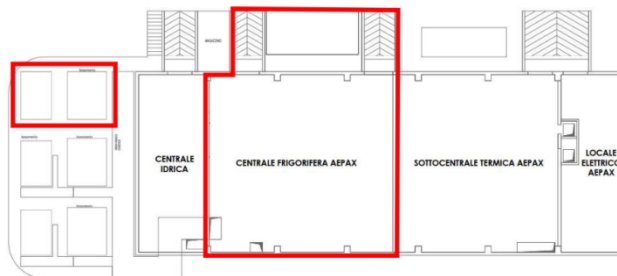


Figure 33 AEPAX cooling station, External space for the absorber and evaporative tower



Figure 34 Heat Exchangers AEPAX (left) and pumps (right)

To maximize the thermal recovery in the middle and summer seasons a lithium bromide absorber will be install in the refrigeration station. Due to the huge volume of the machine, the refrigerant group will be installed in a cabin outside the station, while the internal basement will be useful for install the auxiliary pumps for the correct operation of the machine. Further analysis will be needed to install the evaporative tower.



Figure 35 Evaporative towers

- **Substation BHS**

From the principal substation, a circuit for the hot water arrive up to the BHS, from the BHS there are two collectors that divide the circuit in smaller circuit. In this building new electro pumps will be needed to allow a modulation of the power.



Figure 36 Collectors BHS (left), heat exchangers BHS (right)

- **Hot water network**

The pipes of the hot water network are not well insulated, because was observed that the water from the principal thermal station up to the AEPAX (around 200 m of distance), the water lose 5°C. New interventions will be needed to improve the present situation. The two underground circuits that today reach the S.T.S. Aepax and S.T.S. BHS will be merged into a single circuit that will reach only Aepax secondary thermal station.

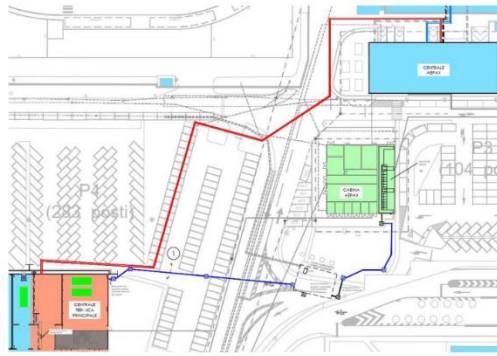


Figure 37 New underground hot water network (red), subservices (grey)

- **Electrical part**

Actually, in the airport there is not the presence of any device for the production in loco of electricity. The electrical network it is composed of different stations supplied from the general electrical panel at 27kV, others are connected with the middle voltage panel at 9 kV. There are two transformers with a ratio 27/9 kV. The three cells should be connected with the low voltage network of the airport. The point of interface will be in the AEPAX, where there is the transformation station.

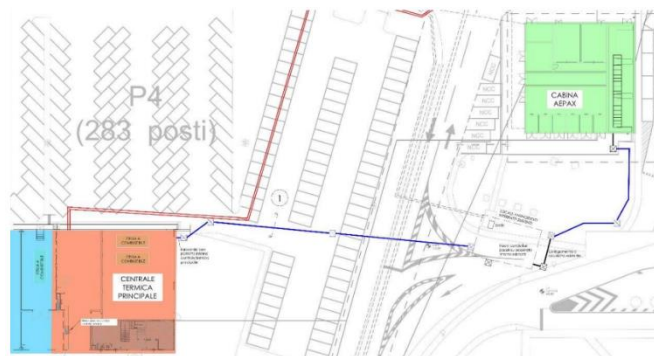


Figure 38 Thermal station and electrical station AEPAX

New lines will be needed at low voltage, in order to deliver 400 V of the fuel cells. From the cells up to the inverter the connection will be in charge of SNAM from the inverter SAGAT will be in charge to make a connection in low voltage up to the AEPAX, the cable will be able to sustain a maximum power of 400 kWe for 1200 kWe total.

7.2 Airport buildings served

STEAM, an energetic company, makes an analysis on the plants at the service of the airport of Turin. The data provided from the study are used as reference in this work and

discussed. SAGAT since 2015 adopted an energetic and efficiency plan to improve the situation of the existing plants, both from an economical and a technological point of view. During 2019 an analysis was conducted to have a complete view of the data and to understand the required interventions. Further possible activities will be the realization of a PV plant and the substitution of the oldest ATU (Air Treatment Unit) build in the '90. All the energy that will be produced from the fuel cells and from the PV plant, will be auto-consumed internally from the Airport. No electricity is sold to the grid. The data available with the consumptions of the Airport are of the year 2019.

The part of the airport that requires more thermal energy is the central south, in fact, in that area there are the majority of the plants for the production of thermal and cooling energy. The north part of the airport requires less energy and it is served from traditional oil boilers, except for the General Aviation that rely on natural gas boilers. All the other parts of the airport are fed with natural gas.

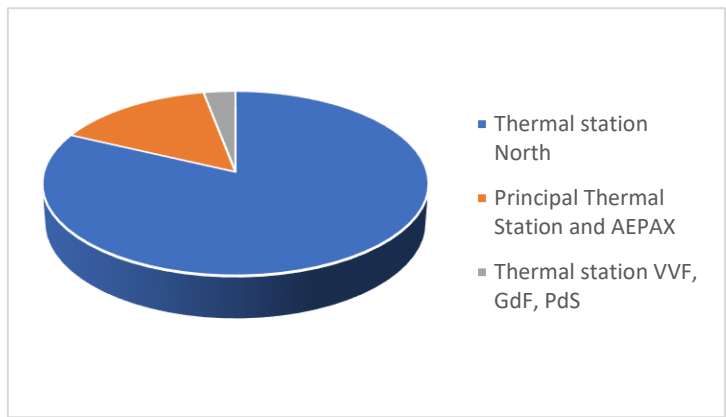


Figure 39 Thermal power installed

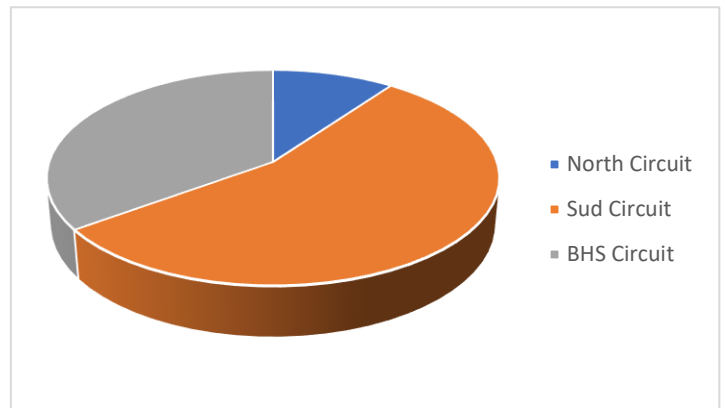


Figure 40 Power installed in the heat exchangers in the secondary sub stations

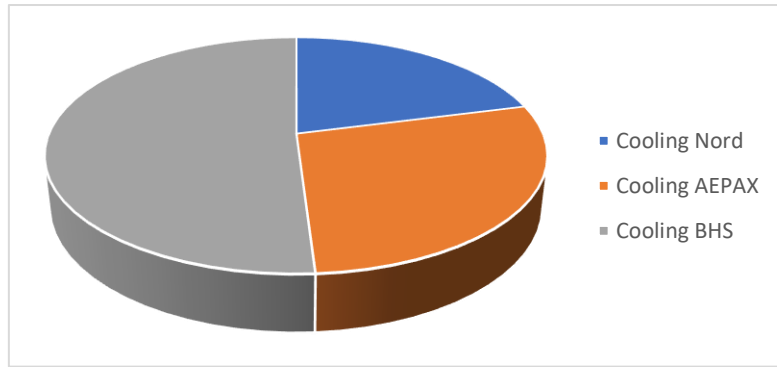


Figure 41 Installed power in the cooling stations

To limit the economical weight of the new interventions and the numbers of infrastructures, the already existing district heating network it will not be further expanded. The building that will be served are:

- Passenger Terminal Building (AEPAX)
- SAGAT office building (AP-PU-M)
- Buildings near opening 3 (QVAR-3)
- Building of the State Bodies (ES)
- Building Baggage Handling System (BHS)
- Freight terminal (AEMERCI)
- Technical Area (AT) + Electrical station (CE)
- Remote check (CKR)

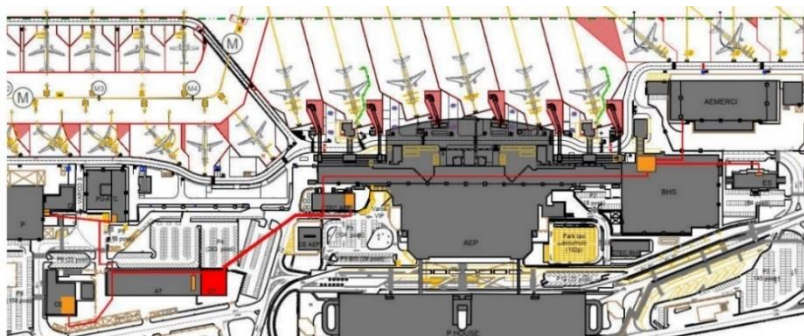


Figure 42 Building, in green, served from the trigeneration plants

From the point of view of electrical production, the electricity produced from the new plants will be used for all the parts of the airport without distinction.

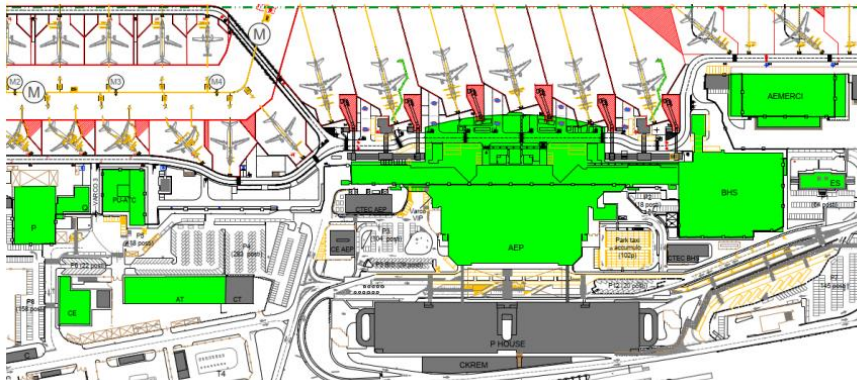


Figure 43 Principal thermal station, in red, and the other connections to the substations, in orange

During the period 2015-2019 some interventions were done in order to improve the energy savings of the airport. There was the upgrading of the air conditioning systems with the substitution of pumps groups and refrigeration unit in the AEPAX, the prevention of the leakages in the hot water pipes. The installation of LED for an internal and external lighting. Other upgrades were the installation of devices for the control of the consumptions of natural gas and for a dynamic management of the ATU (Air Treatment Unit). The thermal production of the new plants will be used only for buildings actually served from diesel oil boilers. The General Aviation will be not served from the new machines because the distance from the Principal Thermal Station. In the principal thermal station, there are actually four natural gas boilers to produce hot water. Outside the station, in the external area it could be necessary the installation of a 100-200 mc storage useful to store the heat produced from the fuel cells in particular during the night when the load is near zero for almost all the year. Further, the storage will minimize ignition and shutdown of the machines. The heat produced from the fuel cells, it is at high temperature and an absorber near the thermal production should be installed. With a double stage absorber, the efficiency doubled the mono-stage absorber (EER=1.3-1.2 with respect 0.7). There will be needed a link between the absorber and the principal thermal power station to the already existing network for transport the cooling water. This could be done with using the existing collectors inside the substation AEPAX.

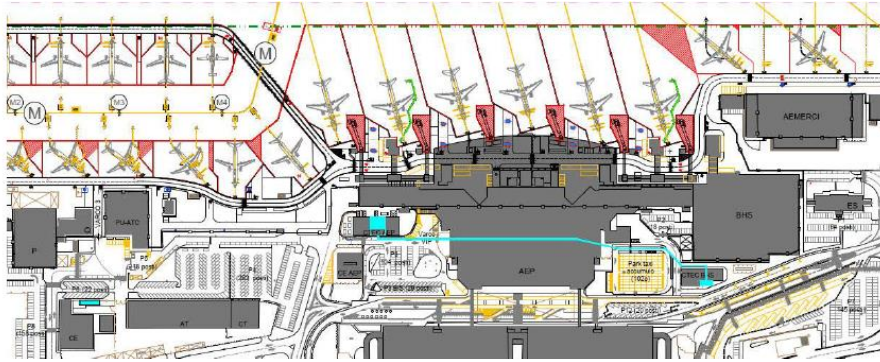


Figure 44 Cooling station (blue) and network for cooling water

7.3 Energetic Model and Energy needs of the airport

To understand the optimal strategy for the airport, an analysis on the energy needs of the airport is needed. SAGAT provide the data for the 2019 with an hour resolution divided in *refrigeration needs [kWh]*, *thermal needs [kWh]*, *electrical needs without absorber [kWh]*, *electrical needs with absorber [kWh]*. The data available are for every hour of each day of the year. Summing all the energy consumptions the yearly needs can be obtained:

- The thermal needs for one year are 5.658 [MWh]
- The cooling needs for one year are 4.830 [MWh]
- The electrical needs without absorber are 15.835.260 [MWh]
- The electrical needs with absorber are 16.444.888 [MWh]

	refrigeration needs [kWh]	thermal needs [kWh]	electrical needs without absorber [kWh]	electrical needs with absorber [kWh]
January	0	1.436.106	1.503.321	1.503.321
February	-2.203	965.276	1.308.266	1.308.266
March	-9.580	649.035	1.367.467	1.367.467
April	-11.540	237.099	1.216.579	1.216.579
May	-123.069	6.940	1.217.196	1.245.949
June	-1.106.551	593	1.298.710	1.432.030
July	-1.494.716	150	1.443.009	1.646.238
August	-1.409.872	32	1.286.945	1.472.685
September	-619.174	1.141	1.197.813	1.245.667
October	-53.751	119.875	1.228.389	1.239.121

November	0	984.848	1.341.531	1.341.531
December	0	1.256.492	1.426.036	1.426.036
	-4.830.455	5.657.588	15.835.260	16.444.888

Table 4 Energy needs of the Airport

As clearly visible, there is a huge mismatch between summer and winter: for this reason, an absorber will be introduced in the plant to have an overall load profile more uniform during the year. The thermal needs in summer are poor, or even zero, because the hot water it is produced using electrical resistances in boilers and the humidify section and post-heating of the air treatment units are switched-off. With the absorber the refrigeration needs are transformed in thermal needs. With the absorber, also in summer there will be a thermal load that increase the number of hours of operation of the cogeneration unit. In winter and in some parts of the intermediate seasons some locals can be cooled in free cooling, reducing in May and October the thermal and cooling needs.

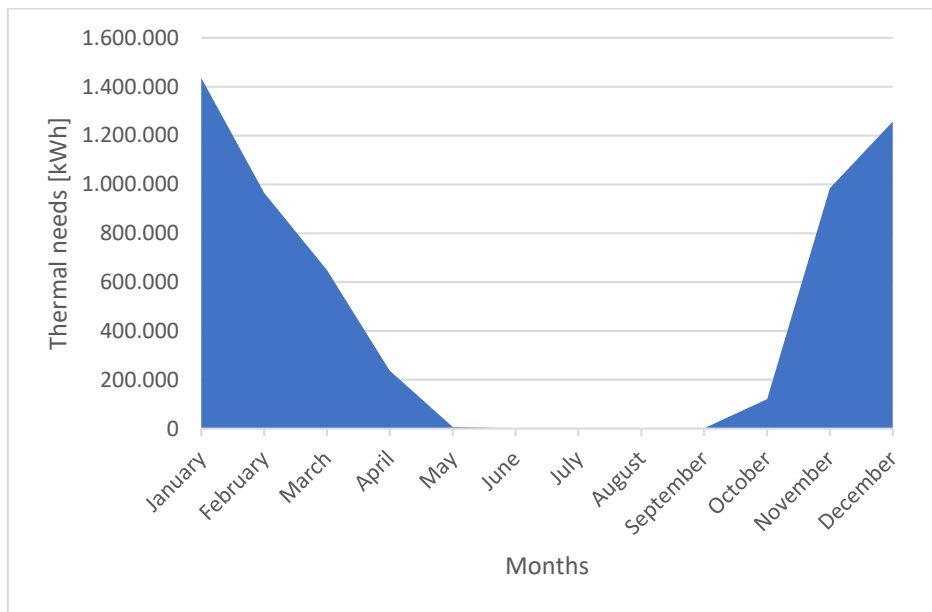


Figure 45 Thermal Needs of the Airport

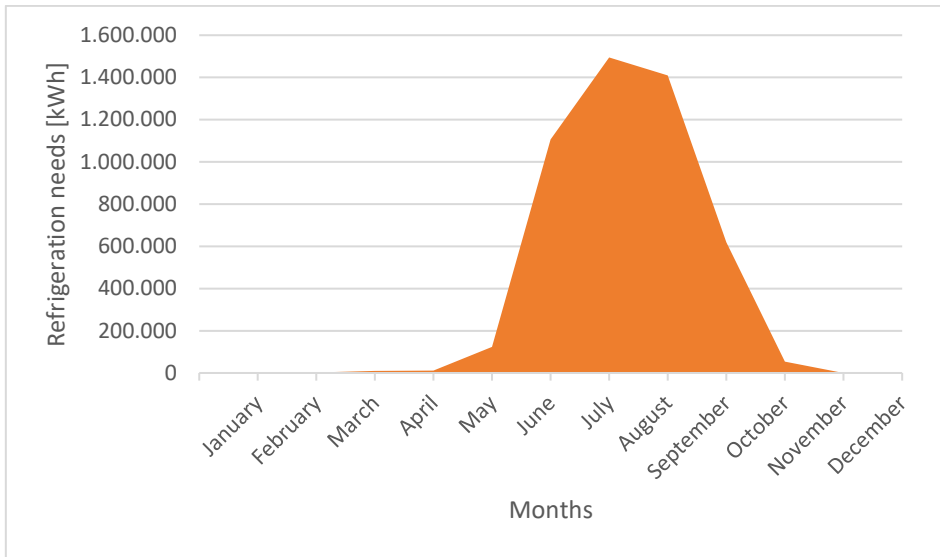


Figure 46 Refrigeration Needs of the Airport

In the graphs are reported the actual thermal needs of the airport, and the cumulated load profile of the actual thermal needs plus the refrigerant load converted in thermal. There are two graphs, one with an EER of 0.7 for a single stage absorber and another with EER of 1.2 for a double stage absorber.

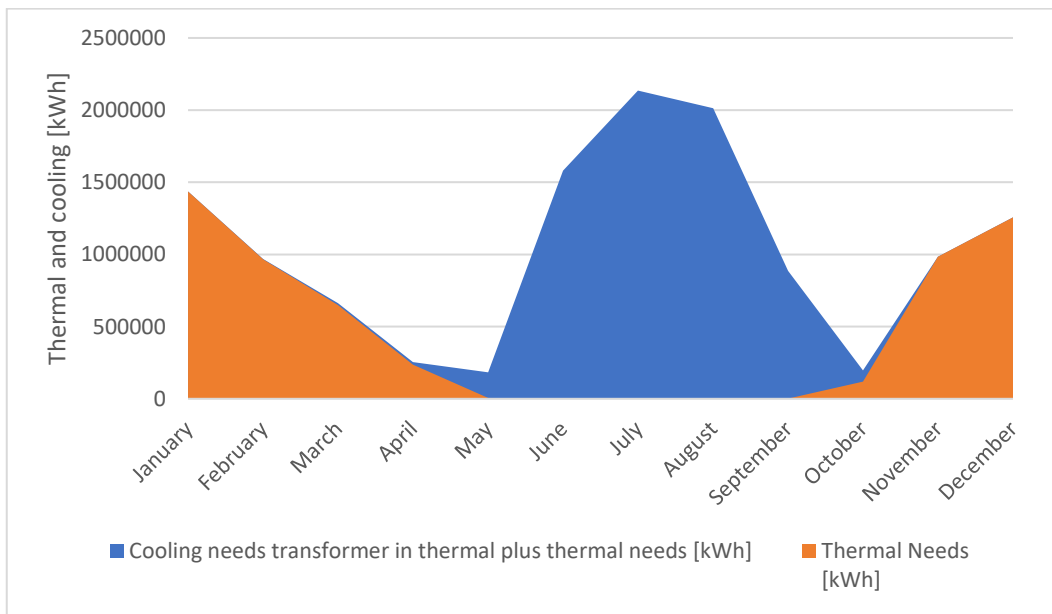


Figure 47 Thermal load profile EER=0.7

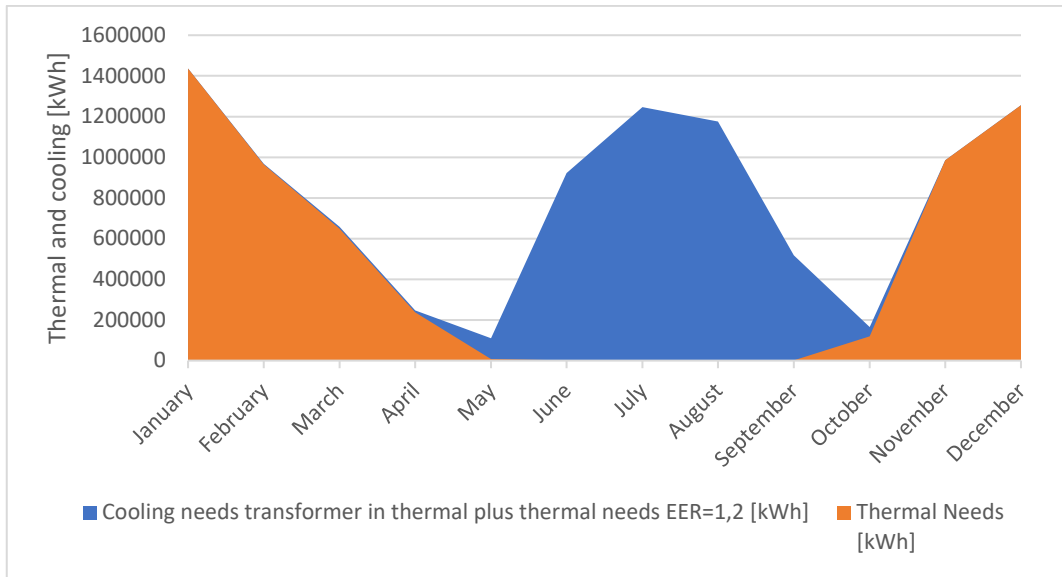


Figure 48 Thermal load profile EER=1.2

The cooling needs are necessary to keep the cogeneration plant turned-on also during summer. In this way the capacity factor of the plant increase. The capacity factor is defined as the numbers of hours in which the plant work with respect the total hours in one year.

$$CF = \frac{\text{numbers of working hours}}{\text{numbers of hours in one year}}$$

The CF is particularly relevant in the economical part.

The electrical load of the airport was determined using the data available from the meters for the airport zones and from the consumptions of electrical energy due to the absorber groups. The data presented are the net consumptions without the consumptions for the air conditioning. From the load profile, in July there are the peaks of consumptions, due to the traditional refrigeration units. For higher cooling energy produced from the absorber the less will be the electrical energy absorbed from the traditional refrigeration units. The annual electricity need is around 16.600 MWh.

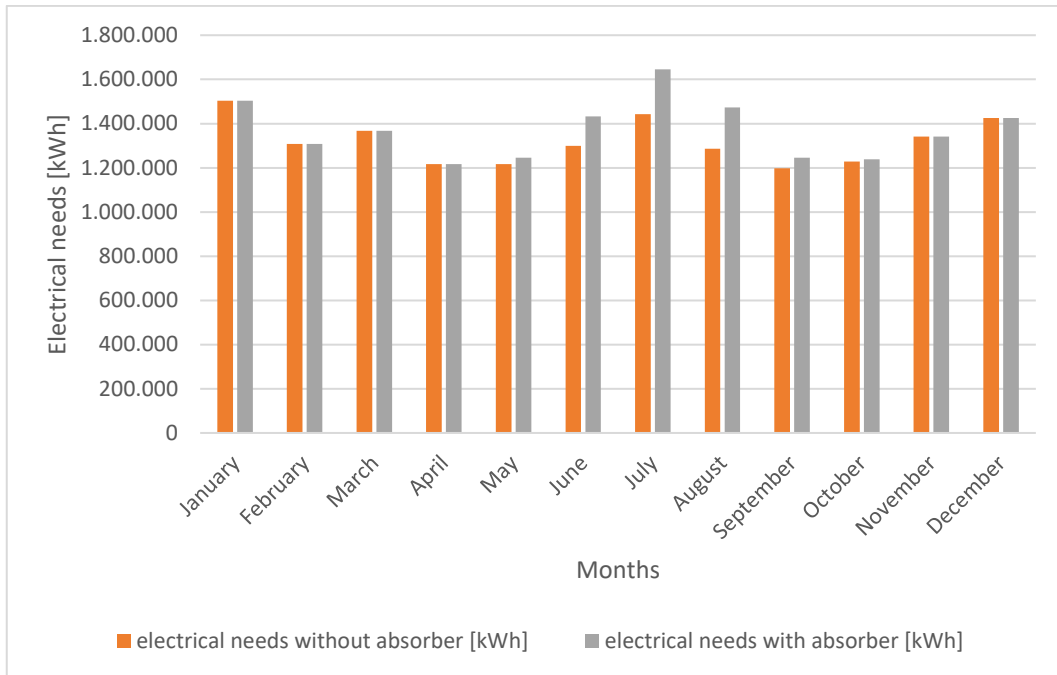


Figure 49 Electrical Needs with and without absorber

SAGAT seeing for market ESCo, is trying to make a cogeneration plant with the adoption of fuel cell. The three modules can be partialized at 40% of the nominal power. Since the high temperature of operation, the fuel cell will be switched off only when the load is really pour, generally in May and October. These stationary machines are not dynamic. Has been decided to make the fuel cell working at maximum load for the majority of the year. A hot water storage of 100-200 cubic meter will be installed to dissipate into the atmosphere less thermal energy during the year. The fuel cells will be exploited when the thermal load is low to charge the storage, then when the thermal load is higher than the production, the storage will be used to compensate the gap. Further, this strategy reduces the energy needs from the traditional boilers reducing also the annual emissions into the atmosphere of CO_2 , CO and NO_x . The storage can be seen as an additional load to be covered from the cogeneration unit. This increase consequently the numbers of annual working hours required from the plant making easier to obtain the High Efficiency Certificates for the cogeneration units. In May and October, the plants will be switched off, and the maintenance could be done in that period. During that month, all the needs of the airport should be covered from the existing plant and the national grid. The information on thermal and electrical power should be known to determine the size and numbers of the cells and the size of the absorber. Several simulations have been done.

The following picture represent the cumulative curve for the thermal power with respect the working hours. Every point in the graph represents the numbers of hours that the plant is expected to operate with the level of power to cover all the energy. In this analysis the storage it is not considered. The effects of the storage results in a translation in time of the curves. With the storage the overall thermal energy produced from the plant doesn't change but change the way the energy is managed. The storage can cumulate energy, for instance during night or when the load is low, and release it during the day, so avoiding dispersion of useful heat into the atmosphere.

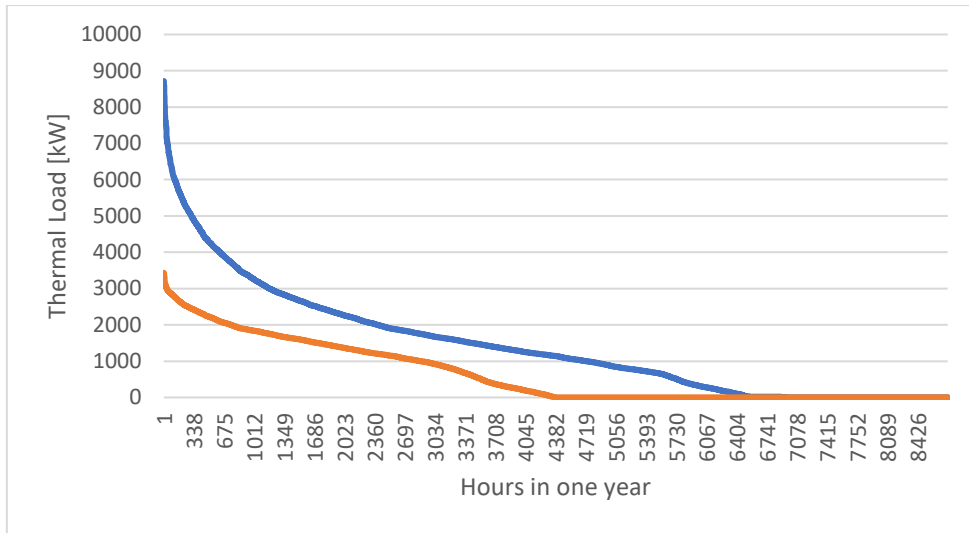


Figure 50 Cumulated curve of the thermal load and cooling load transformed in thermal with a double stage absorber

To allow the machines to work for a high number of hours, it is necessary predispose a plant with a thermal power not higher than 800 kW. The numbers of hours in operation for a plant of 800 kW_{th} are more than 5200, that means a capacity factor near 60%, not considering the two months of stop for maintenance. The electrical energy demand is higher than 1.2 MW for almost all the hours of the year. A cogenerator with 1500 kW size can be suitable to satisfy the electrical needs for 8000 hours, but in order to avoid excessive thermal dispersions into the atmosphere, the size of the cogenerator should be lower.

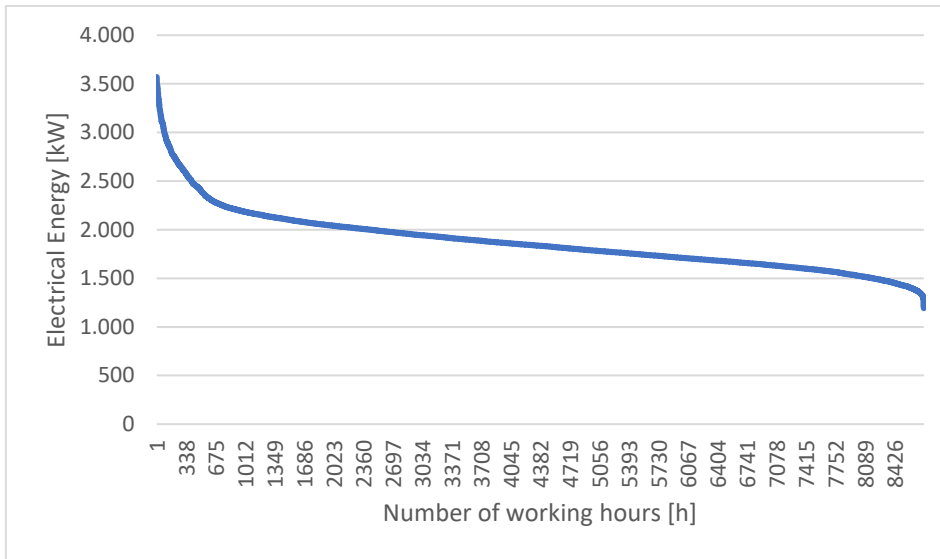


Figure 51 Cumulated curve of the electrical load with absorber

A double stage absorber with an EER=1.3 have been also considered.

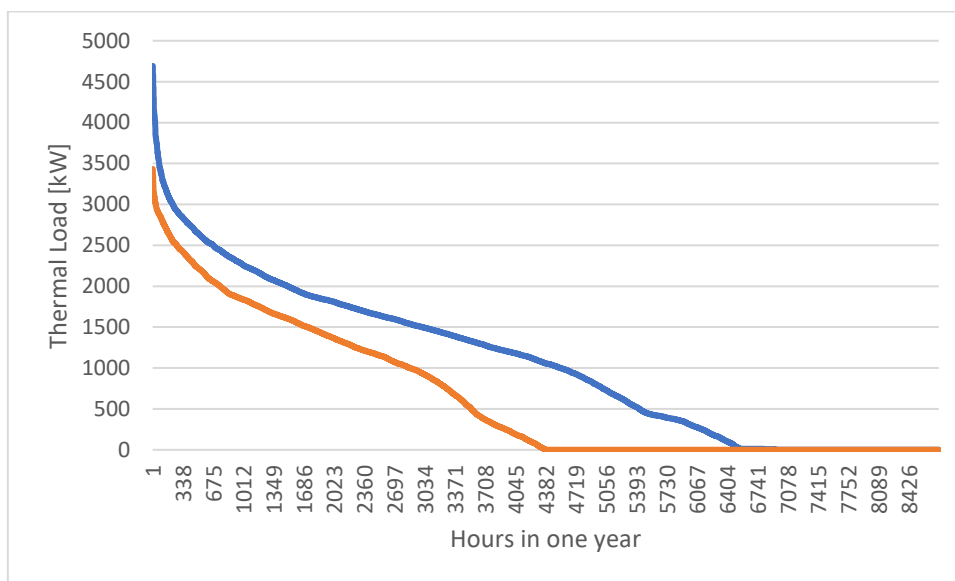


Figure 52 Cumulated curve of thermal load EER=1.3

The fuel cells will be installed in parallel. The minimum thermal energy required to avoid too high dissipations and work high numbers of hours remain 400 kW.

7.3.1 Results of the simulations for 10 months operation

The following table summarize the contributions of the fuel cells to the electrical, thermal, and cooling needs. In this simulation in May and October, the fuel cells are switched off. The capacity factor is 0.83.

Summing the energies for each hour, it is possible to determine, on a monthly basis, the amount of electrical needs with and without the absorber, the thermal and the cooling loads. Knowing the nominal electrical power of one module of 400 kW, and thermal 281 kW_t , it is possible to determine the contribution of the fuel cells to the loads of the Airport.

	% Electrical load without absorber covered from the cells	% Electrical load with absorber covered from the cells	% Thermal load covered from the cells	% Cooling load covered from the cells
January	58,92%	58,92%	43,30%	100%
February	61,10%	61,10%	58,14%	100%
March	57,57%	57,57%	85,17%	100%
April	39,52%	39,52%	100%	100%
June	57,26%	51,93%	100%	37%
July	58,89%	51,62%	100%	31%
August	65,74%	57,45%	100%	33%
September	51,79%	49,80%	100%	48%
November	63,51%	63,51%	60,74%	100%
December	62,61%	62,61%	49,89%	100%

Table 5 Contribution of the fuel cells with the storage to the energy needs of the airport

In summer, it is frequent that the thermal load is null, and there are only refrigerants needs. The maximum amount of cooling energy that can be produced from three modules is:

$$Q_{cool,max} = 281 * 3 * 1.3 = 1095.32 \text{ [kWh}_f\text{]} \quad (10)$$

There are hours in which the refrigerants need cannot be completely satisfied from the fuel cells. Traditional chillers should be used to satisfy all the demand. Also the storage contributes to cover the cooling demand, as average 5% more in the summer months.

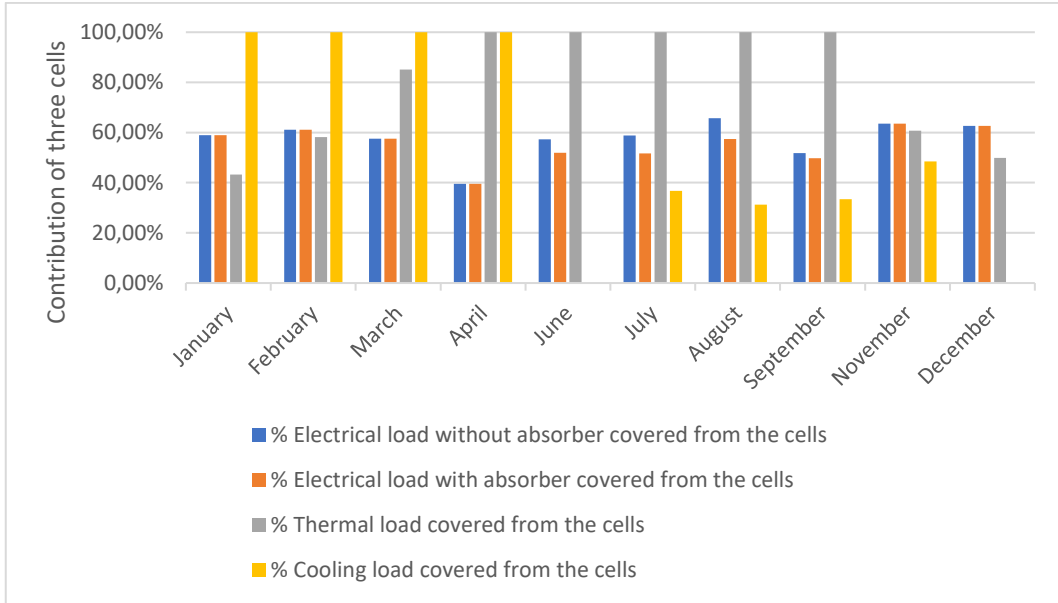


Figure 53 %Monthly contribution of the cells

For each hour can be calculate the net heat from the fuel cells.

$$Q = Q_{fuel_{cells}} - Q_{total_therma_load} \text{ [kWh]} \quad (11)$$

The total thermal energy can be calculated considering the base thermal load plus the refrigerants needs transformed in thermal.

$$Q_{total_thermal_load} = Q_{thermal_load} + \frac{Q_{refrigerant}}{COP} \text{ [kWh]} \quad (12)$$

The COP of the absorber for the simulation has been assumed equal to 1.3.

When Q is higher than zero, it means that the fuel cells produced more thermal energy with respect the demand. So, the energy in surplus can be stored into the water storage. When Q is negative, it means that the thermal demand is higher than the energy produced from the cells.

For each hour can be determined the state of charge of the storage.

$$Q_{SoC_h} = Q_{h-1} + Q_h \quad (13)$$

Where Q_{SoC_h} is the state of charge energy cumulated inside the storage at the h-th hour. The storage cannot exceed 2000 kWh.

$$0 < Q_{SoC_h} < 2000 \text{ kWh} \quad (14)$$

When the Q_{SoC_h} is at the maximum level, the storage cannot accept further heat, and when the heat produced from the fuel cells exceed the demand ($Q_h > 0$), the extra heat is dissipated into the atmosphere. This is a lost for the plant.

The maximum thermal energy that can be cumulated in the storage

$$Q_{SoC_MAX} = c_{water} \cdot \rho_{water} \cdot V \cdot \Delta T \quad (15)$$

Where c_{water} is the specific heat for water $4.186 \left[\frac{J}{Kg \cdot K} \right]$, ρ_{water} is the density $1000 \left[\frac{Kg}{m^3} \right]$, V is the volume of the storage equal to $200 m^3$, ΔT is the delta temperature in the storage. The ΔT for $200 m^3$ is around $10^\circ C$. The value obtained must be multiplied for $\frac{1}{3600} \left[\frac{kWh}{kJ} \right]$.

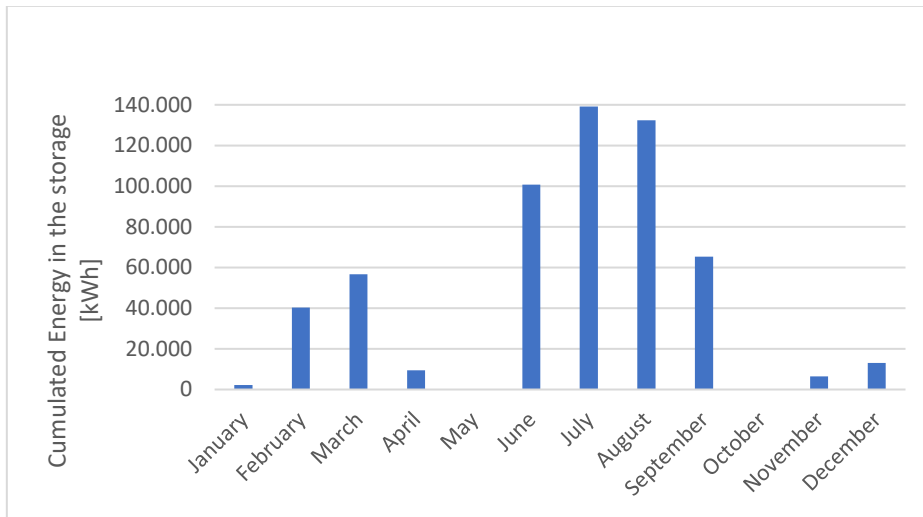


Figure 54 Energy in the thermal storage during 2019

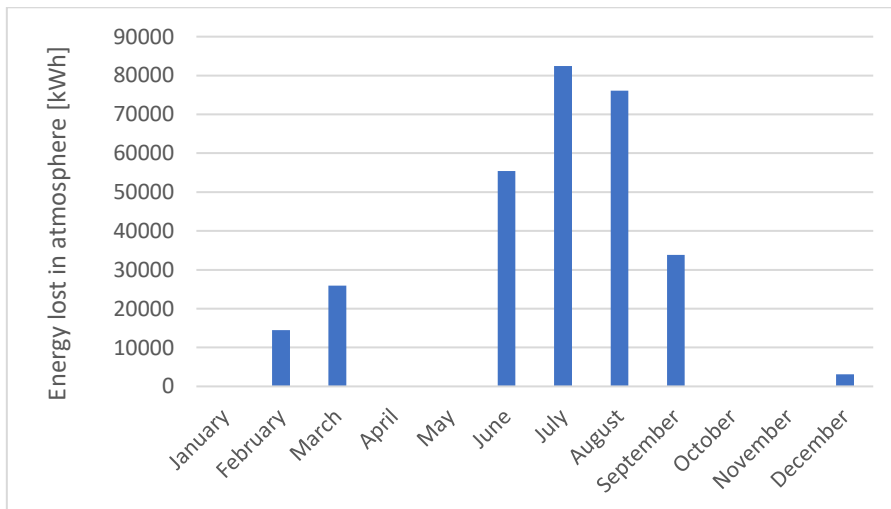


Figure 55 Thermal energy dispersed in atmosphere

In July, when the thermal needs are closer to zero, and there is high demand for refrigeration, the dissipations of extra-energy into the atmosphere increase. In June, July, August and September there is a huge mismatch between the thermal load close to zero, and the higher refrigerant needs. The cumulated energy into the storage can be exploited to cover the refrigerant needs.

$$Q_{refrigerant} = COP \cdot Q_{Thermal_{Release}} = 1.3 \cdot Q_{Thermal_{Release}} \quad (16)$$

The thermal energy release from the storage, discharging phase, can be exploited to cover the cooling needs.

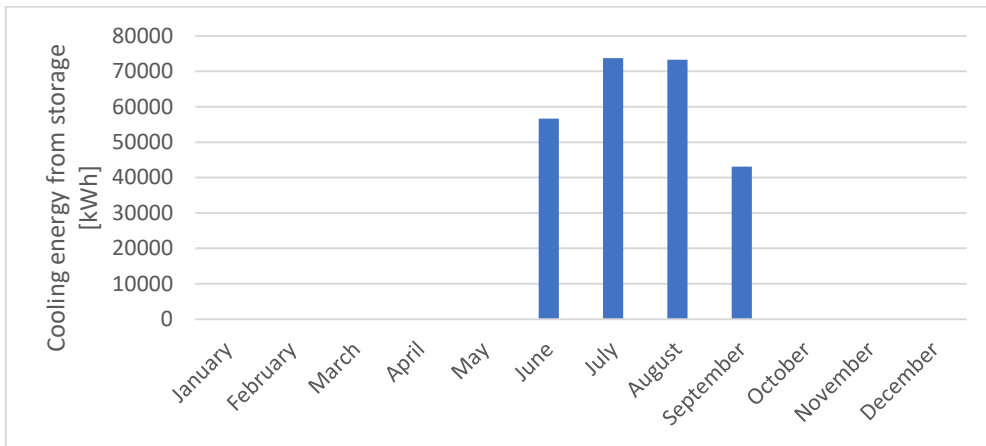


Figure 56 Cooling energy during discharging phase of the storage

When the cooling needs cannot be all satisfied from the fuel cells, traditional chillers are used to satisfy the demand.

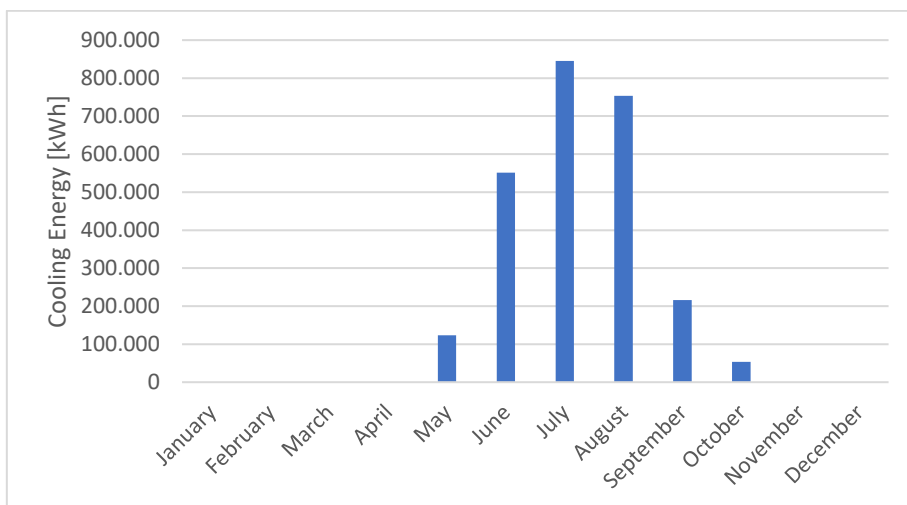


Figure 57 Cooling energy from traditional chillers

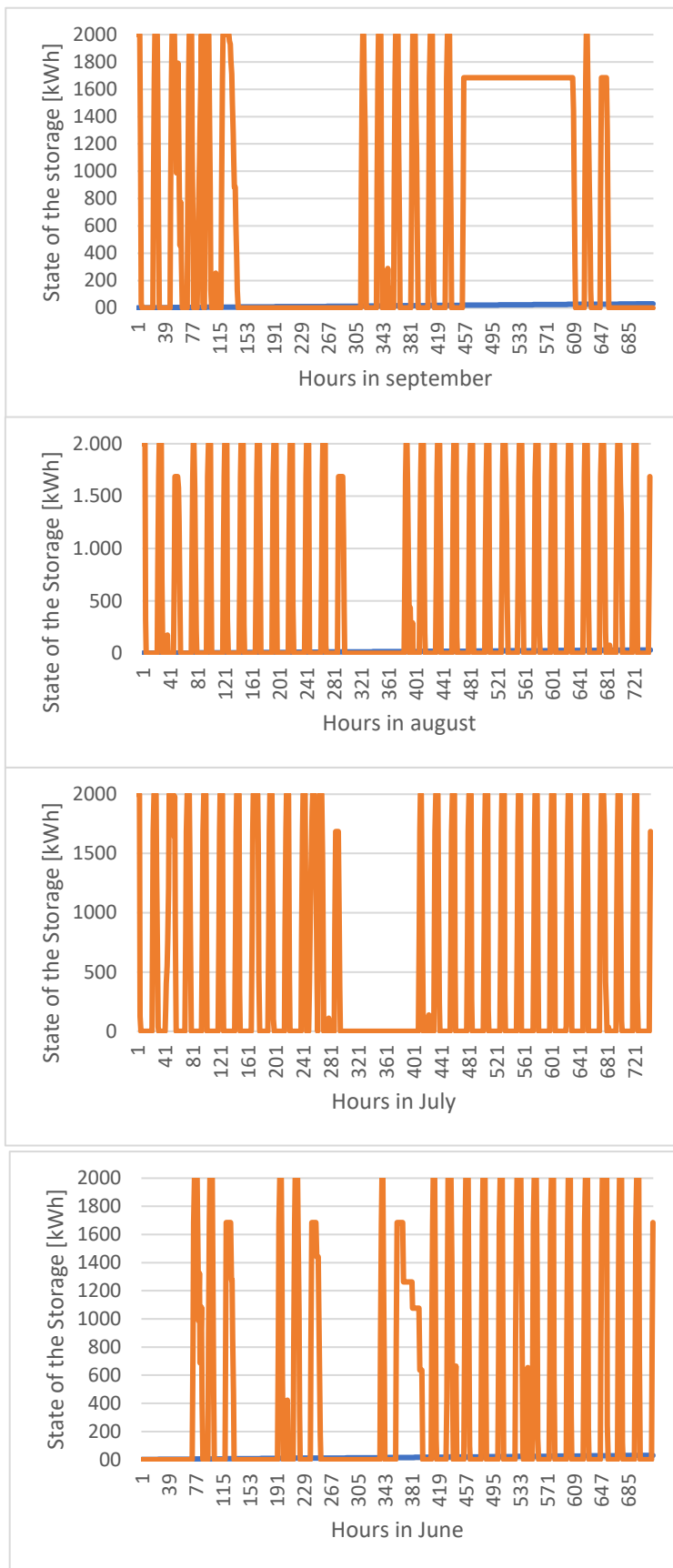


Figure 58 State of the storage in summers months

In September the storage has been kept at 1685 kWh, the thermal needs during that days were not relevant and the small amount of refrigerants demand could be covered from the fuel cells. The fuel cells that work at high temperature (HTFC), cannot be easily switched on and off without damaging the machine and lost time at the start-up. To avoid unwanted switch-off in some hours, extra heat is produced and wasted into the atmosphere.

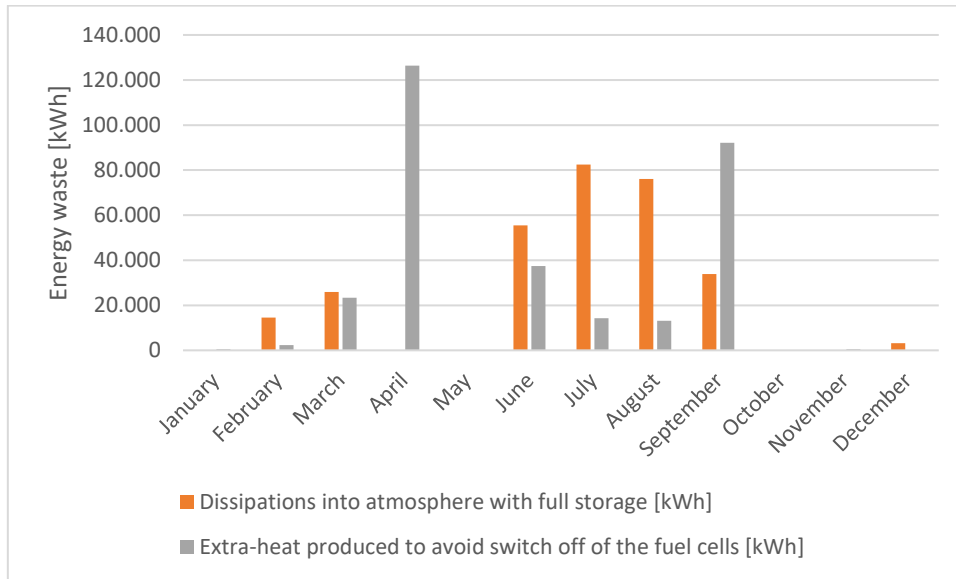


Figure 59 Energy wasted into atmosphere

All the electricity produced from the fuel cells is auto-consumed in the Airport. The amount of electrical energy produced from the fuel cells is not sufficient to cover all the demand, the rest is bought from the national grid.

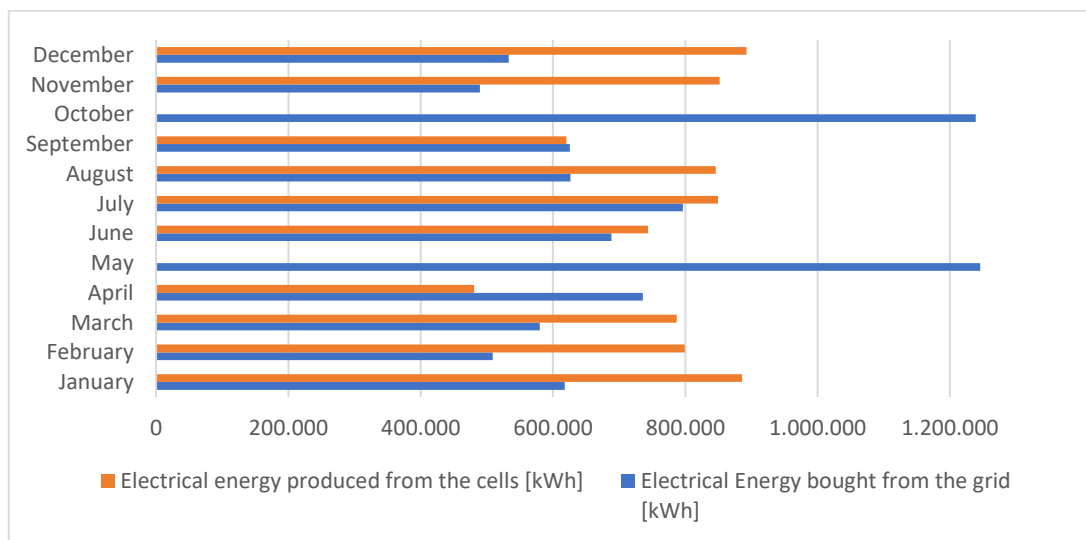


Figure 60 Electrical energy produced from the fuel cells and bought from the grid

In May and October, all the electricity is bought from the grid. The total monthly electrical consumptions bought from the grid is 1.240.000 [kWh], even if the two months are in two different seasons of the year. Summing the two contributions, the yearly electricity consumption is 16.444.888 [kWh].

Each module consumes $80 \left[\frac{Sm^3}{h} \right]$. In April, is the month, when the fuel cells are in operations, with the smallest thermal loads, the amount of natural gas required is the lowest. April is also the month with the biggest energy wasted into the atmosphere to avoid the shutdown of the cells. The annual natural gas consumptions are $1.542.609 Sm^3$. Equivalently the yearly energy of the fuel is 16.505.920 [kWh], considering a standard cubic meter [Sm^3] equivalent to 10.7 [kWh].

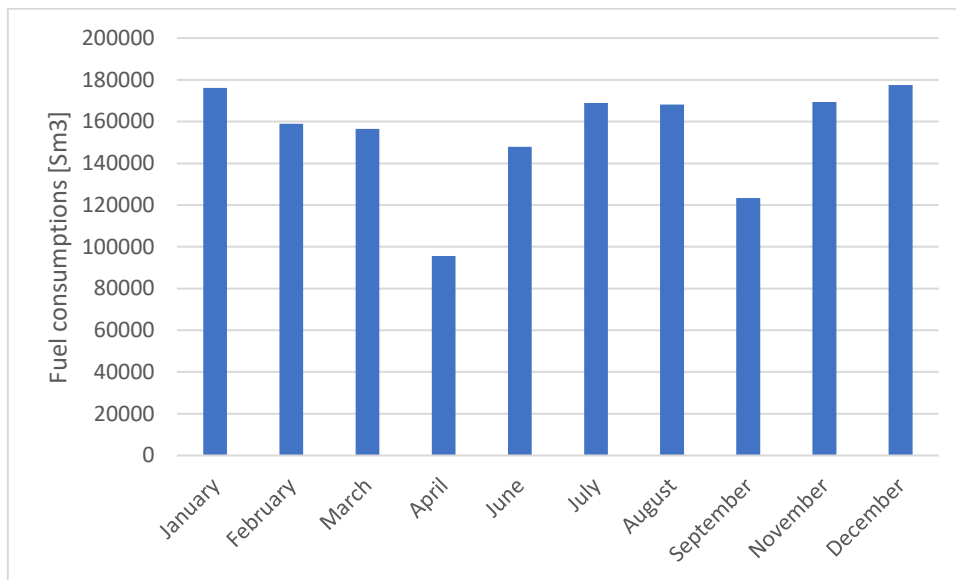


Figure 61 Monthly natural gas consumptions

A simulation has been carried out using a CF equal 0.9 and another with 0.8, no entire months of stop have been considered, the number of hours lost for maintenance are accounted in the capacity factor.

The table shows the contribution of the fuel cells in covering the demand. During summer, about half of the refrigerant loads would be satisfy. During the months of a year, more than half of electricity will be produced from the cells.

	% Electrical Energy without absorber covered with fuel cells	% Electrical Energy with absorber covered with fuel cells	% of thermal load covered from the cells	% of cooling load covered from the cells
January	53%	53%	39%	100%
February	61%	61%	53%	100%
March	59%	59%	87%	100%
April	66%	66%	100%	100%
May	66%	64%	100%	100%
June	62%	56%	100%	46%
July	56%	49%	100%	37%
August	62%	55%	100%	40%
September	67%	65%	100%	88%
October	65%	65%	100%	0%
November	60%	60%	55%	0%
December	56%	56%	45%	0%

Table 6 Contribution from the fuel cells to the loads CF=0.9

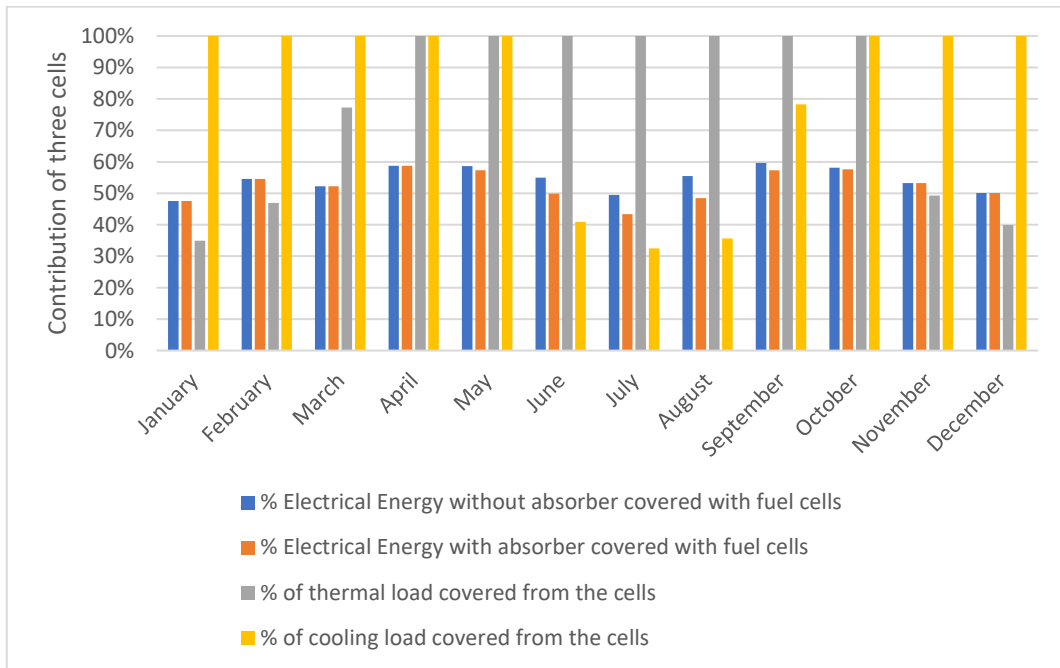


Figure 62 Contribution from the fuel cells to the loads CF=0.9

	% Electrical Energy without absorber covered with fuel cells	% Electrical Energy with absorber covered with fuel cells	% of thermal load covered from the cells	% of cooling load covered from the cells
January	48%	48%	35%	100%
February	55%	55%	47%	100%
March	52%	52%	77%	100%
April	59%	59%	100%	100%
May	59%	57%	100%	100%
June	55%	50%	100%	41%
July	49%	43%	100%	32%
August	55%	48%	100%	36%
September	60%	57%	100%	78%
October	58%	58%	100%	100%
November	53%	53%	49%	100%
December	50%	50%	40%	100%

Table 7 Contribution fuel cells to the load CF=0.8

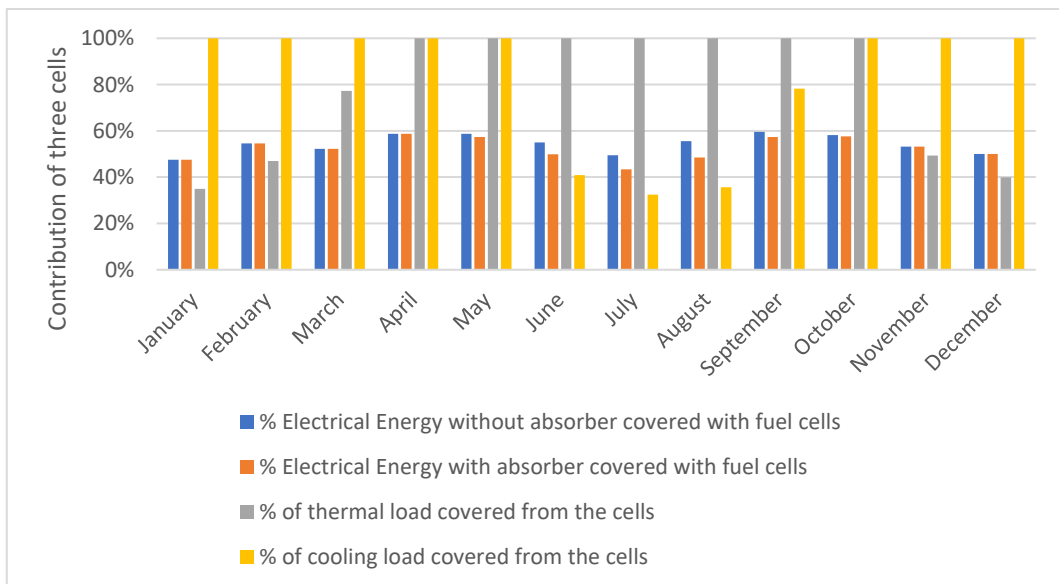


Figure 63 Contribution fuel cells to the load CF=0.8

7.4 Storage

There are two possible size of storage that can be selected, 200 m^3 and 100 m^3 . With a maximum storage capacity of 2000 kWh for 200 m^3 size and 1000 kWh for 100 m^3 . The

installation cost for a 200 m^3 storage, including the connections, the instrumentations and the accessory needed to the installation, is 216.280 €.

Considering the effect of capacity on purchased equipment cost the following formula can be used:

$$\frac{C_1}{C_0} = \left(\frac{S_1}{S_0}\right)^n \quad (17)$$

Where C_0 is the cost of the component of size S_0 , C_1 and S_1 are respectively the cost and the size to be determined, n is a scaling factor that depends from the type of equipment, the units in which the capacity is measured, the range capacity. A value of 0.6 has been used in this analysis. The estimated cost of the storage of size 100 m^3 is 142.691 €.

The maximum dissipated energy during a year is 843 kWh. A 2843 kWh storage size could be necessary to be installed in order to avoid dispersion in the atmosphere. The estimated cost would be 266.360 €. The annual amount of heat dispersed for a 200 m^3 storage is 291.395 kWh. The annual dispersed heat for a 100 m^3 would be 1.061.140 m^3 . The numbers of hours in a year with the 200 m^3 storage full are 451 h, instead 1023 h with a 100 m^3 storage. Being the dispersion for a smaller storage too high, it is advisable insert a 200 m^3 .

7.5 Fuel cell stack datasheet

The fuel cell is the SureSource 400. The fuel cell size is 400 kW that means that it can produce 400 kWh in one hour. The declared key features from FuelCellEnergy that is the producer are:

- Continuous Power
- Highly Efficient
- Fuel Flexible
- Ultra-Clean
- Scalable
- Modest Footprint
- Quiet Operation

From data sheet "This solution is ideal for on-site power generation requiring continuous power and value high-quality facility heating and/or absorption chilling; including industrial facilities, hospitals, universities and wastewater treatment plants."

Power Output		Pollutant Emissions	
Power @ Plant Rating	400 kW	NOx	0.0045 g/kWh
Voltage AC (standard)	400 V	SOx	0.000045 g/kWh
Frequency (standard)	50 Hz	PM10	0.000009 g/kWh
Electrical Efficiency	47 +/- 2%		
Available Heat		Greenhouse Gas Emissions	
Exhaust Temperature	420 +/- 25°C	CO2	445 g/kWh
Exhaust Flow	2500 Kg/h	CO2 (with waste heat recovery)	236-309 g/kWh
Allowable BackPressure	15 mbar		
Heat Energy Available for Recovery		Sound Level	
At 120 °C Exhaust Temperature	260 kW	Standard	81 dB(A) at 1 m
At 50°C Exhaust Temperature	370 kW	Optional	66 dB(A) at 1 m
Fuel Consumption		Average Water Consumption	
Natural Gas (at LHV=10.1 kWh/m3)	84 Nm3/h	High Purity Water	150 l/h
Biogas (60% methane)	142 Nm3/h	Untreated Water	250 l/h
		Average Water Discharge	100 l/h

Table 8 FuelCellEnergy datasheet of the cell

Fuel Cell Module			Electrical Balance of plant		
Height	3,9	m	Height	2,2	m
Weight	22	t	Weight	5,7	t
Media Supply			Desulfurization		
Height	2,5	m	Height	2,8	m
Weight	4,5	t	Weight	2	t

Table 9 Dimensions and weight of the machine

The producer of the fuel cells, FuelCellEnergy, provides the data of the molten carbonate fuel cell for different fuel blending compositions. FCE has extensive experience with fuel blending, especially with renewable biogas. FCE declared that the system is fully capable of blending up to 50% Hydrogen with Natural Gas without experiencing significant (more than 10%) reduction in power output.

%CH4	%H2	Blend [Nm3/h]	CH4 [Nm3/h]	H2 [Nm3/h]	LHV [Mcal/Nm3]	%El. Eff	%El. Eff respect power output
100%	0%	85,5	85,5	0	8,557	47%	100
90%	10%	89,5	80,6	8,9	7,959	46%	95,7
80%	20%	96,9	77,5	19,4	7,336	45%	94,1
70%	30%	105,7	74	31,7	6,763	45%	92,7
60%	40%	116,2	67,7	46,5	6,165	44%	91,2
50%	50%	129,2	64,6	64,6	5,568	43%	89,7

Table 10 Input data from FCE

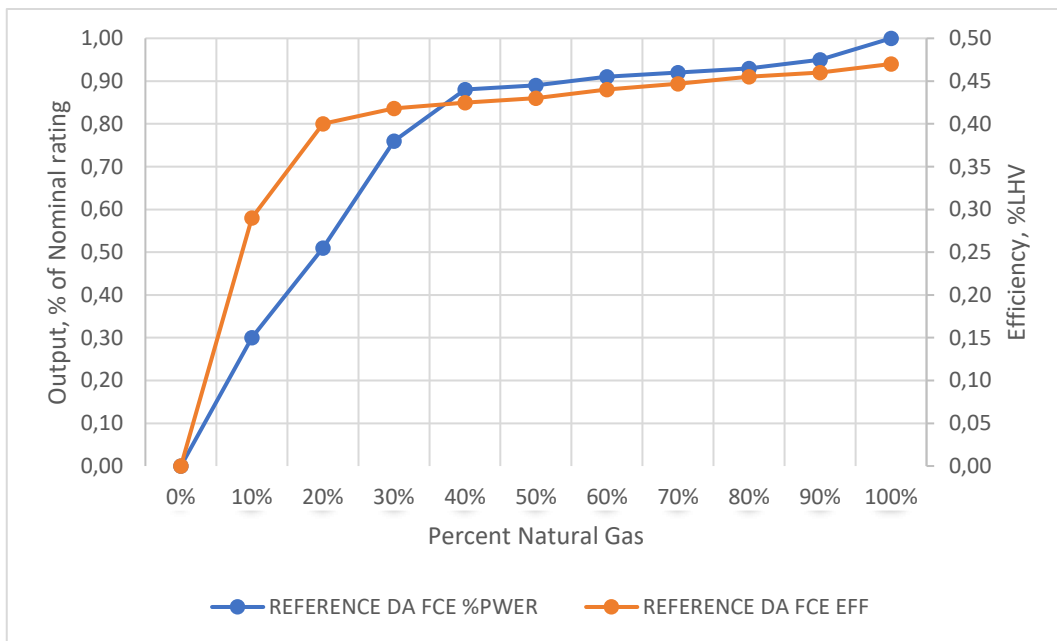


Figure 64 FCE efficiency and power output

For a low percentage of natural gas, the reduction in efficiency and power is too high. In this work has been considered reliable the data up to a blend ratio of 0.5. The volume flow rate and the mass flow rate change proportionally for different blend compositions. For higher volume flow rate there is a reduction in the mass flow rate.

Knowing the value of the volume flow rate is possible calculate:

$$\dot{n} = \frac{Q_{vol} \left[\frac{Nm^3}{h} \right] \cdot 1000 \left[\frac{Nl}{Nm^3} \right]}{22.4 \left[\frac{Nl}{mol} \right] \cdot 3600 \left[\frac{s}{h} \right]} \quad \left[\frac{mol}{s} \right] \quad (18)$$

$$\dot{m} = \dot{n} \cdot \frac{MW_{mixture}}{1000} \left[\frac{Kg}{s} \right] \quad (19)$$

Where \dot{n} is the molar flow rate, \dot{m} the mass flow rate, MW the molecular weight.

%CH4	%H2	Molar flow rate [mol/s]	Molecular Weight of the mixture [g/mol]	Mass flow rate [Kg/s]	Blend [Nm3/h]
100%	0%	1,060	17,4078494	0,018	85,5
90%	10%	1,110	15,8810624	0,018	89,5
80%	20%	1,202	14,3402485	0,017	96,9
70%	30%	1,311	12,8166875	0,017	105,7
60%	40%	1,441	11,2774129	0,016	116,2
50%	50%	1,602	9,77242802	0,016	129,2

Table 11 Molar, mass, volume flow rate FCE simulation

7.6 PV plant

SAGAT want install a photovoltaic system in some areas in the airport, with an estimated producibility of 2.554.803 kWh at the first year.



Figure 65 Space for PV installations

The total power calculated is 2207.16 kW_p with the adoption of 6131 modules 360 Wp each. The monocrystalline panel has an efficiency of 21.28%. The adoption of a null tilted angle it is due to the desire to limit the visual impact, only in the area near the railway the panels will be tilted of an angle equal to the natural slopes of the area. To support the

panels, it is planned to use an anchor system made by means of cement conglomerate ballast and connection to the panel by a universal clamp. The total power of the photovoltaic system was determined in order to not have more energy with respect the energy request, thus the study ensure that no energy will be injected into the national grid, but all the energy will be auto consumed. Due to the deterioration of the modules the annual energy will be reduced of 1% after one year and 0.4% for the successive years.

7.7 PV plant and electrolyze for the production of green hydrogen

A solution to be considered is the production of green hydrogen directly in the airport. A possibility it is to install a PV plant coupled with an electrolyzer. For this purpose, a storage will be needed when the production from the panels it is low or not sufficient. There are two possible paths: the first it is to install a electrochemical storage, but actually this type of technology it is not suitable for economical reason. The second option it is to adopt an hydrogen pressurized storage. The size of the storage and the PV plants will be in function of the percentage of the blending that it is required. Being for Turin an electricity annual producible on peak installed power for photovoltaic systems equal to 1,150 kWh/kWp, starting from the annual electrical absorption of the absorber is possible evaluate the size of the photovoltaic system that could be necessary. Below a first estimation it is provided.

7.8 Problems regarding the adoption of a fuel cell

In this section are summarized the main problematics that could be presented when fuel cells are used.

- Vulnerability. An eventual installation of these devices in place of the traditional natural gas boilers, would bind the airport in using a technology that could be fed with a fuel different from natural gas, but with no certainty about the effective penetration in future of this fuel, hydrogen, in the market.
- UPS of the airport. Uninterruptible power supply, the airport must guarantee every hour of the years a reliable supply of energy. Period without electrical energy cannot be accepted, for this reason there are auxiliaries' generators. The maintenance is planned for two months in a year, the loads in this period must be covered with others machines.

- Costs. The costs of this technology are still very high, despite this the installation of fuel cells can be economical profitable.
- Maintenance and Change of the stack. Every 7 years an extraordinary maintenance is necessary.
- Operation, high Purity water is required.

8. Plant model in Aspen Plus

In Aspen doesn't exist a component that can directly model a fuel cell. So, in this work the fuel cell is modelled using available components from the model palette. To develop the electrochemical model, a reference paper is considered [15].

In the model there are two main branches: the cathode branch and the anode branch. The anode line is composed of a blower, a heat exchanger, a mixer, a reformer, the anode electrode and a splitter. The anode of the fuel cell is modelled using an ideal R-Gibbs reactor. The reformer, where the natural gas reacts in favor of hydrogen is an R-Gibbs reactor. In the model an internal reforming strategy has been adopted.

The cathode line is composed of a blower, a mixer, two heat exchangers, the cathode electrode. The cathode electrode is modelled with a separator block. The first heat exchanger is needed to preheat the inlet air to a temperature of 560°C suitable for the working conditions of the fuel cell. The second heat exchanger is a fictitious component used to simulate the increase of temperature due to the electrochemical reaction inside the cell. The ions through the electrolyte CO_3^{2-} are modelled with two different streams, one for the O_2 and another for CO_2 . Respectively the streams are "O2-AN" and "CO2-AN".

Literature on MCFC has been investigated[16]–[19] and several approaches have been found to describe the fuel cells. Although the high numbers of papers, most of them are dedicated in studies in which the MCFC is integrated in plants for carbon capture (CC). Due to the necessity to have CO_2 as reactant at the cathode, the MCFC are generally inserted downstream the exhausts of a plant, where CO_2 is available in high concentrations. With this configuration the MCFC are used to produce electricity and simultaneously capture the CO_2 that otherwise would be emitted directly into the atmosphere. In the airport, instead, the MCFC is stand-alone since no others stream with a high concentration of CO_2 are available to feed the cell. The fuel anode will be natural

gas taken from the grid or in future scenarios a blending mixture with hydrogen. In any case, at the state of the art, the fuel cell will be fed with natural gas, at least in the first years of operation; still there are concerns regarding the possibility to have some percentage of hydrogen in the pipelines. Another possible scenario is the production of hydrogen directly in loco at the airport, but this solution has several constraints, also from an economical perspective.

The model presented can describe the behavior of the fuel cell for an input fuel of natural gas or for variable blending mixture of hydrogen or other gases. The aim of the model is to understand and simulate the fuel cell performances for different fuel inlet composition. The software used to build the model is Aspen plus. The following sections describe the steps for the construction of the model, others are devoted to the investigation of some parameters used to describe the behavior of the machine in different working conditions.

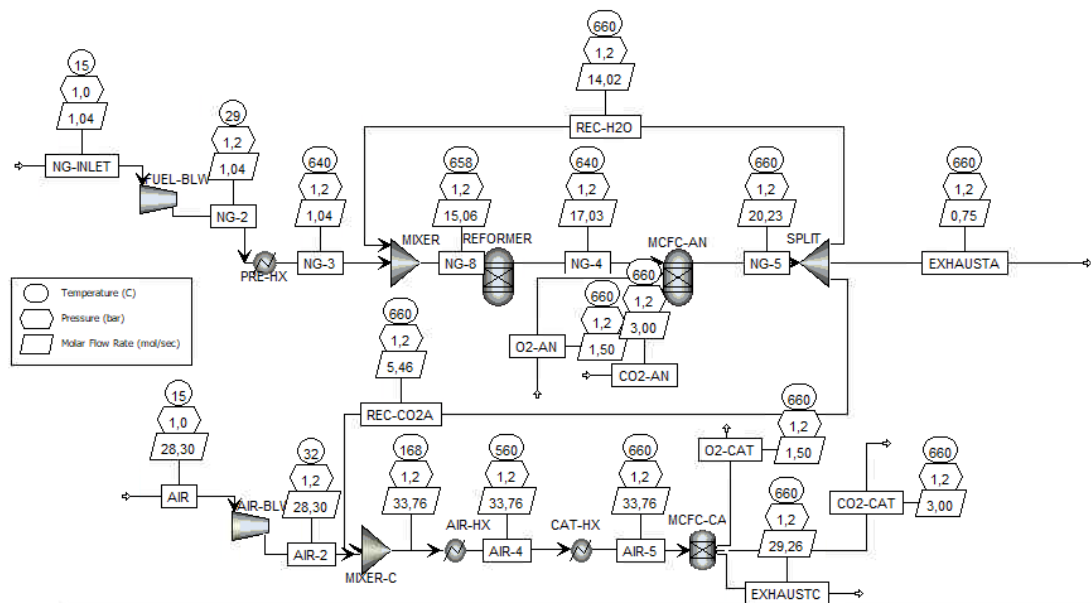


Figure 66 MCFC model Aspen

The water recirculation loop, "REC-H2O" is useful to control the steam-to-carbon ratio at the inlet of the machine. A design specification has been created in Aspen to guarantee a value of 3.5 in the stream "NG-8" before the reforming section. Since, for this application, there is not a stream rich in CO_2 , a recirculation loop from anode to cathode has been adopted to exploit the CO_2 produced inside the anode electrode. The "REC-CO2A" is a stream rich in CO_2 for recirculate to the cathode the carbon dioxide produced at the anode.

8.1 Model equations

The equations of the electrochemical model are based on thermodynamic considerations and experimental results. The open circuit voltage (OCV) is determined with the Nerst equation. The Nerst equation provides a relationship between the ideal standard potential (E_0) of the cell reactions and the ideal equilibrium potential for a given temperature and partial pressure (p_k) of reactants and products. Fuel cell irreversible losses could be estimated through local calculation of the three primary bulk losses [20]. The methodology followed in this work [20]-[15], combines a general, macro-homogeneous concept of the active reaction sites with a specific micro-geometric representation of the gas transport and current conduction in the electrode. It is known as the agglomerate model, the porous electrode is divided spatially into two regions, one consisting of agglomerates of solid particles having liquid filled micro pores, and the other consisting of macro-pores. Has been observed that the same equations appear in different papers [18]-[21].

The electrochemical model is here represented [15]:

$$E_{NERST} = \frac{\Delta G}{n \cdot F} + \frac{R \cdot T}{n \cdot F} \cdot \ln \left[\frac{p_{h_2,an} \cdot (p_{O_2,ca})^{\frac{1}{2}} \cdot p_{CO_2,ca}}{p_{H_2O,an} \cdot p_{CO_2,an}} \right] \quad (20)$$

$$\Delta G = 242000 - 45.8 \cdot T \left[\frac{J}{mol \cdot K} \right] \quad (21)$$

$$V_{op} = E_{nernst} - (R_{an} + R_{ca} + R_{ohm}) \cdot i_c [V] \quad (22)$$

$$R_{an} = 2.27 \cdot 10^{-9} \cdot \exp\left(\frac{E_{act_a}}{R \cdot T}\right) \cdot p_{h_2}^{-0.42} \cdot p_{CO_2}^{-0.17} \cdot p_{H_2O}^{-1.0} \left[\frac{\Omega}{m^2} \right] \quad (23)$$

$$R_{ca} = 7.505 \cdot 10^{-10} \cdot \exp\left(\frac{E_{act_{ca}}}{R \cdot T}\right) \cdot p_{O_2}^{-0.43} \cdot p_{CO_2}^{-0.09} \left[\frac{\Omega}{m^2} \right] \quad (24)$$

$$R_{ohm} = 0.5 \cdot 10^{-4} \cdot \exp\left[3016 \cdot \left(\frac{1}{T} - \frac{1}{923}\right)\right] \left[\frac{\Omega}{m^2} \right] \quad (25)$$

Where:

- n is the number of electrons released in the dissociation of an h_2 molecule, in this case equal to 2
- F is the Faraday's constant ($96\,487 \frac{C}{mol}$)
- p_k is the partial pressure of the specie "k-th"

- E_{act} is the anode and cathode activation energy assumed to be $E_{act_{an}} = 53500 \frac{KJ}{kmol}$; $E_{act_{ca}} = 77229 \frac{KJ}{kmol}$
- T is the cell temperature calculate as average value between the cathode conditions at inlet and outlet.
- i_c is the current density, $i_c = \frac{I}{A_c} \left[\frac{A}{m^2} \right]$, A_c is the area of a single cell.

The increases of the reagent partial pressure cause an increase of E. Since the partial pressure is calculated as the product of the total pressure time the molar fraction, an increase in composition of the reagent in the mixture increases the OCV of the cell as well. Simultaneously, an increase in the total pressure means an increase in the OCV. On the other hand, a too high total pressure can only be sustained from blowers that require a big amount of energy and so, even if the cell efficiency could increase, the one of the entire system decreases. A decrease in the product partial pressure causes an increase of OCV, so it is a good practice to remove as fast as possible the product of the reaction from the point where the reaction occurs. A too high concentration of the products increases the partial pressure and so the equilibrium of the reaction is shifted towards the reaction instead of products and the entire process slows down.

Starting from a known value of inlet flow rate, it is possible calculate the current produced by one cell. To facilitate the conversions in the different expressions of flow rate, In Aspen has been implemented a procedure that considers different fuel compositions. Properties sets have been defined “LHV15MB” and “MW-MIX” automatically calculate the lower heating value at 15°C on mass basis $\left[\frac{MJ}{Kg} \right]$ and the molecular weight $\left[\frac{g}{mol} \right]$ of the inlet mixture of the stream “NG-INLET”.

Starting from an input value of volume flow rate, generally indicated in $\left[\frac{Nm^3}{h} \right]$ is possible to obtain the molar flow rate.

$$\dot{n}_{fuel} \left[\frac{mol}{s} \right] = Q_{fuel_NG} \left[\frac{Nm^3}{h} \right] \cdot \frac{1}{3600} \left[\frac{h}{s} \right] \cdot \frac{1}{22.4} \left[\frac{mol}{NL} \right] \cdot 1000 \left[\frac{NL}{Nm^3} \right] \quad (26)$$

Once the fuel flow rate at molar basis is known, the total current CTOT can be determine considering the fuel composition.

$$CTOT = \dot{n}_{fuel} \cdot FU \cdot F \cdot \left(\sum_i^N y_i \cdot Z_i \right) [A] \quad (27)$$

$$CTOT = I \cdot n_{cell} [A] \quad (28)$$

Where Z_i is the charge number of the substance. The charge number can be calculated for a substance $C_xH_yO_z$ using the expression:

$$Z_i = 4x + y - 2z \quad (29)$$

Component	Name	x	y	z	Z
CH4	Methane	1	4	0	8
H2	Hydrogen	0	2	0	2
CO	Carbon monoxide	1	0	1	2
C2H6	Ethane	2	6	0	14
C3H8	Propane	3	8	0	20
C4H10	Butane	4	10	0	26

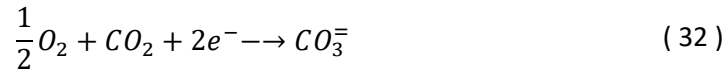
Table 12 Value of the charge number Z

The amount of stoichiometric oxygen and carbon dioxide required in the reactions are calculated with the Faraday law.

$$\dot{n}_{O_2} = \frac{CTOT}{4 \cdot F} \left[\frac{mol}{s} \right] \quad (30)$$

$$\dot{n}_{CO_2} = 2 \cdot \dot{n}_{O_2} \left[\frac{mol}{s} \right] \quad (31)$$

The amount of carbon dioxide is calculated in accordance to the stoichiometric reaction.



These values of the molar flow are assigned respectively in the streams "O2-AN" and "CO2-AN" to model the ions through the electrolyte. Another possibility is to determine the amount of oxygen and carbon dioxide by using the utilization factors.

$$\dot{n}_{O_2} = U_{O_2} \cdot \dot{n}_{O_2_CATIN} \left[\frac{mol}{s} \right] \quad (33)$$

$$\dot{n}_{CO_2} = \dot{n}_{CO_2_CATIN} \left[\frac{mol}{s} \right] \quad (34)$$

The utilization factors are defined as the ratio between the flow rate of CO_2 transferred through the cell as carbonate CO_3^- ions with respect to the amount of CO_2 flow rate introduced at the cathode inlet. The values used in the simulation has been selected in accordance with the reference paper.

A calculator block has been created in order to have equality in the streams "O2-AN" with "O2-CAT" and "CO2-AN" with "CO2-CAT":

$$\dot{n}_{O_2_{AN}} = \dot{n}_{O_2_{CAT}} \left[\frac{mol}{s} \right] \quad (35)$$

$$\dot{n}_{CO_2_{AN}} = \dot{n}_{CO_2_{CAT}} \left[\frac{mol}{s} \right] \quad (36)$$

Finally, from the electrochemical model the working operating voltage V_{op} of the cell can be calculated and so the output power produced from the cell.

$$V_{op} = V_{Nerst} - ASR \cdot i_c [V] \quad (37)$$

$$P_{FC,out} = V_{op} \cdot I \cdot n_{cell} = V_{op} \cdot CTOT [W] \quad (38)$$

The electrical efficiency of the stack has been defined to the energy of the fuel inlet.

$$\eta_{el} = \frac{P_{FCout}}{\dot{m}_{fuel} \cdot LHV_{fuel}} \quad (39)$$

8.2 Aspen Plus model assumptions and results

The working conditions of the components in the plant are summarized in the table.

	Temperature	Pressure Drop	Isentropic efficiency	Mechanical Efficiency	Reference
FuelBlower			0,9	0,8	
AirBlower			0,9	0,8	
Pre-Heat Exchanger fuel	640 °C	0			Hypothesis [22]
Air Heat Exchanger	560 °C	0			Hypothesis [22]
Cathode Heat Exchanger	660 °C ($\Delta T_{cathode} = 100^\circ C$)	0			Hypothesis [22]
Reformer	640 °C	0			[23]
MCFC Anode electrode	660 °C ($\Delta T_{anode} = 20^\circ C$)	0			[15]

Table 13 Working condition of the components in the Aspen Plus Model

The fuel flow-rate used in the model, in accordance to the datasheet, is $84 \left[\frac{Nm^3}{h} \right]$. The $\Delta T_{cathode}$ of 100°C has been selected through a literature review and relying on a

sensitivity analysis of the air inlet flow rate and blower consumptions in function of the increase of temperature in the cathode electrode ($\Delta T_{cathode}$).

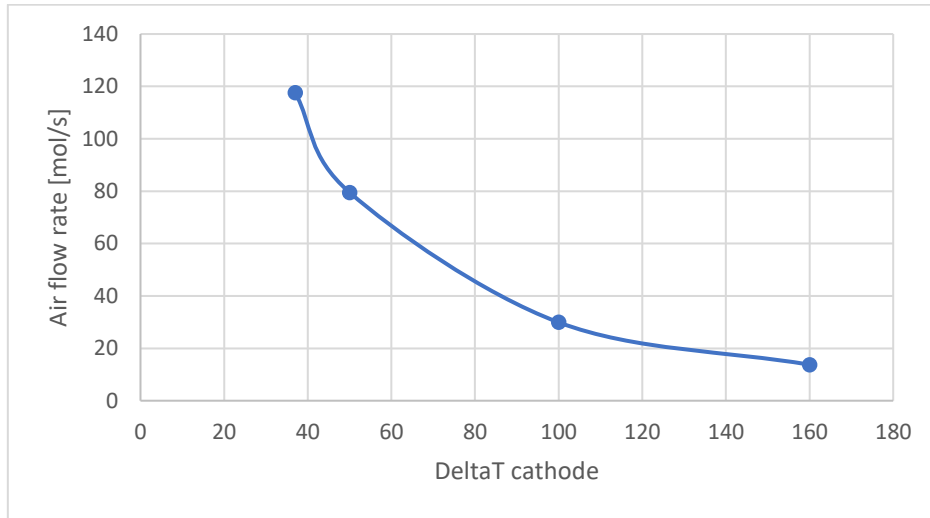


Figure 67 Air flow rate in function of the $\Delta T_{cathode}$

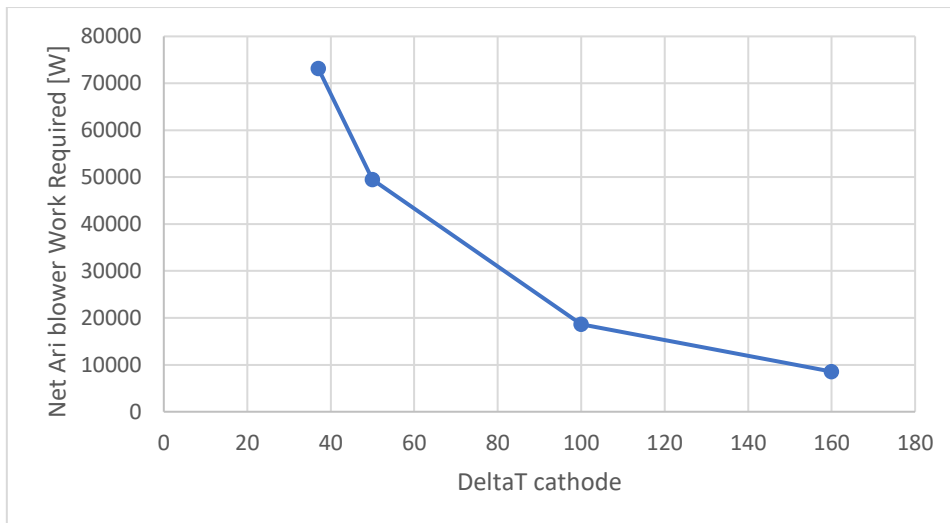


Figure 68 Net Air Blower work in function of $\Delta T_{cathode}$

The selected $\Delta T_{cathode}$ of 100°C is a trade-off between the required inlet flow rate and the electrical work of the blower. The air in the stack acts as cooling fluid so if the $\Delta T_{cathode}$ increase the mass flow of air decrease.

Fuel utilization factor	75%
CO2 utilization factor, U_{CO_2}	70%
O2 utilization factor, U_{O_2}	11%
Steam to carbon ratio, S/C	3,5
Cell current density, i_c	1500 $\left[\frac{A}{m^2}\right]$
DC-AC efficiency	95%

Table 14 Assumption for MCFC simulation [10]

The results of the simulation are presented in the table.

Variable	Value read	Units
W_{el}	399776	[W]
C_{TOT}	578307	[A]
$\eta_{electrical}$	46%	[-]
\dot{m}_{fuel}	0,018	[mol/s]
LHV_{mix}	47,451	[MJ/Kg]
V_{op}	0,691	[V]
\dot{n}_{fuel}	1,042	[mol/s]
MW_{mix}	17,408	[g/mol]
ρ_{mix}	0,729	[Kg/m3]
$W_{el Air blower}$	17411	[W]
$W_{el Fuel blower}$	643	[W]
η_{th}	32%	[-]

Table 15 Results from Aspen

The electrical efficiency of the stack founded of 46.46% is closer to the declared value in the datasheet of 47%.

8.3 Validation of the model

The aim of the validation is to compare the results of the reference paper [15] to the one obtained from Aspen using the same equations of the electrochemical model presented. The plant in the paper is an integration of a MCFC with a Gas-turbine. The exhaust from the gas-turbine still contains CO_2 , this stream is directed to the MCFC cathode. A substantial fraction of this CO_2 is then moved from cathode to anode through the electrolyte, along with the oxygen required to oxidize the fuel. This solution offers the possibility to capture carbon dioxide at a low energy cost. The study contains the equations and the information to describe the electrochemical model. The equations consider the anode and cathode stream composition.

The reference paper provides the polarization curve and compositions, temperature, pressure, mass flow rate, molar flow rate of all the streams in the plant.

For the validation a specific model in Aspen has been created. The recirculation loop for the CO_2 has not been considered, neither the recirculation loop at the anode of water. In the equations of the electrochemical model, the partial pressures are function of the inlet composition. This ensures different results in the voltage and in power for different stream compositions.

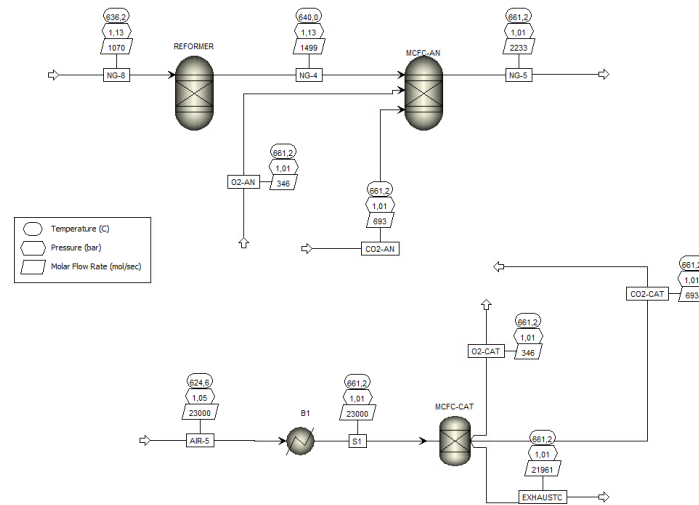


Figure 69 MCFC model for the validation

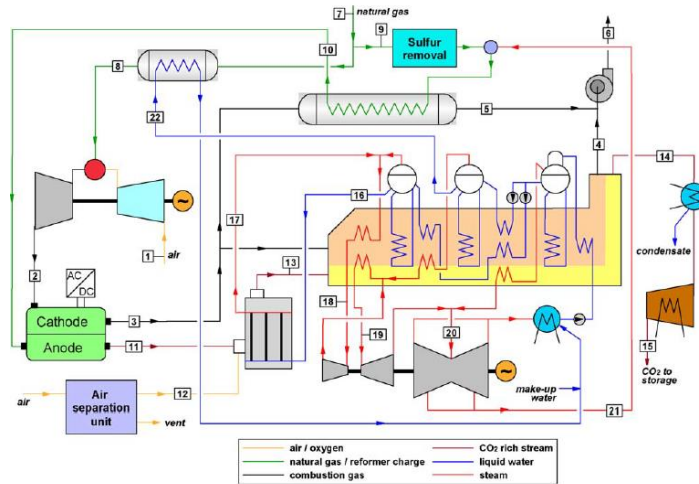


Figure 70 Integration of a MCFC in a plant with GT [15]

Steam is added in order to have a steam to carbon ratio of 3.8 in the stream n.10 in the plant. This value of SC is suitable for the conversion of natural gas by internal reforming at the operating temperature of the cell directly inside the anode of the fuel cell module. The paper indicates that the reforming process occurs in the fuel cell module. The natural

gas is preheated to about 635°C by exploiting the heat from a fraction of the exhaust gases from the cathode side of the MCFC. The internal reforming of hydrocarbons inside the anode sets the composition of the exhaust stream from the electrode, it is supposed that all the reactions will be completed and reach the thermodynamic equilibrium at the cell operating temperature of about 650°C. For these reasons in the model there is no a recirculation loop “REC-H2O” of water in order to obtain the desired steam-to-carbon ratio at anode inlet, the compositions are known and fixed from the reference paper.

steam number	T (°C)	P (bar)	\dot{m} (Kg/s)	\dot{n} (Kmol/s)	Molar concentration (%)								
					Ar	CH_4	CO	CO ₂	C ₂₊	H ₂	H ₂ O	N ₂	O ₂
Cathode “2”	624,6	1,05	653,3	23	0,9			4,1			8,6	74,3	12,2
Anode “10”	636,2	1,13	19,3	1,07		18,6		0,4	1,7		79,1	0,2	

Table 16 Streams inlet composition

Implementing the electrochemical equations in the model, it is observed that the two curves have the same slope, that confirmed the correctness of the expressions, but shifted: the reference curve has a lower value of OCV.

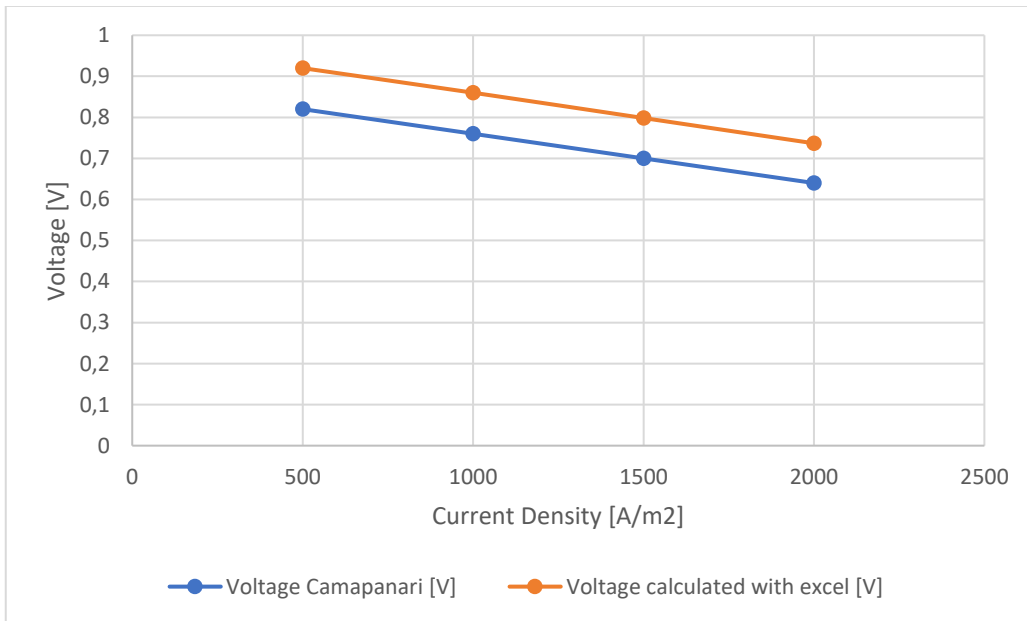


Figure 71 Comparison of the curves

To fit the data, some changes in the pre-exponential terms have been modified. In the expression of R_{ohm} the 0.5 has been substituted with 1.13. This change brings the following results with a maximum error in the voltage at 500 $\left[\frac{A}{m^2}\right]$ of 8%. This

approximation it is acceptable because the fuel cells, during normal operation work always with the same amount of natural gas inlet, and so the working point doesn't change from the nominal. The nominal working point is fixed from the reference paper at $1500 \left[\frac{A}{m^2} \right]$, at that level of current, the voltages of the two curves are really close and the error in that area approaches zero.

The new formulae used to calculate the ohmic resistance

$$R_{ohm} = 1.13 \cdot 10^{-4} \cdot \exp \left[3016 \cdot \left(\frac{1}{T} - \frac{1}{923} \right) \right] \left[\frac{\Omega}{m^2} \right] \quad (40)$$

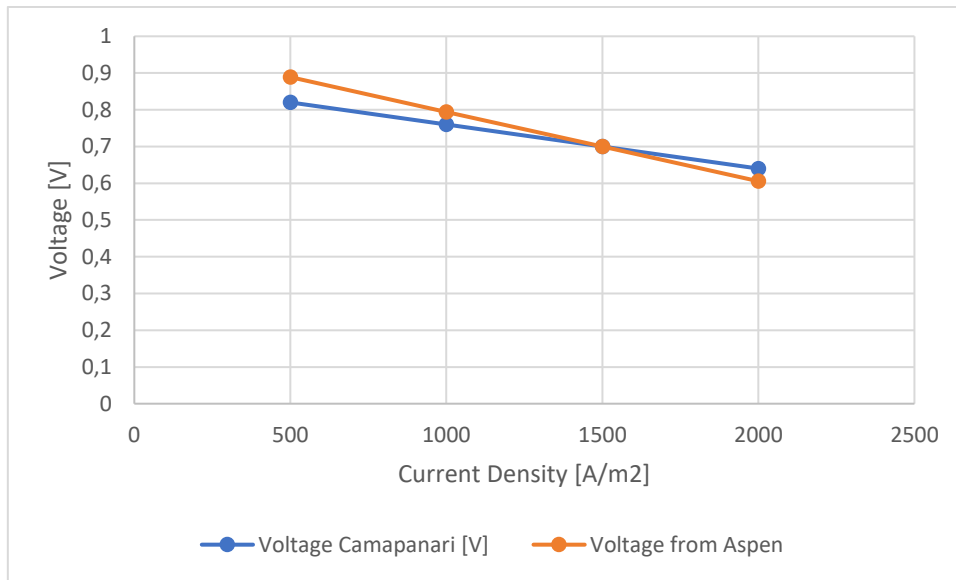


Figure 72 Comparison of the two curves

Fuel utilization factor	75%
CO₂ utilization factor, U_{CO_2}	75%
O₂ utilization factor, U_{O_2}	11%
Steam to carbon ratio, S/C	3,5
Cell current density, i_c	$1500A/m^2$
Cell voltage at nominal conditions, V_{op}	0.699 V
Anode inlet temperature	636 °C
DC-AC efficiency	94%
ΔT_{anode}	25°C
$\Delta T_{cathode}$	37°C

Table 17 Reference Input value from the reference paper

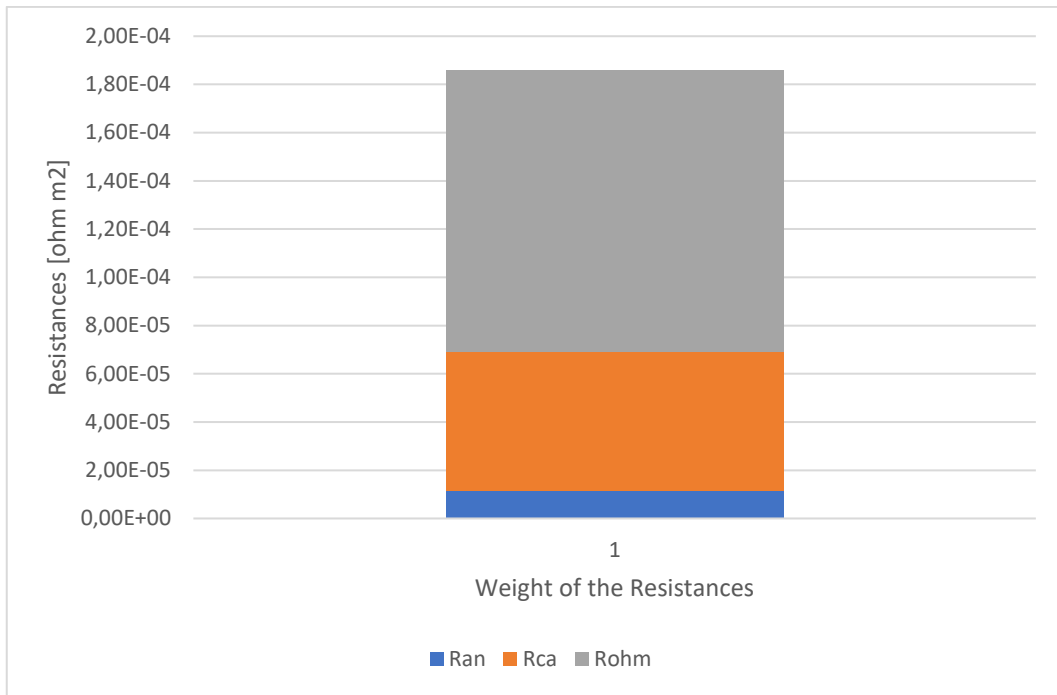


Figure 73 Distribution of the resistances

8.4 Molten Carbonate Fuel Cell Model Balance of Plant

Further components have been added to the base model to exploit the high energy content in the exhaust streams from the cell. An adiabatic after-burner with null pressure drops has been inserted downstream the fuel cell. A heat-recovery-unit, HRU, has been modelled with a double flow heat exchanger to cool down the high temperature gases to increase the water temperature to 120°C. The design temperature of 120°C is a typical value in the district heating networks.

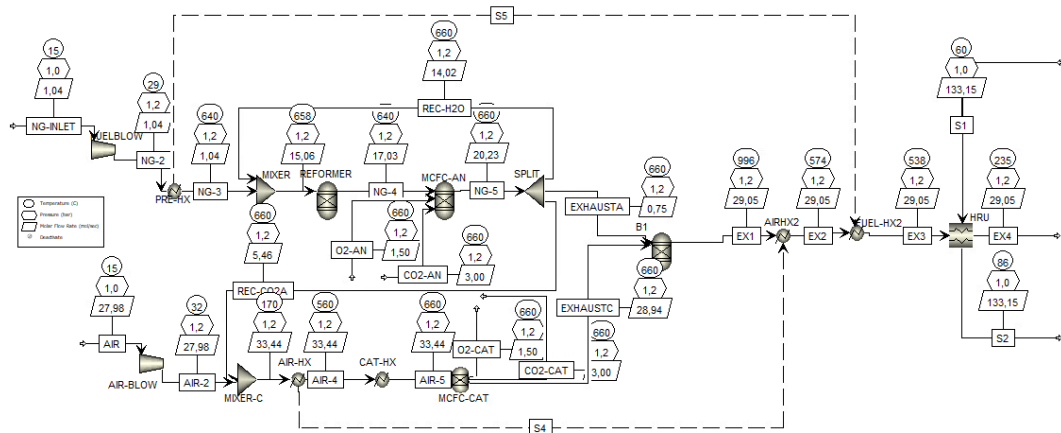


Figure 74 MCFC Balance of Plant model

The volume flow rate of the water is determined in function of the diameter of the pipes.

$$Q = \pi \cdot \frac{d^2}{4} \cdot v$$

Where Q is the volume flow rate in $\left[\frac{m^3}{s}\right]$, d the internal diameter of the pipes in $[m^3]$ and v is the design velocity in the pipe, generally for district heating application is equal to $2 \left[\frac{m}{s}\right]$.

Pipe diameter [mm]	Design Velocity [m/s]	Volume flow rate in [m3/s]	Volume flow rate in [m3/h]
30	2	0.00141	5.089
40	2	0.00251	9.048
50	2	0.00392	14.137

Table 18 Volume flow rate in function of pipe diameters

The heat produced from the cell is

$$Q_{MCFC} = -\Delta H - W_{el} [W] \quad (41)$$

Where $\Delta H [W]$ is the net duty produced and $W_{el} [W]$ is the electrical power produced from the cell. Considering the heat required by the endothermic reforming reactions it is possible calculate the heat produced from the cell

$$Q_{waste} = Q_{MCFC} - Q_{ref} [W] \quad (42)$$

The available heat from the plant is calculated in the heat recovery unit section. The temperature at the outlet of the afterburner is 996°C. The stream after the burner has the uncombusted components.

	Mole Flows		Mole fractions
CH4	3,98E-34	mol/sec	1,37E-35
CO2	1,09896	mol/sec	0,0378
H2	2,65E-07	mol/sec	9,12E-09
CO	2,24E-07	mol/sec	7,70E-09
H2O	2,10623	mol/sec	0,0725
N2	22,1093	mol/sec	0,761
O2	3,73054	mol/sec	0,128
C2H6	0	mol/sec	0
C3H8	0	mol/sec	0
NO	0,00786	mol/sec	0,00027
NO2	7,97E-05	mol/sec	2,74E-06
ISOBU-01	0	mol/sec	0
Total mole flow	29,053	mol/sec	

Table 19 Mol flow and mole fractions after the burner

Two heat-exchangers have been added to heat up the air and the fuel, respectively AIRHX2 and FUELHX2.

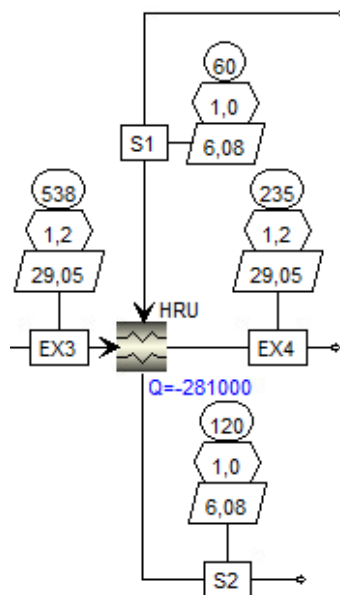


Figure 75 Hear Recovery Unit

The thermal heat available from the cell is 281 kWh_{th} , that amount of heat is imposed in the HRU thus the outlet temperature of the hot stream exhaust is 235°C. The target water

is heated up from 60°C to 120°C. The flow rate has been calculated $6.08 \left[\frac{mol}{s} \right]$, in terms of volume flow rate is $0.39 \left[\frac{Nm^3}{h} \right]$.

The water temperatures in the economizer of the pumping station are 70/90°C. To have a ΔT_{water} of 20°C, a calculated flow rate of $11 \left[\frac{m^3}{h} \right]$ has been determined at the inlet of the HRU. The maximum heat available from the exhaust supposing to cool down the gases at a lower temperature is $580 kW_{th}$.

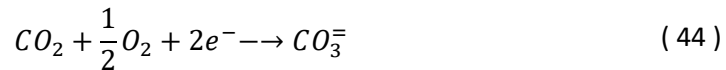
8.5 Design Specifications

Design specifications in Aspen have been created. Before the reformer, a steam-to-carbon ratio equal to 3.5 is imposed. This is an important design parameter, the value is in accordance with the reference paper [15]. A suitable SC ratio is important to avoid carbon depositions inside the cell that can damage or even block the machine. In Aspen, the SC has been calculated in the stream “NG-8”:

$$SC = \frac{\dot{n}_{H_2O}}{\dot{n}_{CH_4}} \quad (43)$$

Accordingly, the stream “REC-H2O” is changed until there is sufficient water to have a value of SC equal to 3.5 in the stream “NG-8”.

Another design specification has been created to determine the amount of CO_2 to be recirculated. The mole flow of carbon dioxide in the stream “RECCO2-AN” has been set equal to the stoichiometric amount of carbon dioxide required for the reduction reaction at the cathode.



In practice the amount of CO_2 in “RECCO2-AN” is equal to the “NCO2-AN” stream.

The value of air flow rate needed at the cathode of the MCFC has been determined defining a design specification. The waste heat produced from the fuel cell has been calculated.

$$Q_{waste} = Q_{MCFC} - Q_{ref} \quad (45)$$

Where Q_{MCFC} is the heat produced from the exothermic reactions of the cells, and Q_{ref} is the amount of heat required at the endothermic reaction of the reformer. This heat has

to be removed to avoid high temperature inside the module. Considering the amount of heat in the fictitious heat exchanger “CAT-HX” to simulate the increment in temperature, the air flow inlet is changed until obtaining

$$Q_{waste} = Q_{HX_air} \quad (46)$$

8.6 Fuel Inlet Composition

The fuel that supplies the MFCs, at least for the first years of operation, will be natural gas. In this model, the reference composition is set equal to the one declared from FuelCellEnergy, one of the biggest producers of fuel cells.

Component	Value
CH4	0.938
CO2	0.011
H2	0
CO	
H2O	
N2	0.011
O2	
C2H6	0.019
C3H8	0.016
C4H10	0.005
NO	
NO2	

Table 20 Reference Natural Gas composition in the models

8.7 Determination of numbers of cells

To determine the number of cells in one stack, according to the datasheet some assumptions have been made. The current density has been assumed $1500 \frac{A}{m^2}$, as the nominal current indicated in the reference paper. Through a literature review [17], [23], [24] the area of a single cell is set at 150 cm^2 .

The total current that passes in the series inside the stack

$$I = i_c \cdot A_c = 1500 \cdot 0.0150 \text{ [A]} \quad (47)$$

From the known value of CTOT at the nominal working condition

$$n_c = \frac{CTOT}{I} = 27539 \text{ cells} \quad (48)$$

The total active area in function of the current density is here reported.

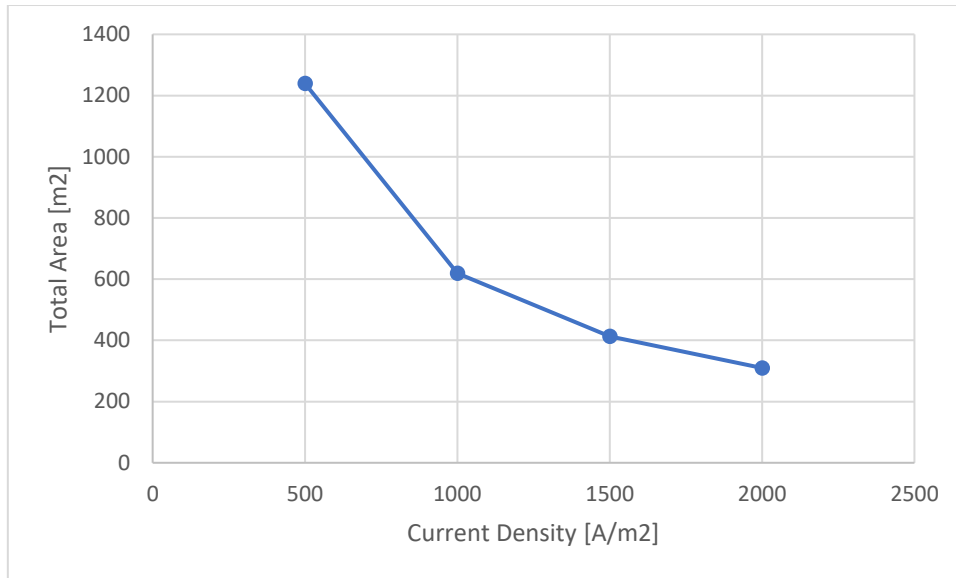


Figure 76 Total area in function of the current Density

8.8 Pressure drops in the components

A literature review has been done to consider the value of pressure drops inside the components.

Pressure Drop in the components			Reference
Pre-Hx	50	mbar	[22], [25]
MCFC anode	36	mbar	[15], [25]
MCFC cathode	24	mbar	[15], [25]
Reformer	50	mbar	[26], [22]
Air HX	100	mbar	[22]
After-Burner	20	Mbar	[25]

Table 21 Pressure Drop in the components

The effects of pressure drop, can be taken into account introducing a valve in the initial part of the branches. The total pressure drops in the anode line are 136 mbar whereas 124 mbar are in the cathode line.

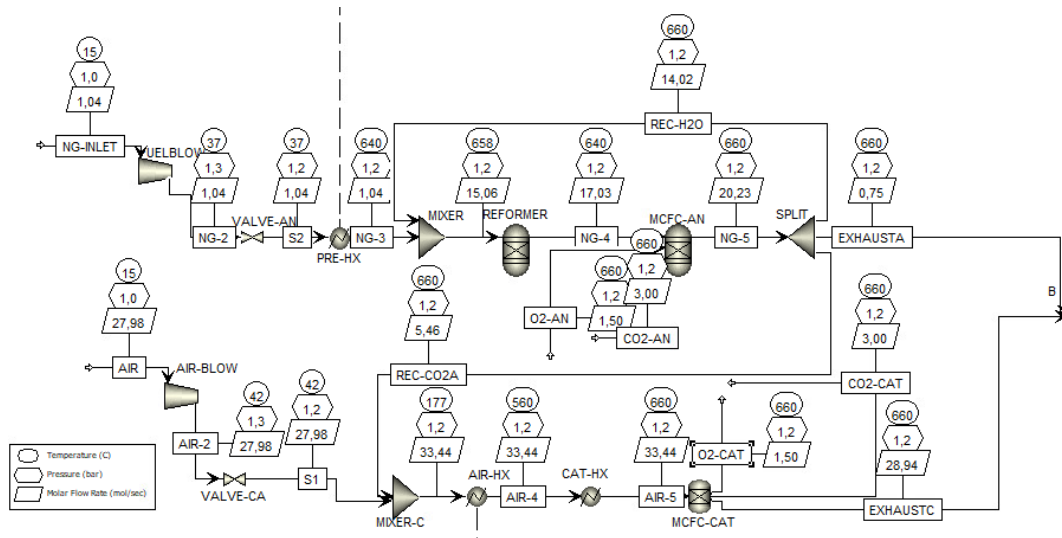


Figure 77 Aspen Model with pressure drops

To counteract the pressure drops, the blowers increase their consumptions and the overall efficiency of the plant decrease.

The system efficiency has been calculated as:

$$\eta_{sys} = \frac{W_{el} * \eta_{DC-AC} - W_{el_{fuel\blower}} - W_{el_{air\blower}}}{LHV_{fuel-in} \cdot \dot{m}_{fuel-in}} \quad (49)$$

Where η_{DC-AC} is the conversion efficiency from direct to alternating current, equal to 0.95. The blowers in the model have been defined with an isentropic efficiency η_{is} equal to 0.9 and a mechanical efficiency η_{mech} equal to 0.8.

	No presure drops	Pressure Drops	
Net work Fuel Blower	0,643	1,035	[kW]
Net work Air Blower	17,41	27,19	[kW]
Eff Syst	42,04%	40.86%	[%]

Table 22 Net-work fuel and air blowers

A sensitivity analysis on pressure drops of the two lines is presented.

	case 1	case 2	case 3	case 4	case 5
Pressure drops cathode [mbar]	124	224	324	424	524
Pressure drops anode [mbar]	136	236	336	436	536
Net work Fuel Blower [kW]	1,03	1,30	1,56	1,80	2,03
Net work Air Blower [kW]	27,19	34,60	41,65	48,38	54,82
Eff Syst	40,86%	39,97%	39,12%	38,31%	37,53%

Table 23 Sensitivity Analysis on pressure drops

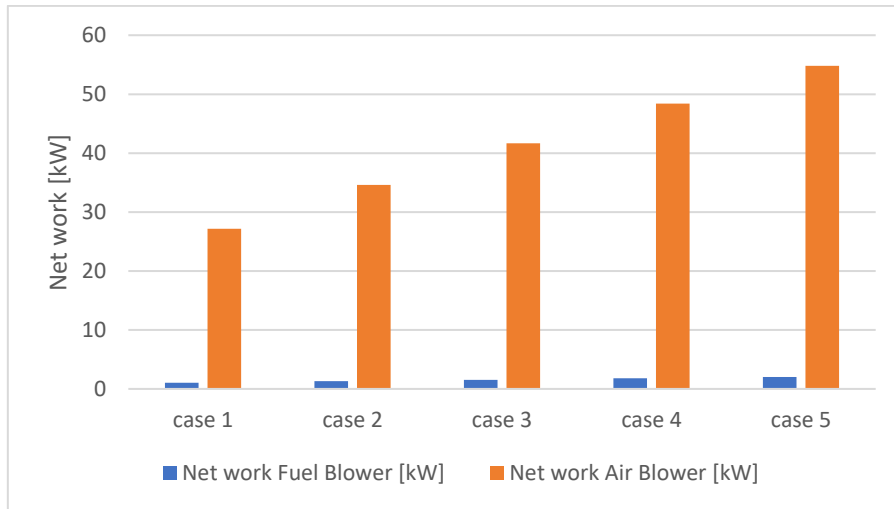


Figure 78 Blower's consumptions

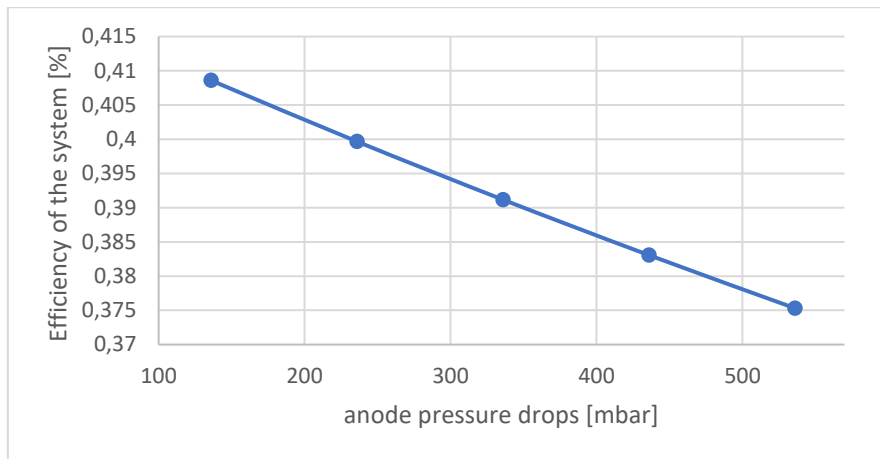


Figure 79 Efficiency of the system in function of the anode pressure drops (the corresponding cathode pressure drops can be determined from the table)

The valve is a concentrated parameter that considers all the pressure drops inside the line. Another possibility is to insert for each component the pressure drops associated, providing a better estimation of the values of pressure inside the cell.

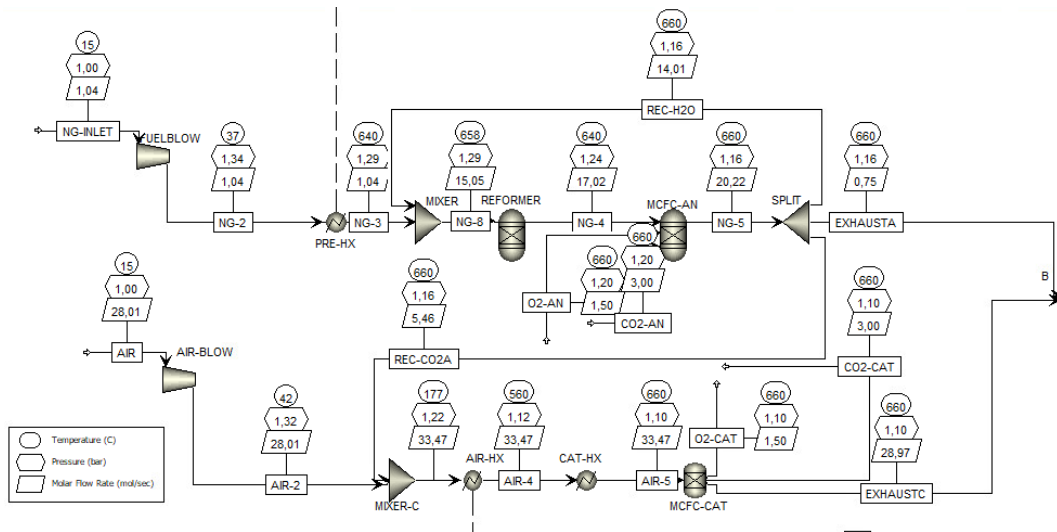


Figure 80 Details on pressure drops

8.1 Parametric and Sensitivity analysis

The analysis has been carried out by using the model complete model in Aspen.

8.1.1 Variation of current density

The MCFC are not dynamic machines, and the amount working point doesn't change considerably from the nominal. The performances of the fuel cells depend on the level of current density, in this model a current density of $1500 \frac{A}{m^2}$ has been selected.

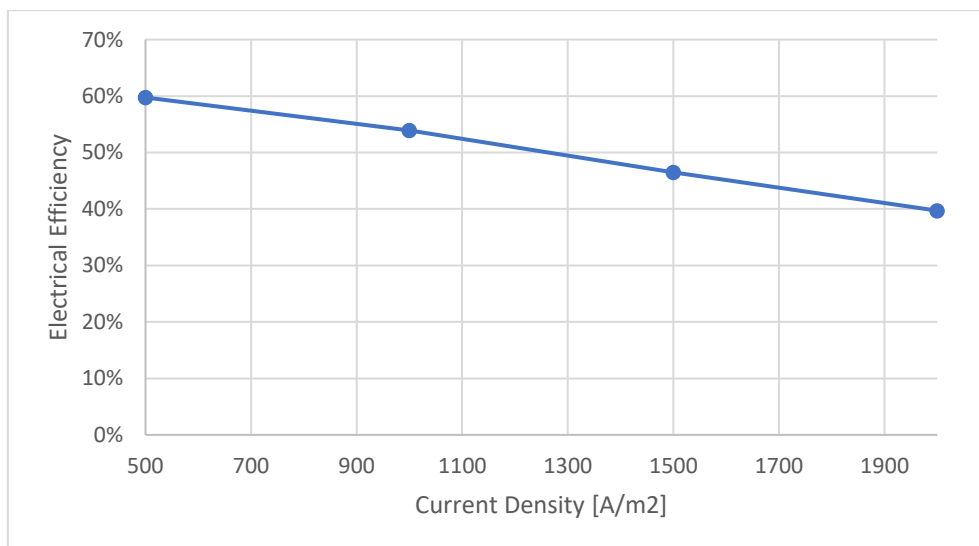


Figure 81 Electrical Efficiency with respect current density [A/m²]

For higher current, the polarization losses increase and consequently the electrical efficiency decrease.

8.1.2 Variation of steam-to-carbon (S/C) ratio

An important design parameter is the steam to carbon ratio. A sufficient amount of steam is recirculated at the anode to avoid carbon depositions inside the cell. There is a slightly decrease in electrical efficiency increasing the steam to carbon ratio, an excessive amount of water affects the reactions inside the cell.

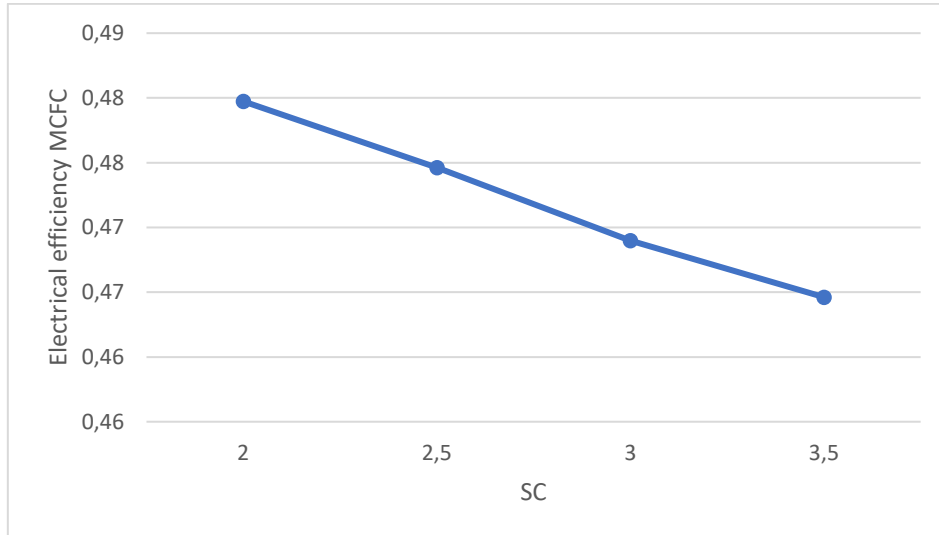


Figure 82 Electrical Efficiency with respect Steam to Carbon Ratio

8.1.3 Variation of temperature of the stack

The cell potential, and consequently the efficiency increases with temperature. The figure shows a strong influence of the operating temperature on the cell potential especially at temperature lower than 625°C. The cell potential increase rapidly with temperature. The thermodynamics calculations showed that the operating cell potential and the efficiency improve as temperature increases, above a certain level the cell potentials reach almost a steady asymptotic value after which it does not change considerably. The kinetics of the reactions inside the cell are governed by temperature.

Generally the carbonate doesn't melt below 520°C. The majority of the MCFC operates at a temperature of 650°C. Lower temperature presents lower performances, instead for value of temperature higher than 650°C the corrosive effects start to become dominant. The common working temperature range for a MCFC are 600-700°C.

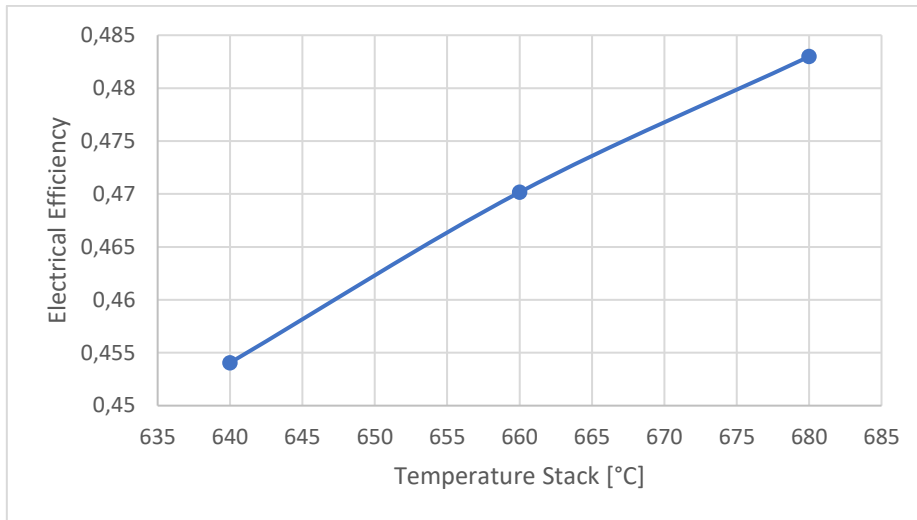


Figure 83 Electrical Efficiency with respect stack temperature

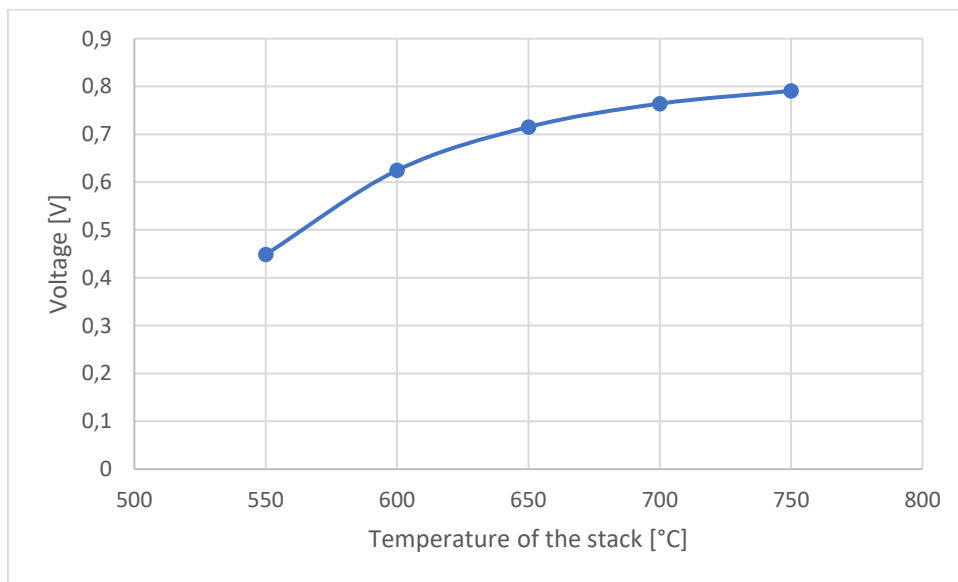


Figure 84 Voltage in function of the cell temperature

8.1.4 Variation of pressure

Considerably effects have the pressure on the performances of the cell. As seen from the figure the cell potentials steadily increase with increase in the operating pressure for both electrolytes. Increase in pressure results in higher operating voltages due to the increased partial pressure of gases and improved gas solubility and mass transport characteristics of the cell. The observed results are in accordance with the Nerst equation. The analysis has been done at the operating cell temperature of about 642°C, founded as the mean value between outlet and inlet temperature streams of the cell.

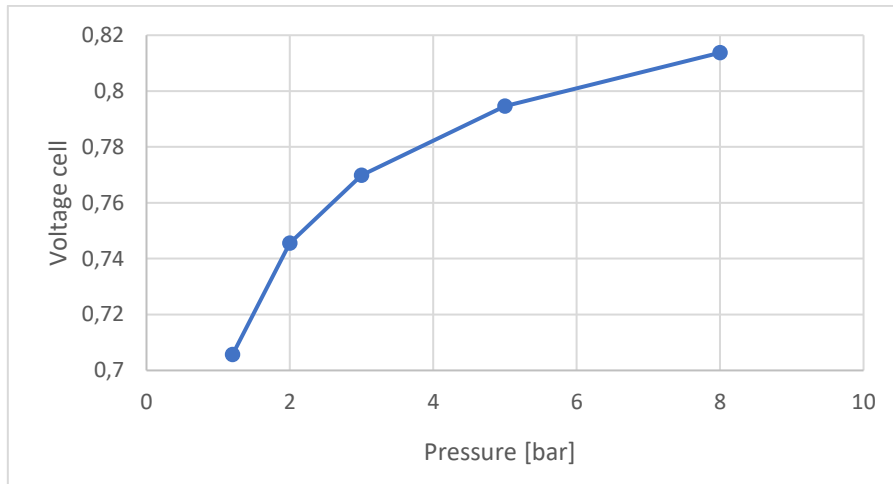


Figure 85 Voltage in function of the pressure

8.1.5 Variation of the fuel utilization factor U_F

The fuel utilization is defined as the amount of fuel that is used to activate the reactions inside the cell. The electrical efficiency accordingly increases with fuel utilization because a larger part of fuel is exploited in the cell, the total current increase.

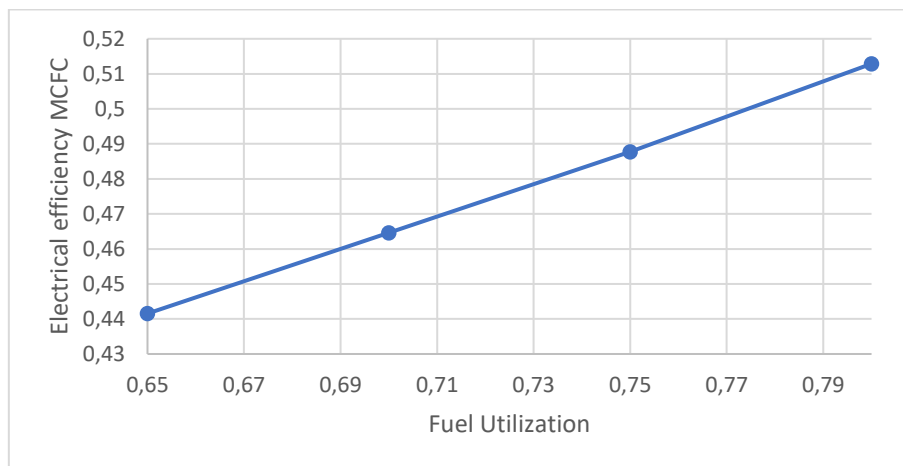


Figure 86 Electrical efficiency in function of Fuel Utilization

9. Partially direct and indirect reforming

A possible system design is partially direct and indirect reforming. Keeping the same working conditions of Table 13 the following configuration is presented.

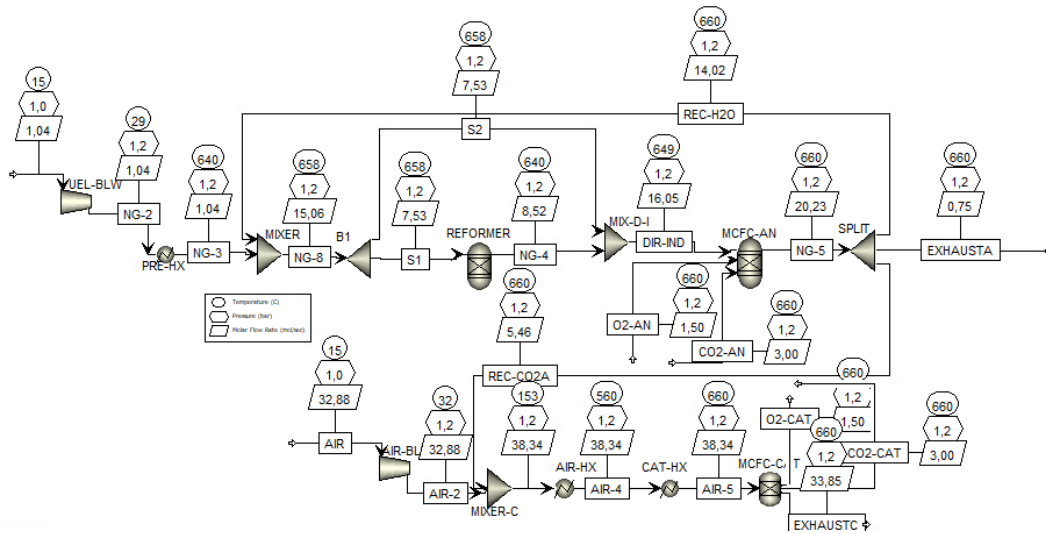


Figure 87 Direct - Indirect MCFC

The reforming processes at the anode enable the heat generation of the polarization losses to directly serve the endothermic steam reformation reactions. Thus, the cell stack cooling requirements and the blower power will be reduced. The net system power and efficiency increase with the grade of internal reforming due to reductions in parasitic power. Capital cost is reduced due to reduction in blower and air preheater capacities and for the elimination of external reforming hardware.

The important variation is in the heat required from the reformer

$$Q_{waste} = Q_{MCFC} - Q_{ref} \quad (50)$$

Being the amount of air determined on the basis of the waste heat

$$Q_{waste} = Q_{HX_air} \quad (51)$$

If the grade of internal indirect reforming decrease there will be a reduction in the heat needed to complete the reforming reactions, Q_{ref} , and the heat produced from the cell Q_{MCFC} . The reduction in Q_{ref} is much stronger than the reduction of Q_{MCFC} , so overall the Q_{waste} increase with decreasing of internal reforming. In accordance to Q_{waste} the air flow rate and the blowers consumption for the air have the same behavior. The power and the stack efficiency increase with the increase of internal reforming [25].

	W_{el} [kW]	η_{el} [%]	W_{airblw} [kW]	$W_{fuelblw}$ [kW]	η_{sys} [%]	\dot{n}_{air} [mol/s]	ΔH [kW]	Q_{ref} [kW]	Q_{waste} [kW]	Q_{MCFC} [kW]
25%IR	374.1	43.5%	22.3	0.643	38.6%	35,88	-573.5	58.4	141	199.4
50%IR	383.9	44.6%	20.5	0.643	39.9%	32,88	-631.9	116.7	131.3	248
100%IR	398.7	46.3%	17.6	0.643	41.9%	28,30	-748.6	233.4	117.6	349.8

Table 24 Performance comparison for different reforming options

When there is an internal reforming of hydrocarbon fuels such methane, there is reduction of the need of external coolant since the water produced in the anode, can be used to directly activate the steam reforming. The SMR is an endothermic reaction, so it acts as a sink for the heat generated by the oxidation reaction.

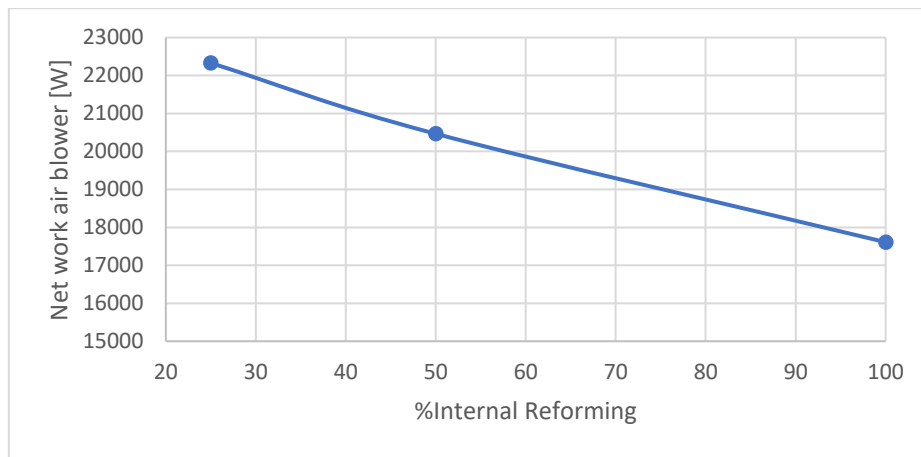


Figure 88 Net-work air blower in function of the grade Internal Reforming

The power and consequently the stack efficiency, calculated respects the same fuel, increase with the grade of internal reforming. This is due to the changes in the molar compositions in the stream “DIR-IND” before entering the anode. The compositions directly affect the value of the Nerst equation. With a higher grade of internal reforming, the amount of hydrogen increases in the stream anode increasing the voltage.

	Vop [V]	H2 mole fraction
25%IR	0,65	0,11988
50%IR	0,66	0,14859
100%IR	0,69	0,20

Table 25 Working voltage and h2 fraction in function of grade IR

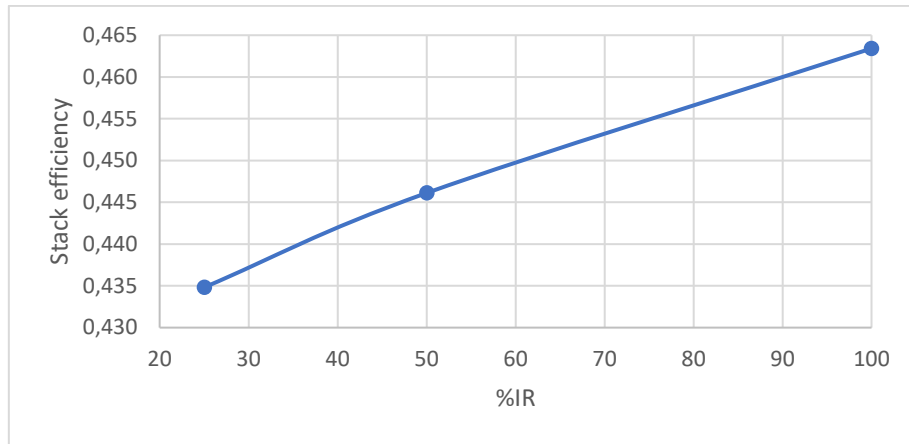


Figure 89 Electrical stack efficiency in function of the grade Internal Reforming

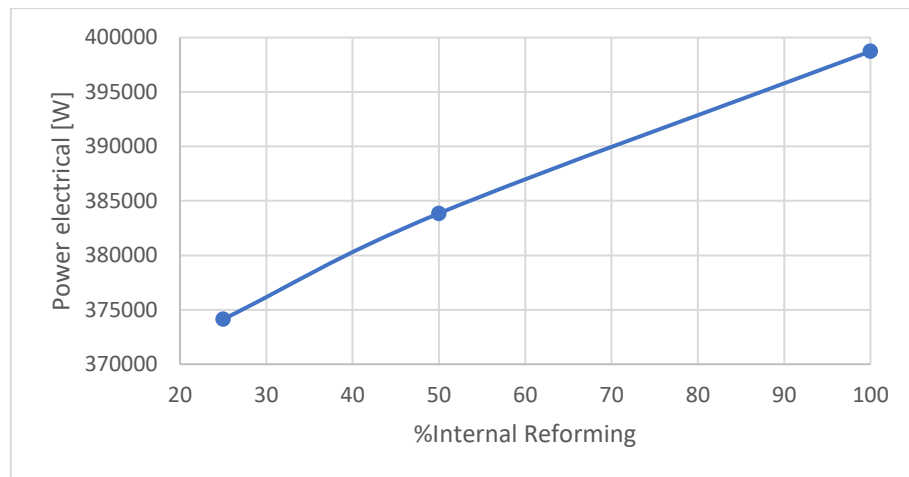


Figure 90 Electrical power in function of the grade Internal Reforming

10. Fuel cell hydrogen fuel capabilities

In this section the performances of the fuel cell have been analyzed for different blend ratio.

Component	Composition of fuel 1	Composition of fuel 2 (typically natural gas)
Hydrogen	100	0
Carbon Monoxide	0	0
Methane	0	93,8
Ethane	0	1,9
Propane	0	1,6
i-Butane	0	0,5
n-Butane	0	0
i-Pentane	0	0

n-Pantane	0	0
Hexane and above	0	0
Ethylene	0	0
Propylene	0	0
Butylene	0	0
Nitrogen	0	1,1
Carbon Dioxide	0	1,1
Water	0	0

Table 26 Compositions of hydrogen and natural gas declared by FCE

The fuel cell can be fed with different value of hydrogen blending, generally up to 50% in volume, while maintaining high performances of the machine. For each fuel composition, has been calculated the electrical efficiency with respect the fuel inlet and the percentage of electrical power producible with respect the nominal. From the datasheet the nominal power of the cell is 400 kW.

In accordance to the equations presented the total current change proportionally to the chemical composition.

$$CTOT = \dot{n}_{fuel} \cdot FU \cdot F \cdot \left(\sum_i^N y_i \cdot Z_i \right) \quad (52)$$

The electrical power can be determined:

$$W_{el} = CTOT \cdot V_{op} \quad (53)$$

The operating voltage of the cell change proportionally with fuel compositions and slightly increase for high hydrogen concentration. The percentage of electrical power producible with respect the power rating and the efficiency of the stack:

$$\%PWERRating = \frac{W_{el}}{400000} \quad (54)$$

$$\eta_{el} = \frac{W_{el}}{\dot{m}_{fuel} \cdot LHV_{mix}} \quad (55)$$

10.1 Fuel cell hydrogen capabilities at constant volume flow rate

The results of the section have been carried out keeping constant the volume flow rate inlet at the rated value in the datasheet of 84 $\left[\frac{Nm^3}{h}\right]$.

%NG	100%	90%	80%	70%	60%	50%	40%	30%	20%	10%	0%
CH_4	93,8	84,4	75,0	65,7	56,3	46,9	37,5	28,1	18,8	9,4	0
CO_2	1,1	0,99	0,88	0,77	0,66	0,55	0,44	0,33	0,22	0,11	0
H_2	0	10	20	30	40	50	60	70	80	90	100
CO	0	0	0	0	0	0	0	0	0	0	0
H_2O	0	0	0	0	0	0	0	0	0	0	0
N_2	1,10	0,99	0,88	0,77	0,66	0,55	0,44	0,33	0,22	0,11	0
O_2	0	0	0	0	0	0	0	0	0	0	0
C_2H_6	1,90	1,71	1,52	1,33	1,14	0,95	0,76	0,57	0,38	0,19	0
C_3H_8	1,60	1,44	1,28	1,12	0,96	0,80	0,64	0,48	0,32	0,16	0
C_4H_{10}	0,50	0,45	0,40	0,35	0,30	0,25	0,20	0,15	0,10	0,05	0
NO	0	0	0	0	0	0	0	0	0	0	0
NO_2	0	0	0	0	0	0	0	0	0	0	0

Table 27 Blend composition in accordance with the amount of hydrogen, in volume basis.

CH4%	H2%	\dot{m}_{fuel} [Kg/s]	\dot{n}_{fuel} [mol/s]	$MW_{mixture}$ [g/mol]
100%	0%	0,018	1,042	17,408
90%	10%	0,017	1,042	15,881
80%	20%	0,015	1,042	14,340
70%	30%	0,013	1,042	12,817
60%	40%	0,012	1,042	11,277
50%	50%	0,010	1,042	9,772

Table 28 Molar and mass flow rate, molecular weight for different compositions of fuels, at fixed volume flow rate 84 Nm³/h

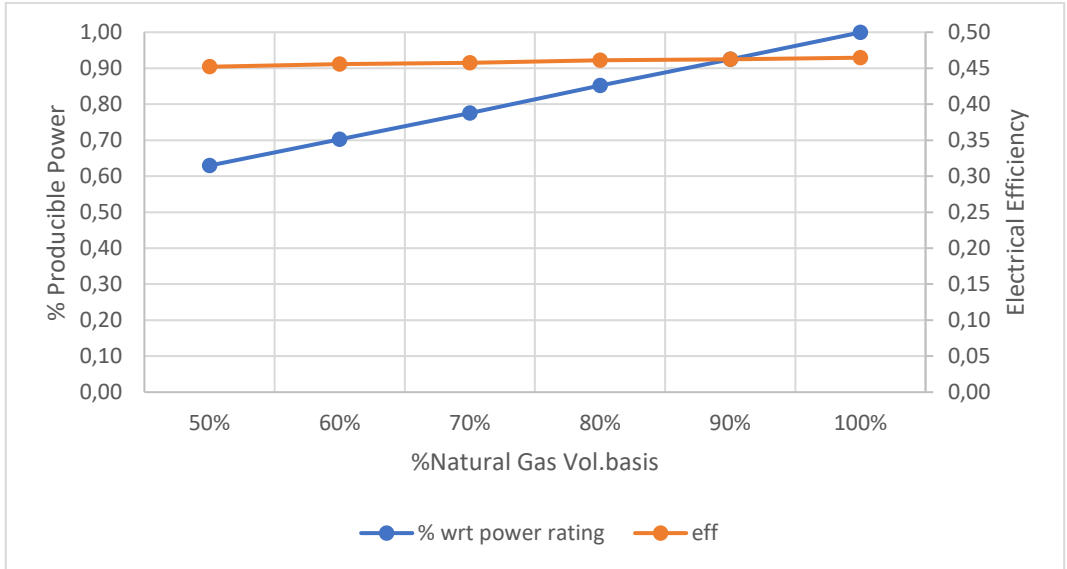


Table 29 Results at constant volume flow rate

The reduction in power output, for the same amount of volume flow rate is 35%, much higher than the 10% declared from FCE. The linearity for the power is due to the equations used in the model. For low percentage of natural gas, there is a high concentration in hydrogen. Being the Nerst equation a function of composition, for higher concentration of hydrogen in the mixture, the partial pressure $p_{h_2,an}$ increases and $p_{CO_2,an}$ decreases. Overall, the argument in the logarithm increase, provoking an increase in the open circuit voltage.

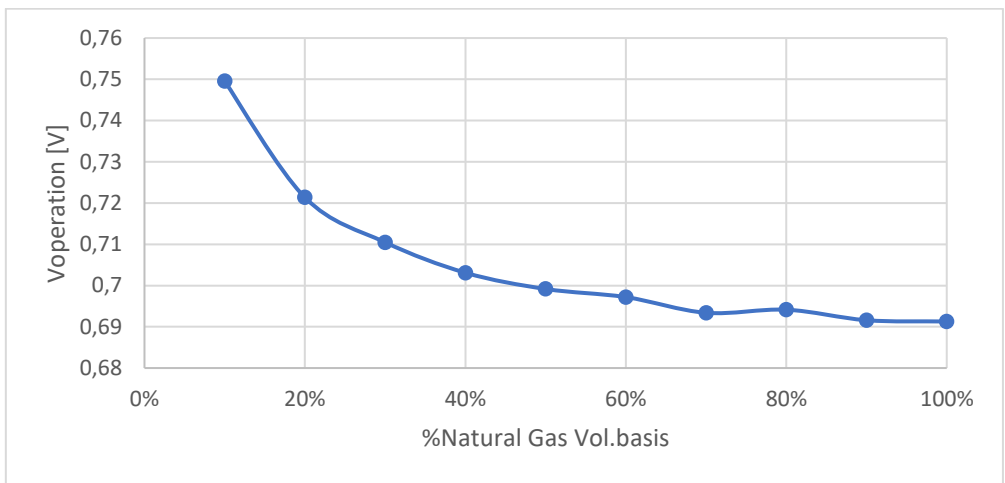


Figure 91 Operating voltage in function of fuel composition

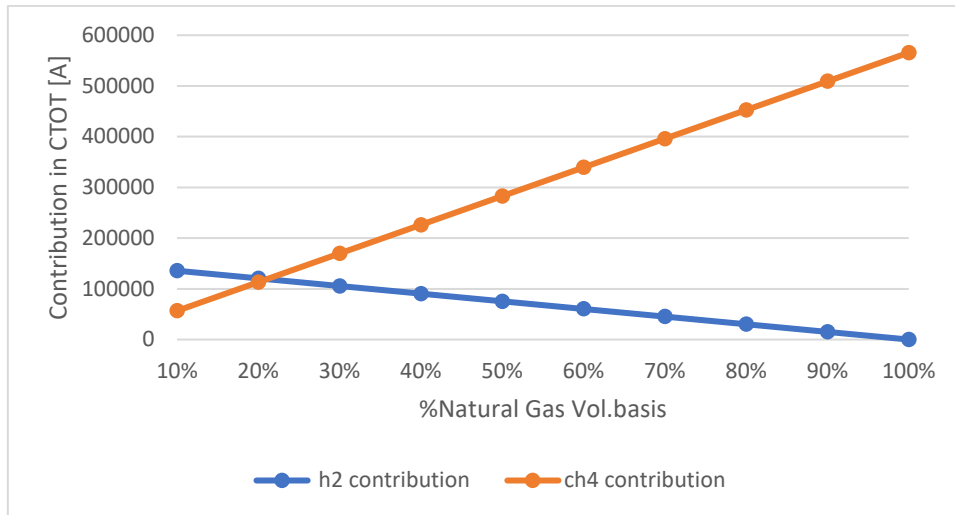


Figure 92 Analysis contribution hydrogen and methane for different compositions

The two contributions have an opposite behavior, the weight of the methane in the determination of the total current remains the prevailing up to 20% of methane. The contribution of hydrocarbons decreasing with methane decreasing.

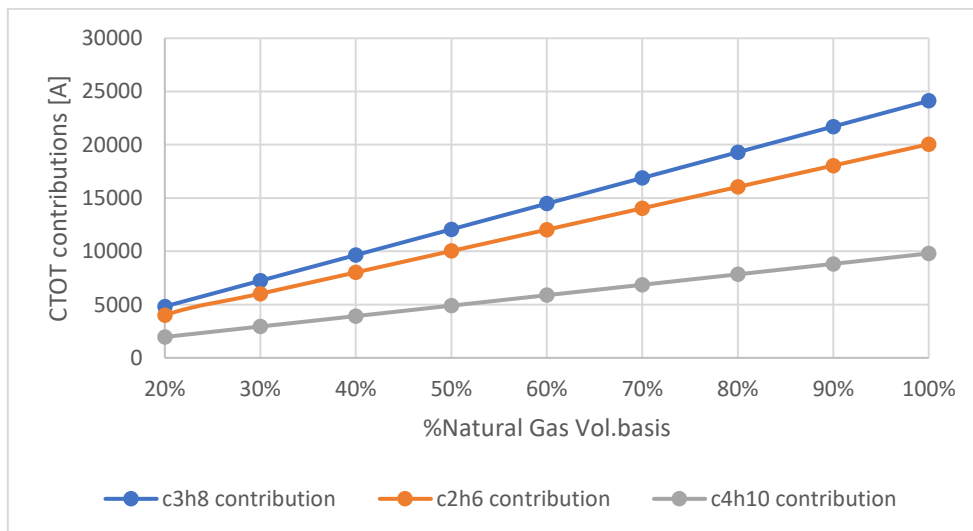


Figure 93 Hydrocarbons contribution

Overall, the total current decrease from a value at 100% natural gas composition of 619614 A to 195638A at 10% natural gas composition. The reduction in total current is more significant respect the increase in the voltage. The power produced calculated as the product of the two terms, overall decrease.

10.2 Blending mixture

The main problem for hydrogen is the low density, $0.084 \left[\frac{Kg}{Nm^3} \right]$. The density of air is $1.25 \left[\frac{Kg}{Nm^3} \right]$ and $0.668 \left[\frac{Kg}{Nm^3} \right]$ for methane. Considering the same heating value, the volume required to store hydrogen is more than seven times the one of methane. The substitution of hydrogen in pipelines has several constraints. The useful energy to the final user would be less respect the methane. Considering $1Nm^3$ of methane, equally $668 g$. The amount of energy that could be exploited considering the heating value for methane of $55.5 \left[\frac{MJ}{Kg} \right]$ is $37.07 [MJ]$. The same volume of hydrogen, corresponding to $84 g$, considering a heating value of $142 \left[\frac{MJ}{Kg} \right]$ contains $11.93 [MJ]$. This show that in terms of energy the complete substitution in volume from 100% methane to 100% hydrogen means a lost in useful energy of two third.

	Methane	Hydrogen
Formula	CH4	H2
Molecular weigth (g/mol)	16	2
Density (kg/m3)	0.668	0.084
Energy Density (MJ/kg)	55.5	142
Energy Density (MJ/m3)	37.3	12

Table 30 Properties of hydrogen and methane

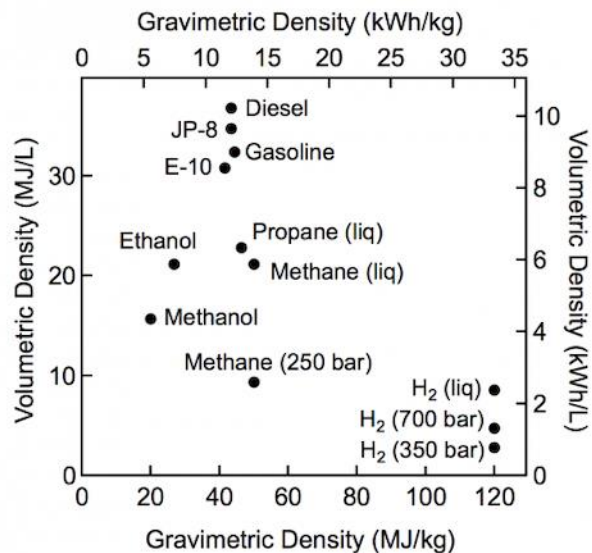


Figure 94 Volumetric and gravimetric density for different compound[27]

The molecular weight of the mixture, as the density, linearly change in accordance to the composition.

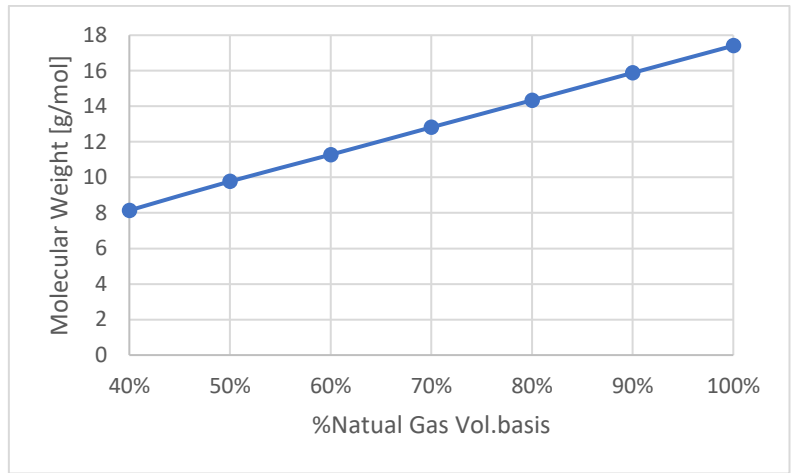


Figure 95 Molecular Weight with respect natural gas composition

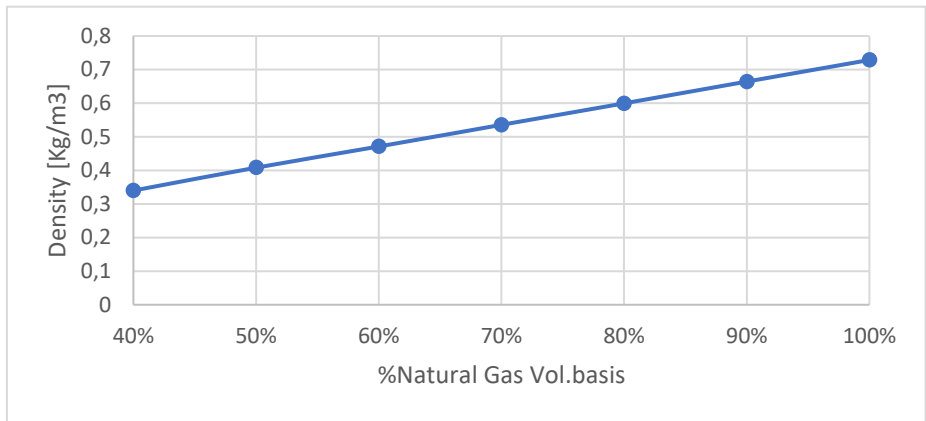


Figure 96 Density with respect natural gas composition

Being the energy density in terms of mass three times higher for hydrogen than methane, for high concentration of hydrogen there is an increase in the heating value.

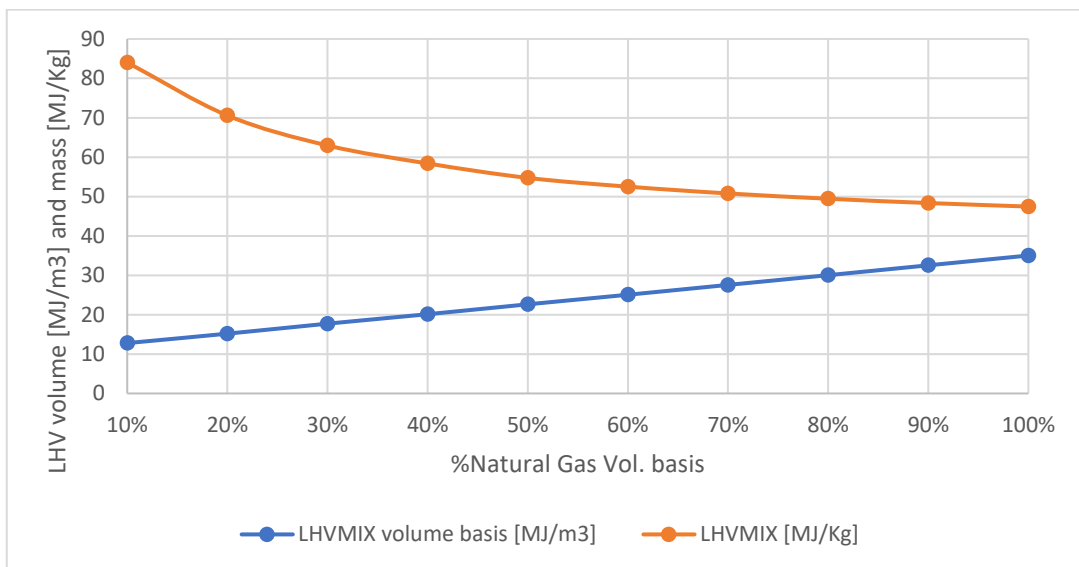


Figure 97 LHV mass [MJ/Kg], LHV volume [MJ/m3] in function of the composition

For the same volume flow rate, the mass flow decreases with increasing hydrogen mixture because the low density of hydrogen respect methane.

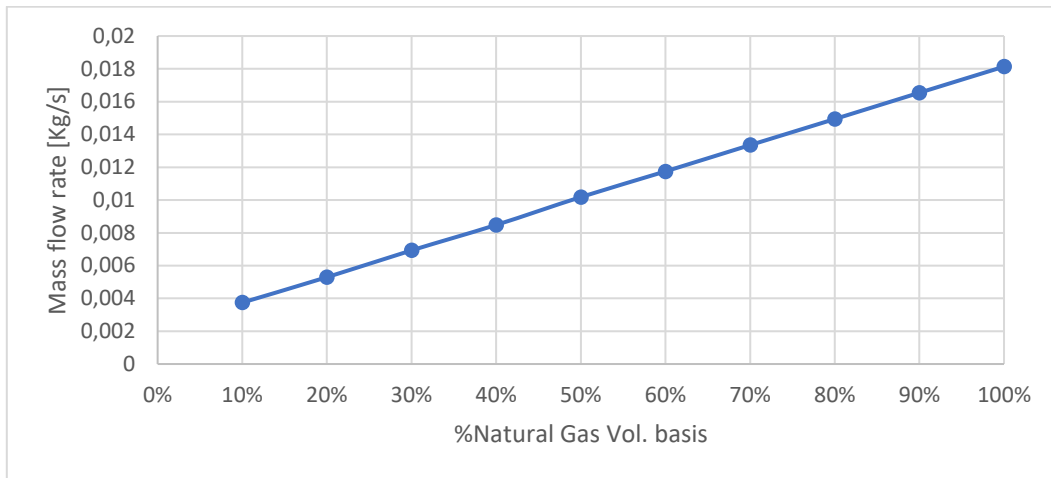


Figure 98 Mass flow rate for different compositions

11. Economical evaluation

There are two possible solutions for managing the investment:

- SAGAT can rely on ESCo for the realization and management of the new plant. SAGAT doesn't invest with own equity and gives part of the incomes to ESCo in the following years.
- SAGAT can decide to invest with own capital relying on financial plans.

The first strategy will be used. The maintenance, in case of EPC (energy procurement contract), or with ESCo, is in charge of the third subject at least for the mechanical and electrical parts. SAGAT have to deal with the maintenance of boilers, substation and absorber. For the absorber, to avoid problems and malfunction it is advisable a full-service contract that guarantee the disservices.

The peculiarity of the contract with ESCo consists in the possibility of upgrading the plant energetically, to achieve over time a better energy performance and therefore a subsequent saving; savings that, for the duration of the contract, will be used by the ESCo to remunerate the investments made. The EPC entrusts ESCo the burden of the investments (works, services, supplies) necessary for the redevelopment of the plant, which will be recovered from the contractually agreed energy savings. There will be a

benefit for the customer in not to have any initial investment expenditure and to repay the redevelopment to ESCo with all or part of the savings.

SAGAT will pay the bills for the natural gas required to feed the boilers (to produce the thermal energy not producible from the congengator) and the electricity bills of the energy bought from the distributor (Enel). In order to track the various voices of cost, the plant should have a meter for the amount of natural gas required from the cells, a meter for the electrical energy produced in cogeneration, a meter for the thermal energy needed to produce hot water, a meter for the thermal energy needed to produce chilled water, a meter for the cooling energy produced.

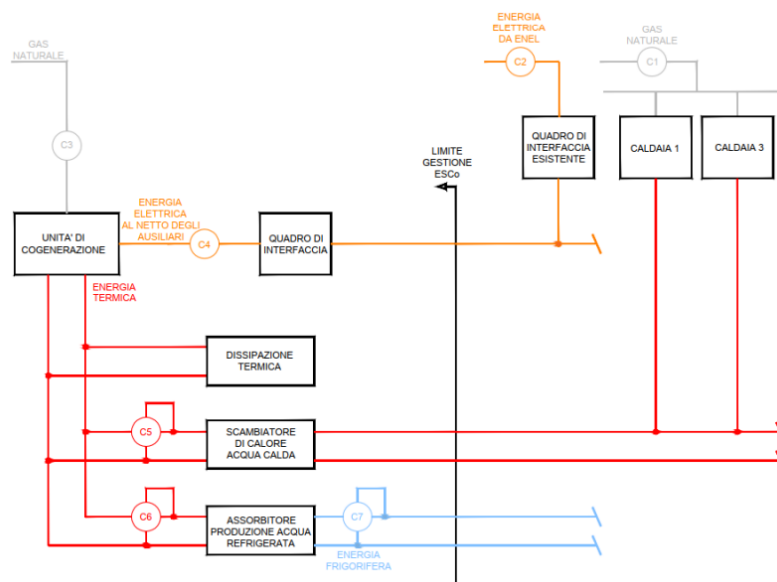


Figure 99 Economical Scheme Strategy for different contracts

SAGAT will pay the energy for C1 and C2, and pay a fee to ESCo proportional to C4 C5 C6 and C7.

The disservices in case of fuel cells are limited, thanks to the adoption of a heat exchanger for every cogeneration unit. For the absorber will be done a full-service maintenance contract with the machine manufacturer and a contract with ESCo that provides a reasonable allowance on the thermal energy guaranteed by SAGAT.

SAGAT pay for:
Electricity from national grid not covered from the cells (ENEL)
Natural gas to feed boilers and fuel cells
Electrical Energy produced from the cell at a design tariff
Fixed annual fee to SNAM

Table 31 Voices of cost SAGAT

11.1 High Efficiency cogenerator certificate (CAR)

A high efficiency cogeneration it is required to take the white certificates, that will be a positive additional contribution to the investment. White certificates, also known as "Energy Efficiency Certificates", give proof of end-use energy savings achieved through projects aimed at increasing energy efficiency in the final uses of energy [28] The WC can be asked from the cogeneration plant of new construction or renovation, after 6 march 2007. White certificates produced are issued for the first 10 years of operation of the plant. If the plants are coupled with a district heating network, the WC are recognized for fifteen years. The parameters to assign the white certificates are the amount of electrical energy produced in one year, the amount of the useful thermal energy produced in one year, the amount of cooling energy produced with the absorber, the amount of fuel used.

To be defined as a high efficiency cogeneration the PES must be higher than 10% if the machine has a size over 1MW, instead PES must be higher than zero if the size it is less than 1 MW.

The subject who applies to the GSE for being recognized CAR, must pay a fee to base on the generation capacity:

P<=50 kW	0 €
50 kW < P<=1 MW	250 €
1 MW <P<=10 MW	1500 €
P>10 MW	5000 €

Table 32 Taxes to GSE accordingly to the size

In addition to the fixed fee, in case of recognition and subsequent withdrawal of TEE by the GSE, there is also a variable fee equal to 1% of the withdrawal price of the same securities. All the requests of CAR, must be done on RICOGE portal, a section of the GSE web site [28].

Starting from the thermal and electrical energy produced for one year, it is possible evaluate the CHP (Combined Heat and Power), the savings in primary energy PES (Primary Energy Saving), and the numbers of white certificate in one year, if there are any. There is a guide for obtaining the CAR certifications [29].

The first principal yield is calculated as the sum of electrical and thermal energy totally produced over one year, divided by the equivalent energy of the fuels in the same period.

$$\eta_{plant} = \frac{H_{CHP} + E_{unit}}{F_{unit}} \quad (56)$$

Where E_{unit} it is the electrical energy produced from one unit, H_{CHP} it is the useful thermal energy produced from one unit without the amount that has been dissipated, F_{unit} is the thermal energy of the fuel. Being all the electricity produced evaluated as cogenerative, E_{unit} coincide with E_{CHP} .

To consider the electricity produced from the plant cogenerative, the primary efficiency must be higher than 75%. In other terms, the machine should be efficient and produce a considerable amount of energy with low fuel inlet.

The formulae to calculate the Primary Energy Saving is

$$PES = \left(1 - \frac{1}{\left(\frac{\eta_{H,CHP}}{\eta_{H,ref}} \right) + \left(\frac{\eta_{e,CHP}}{\eta_{e,ref}} \right)} \right) \cdot 100 \quad (57)$$

Where $\eta_{H,CHP}$ is the thermal efficiency with cogeneration, it is calculated as the ratio H_{CHP} over F_{unit} , $\eta_{e,CHP}$ is the electrical efficiency with cogeneration, it is calculated as the ratio E_{CHP} over F_{unit} , $\eta_{H,ref}$ is the reference thermal efficiency with a separate production, $\eta_{e,ref}$ it is the reference electrical efficiency with a separate production.

It is possible calculate the real saving with respect the reference value of electrical and thermal Italian park.

$$Savings = \frac{E_{CHP}}{\eta_{E,ref}} + \frac{H_{CHP}}{\eta_{T,ref}} - F_{CHP} \quad (58)$$

Where E_{CHP} is the electrical energy in MWh produced during one year, H_{CHP} is the thermal energy in MWh for the same period, F_{CHP} is the energy of the fuels in MWh, $\eta_{E,ref}$ is the yield considered as an average of all the Italian park equal to 46% corrected in function of the voltage, of the amount of energy injected into the grid and the amount of energy self-consumed, $\eta_{T,ref}$ is the average yield for the thermal energy of the Italian park equal to 90% in case of production of hot water and vapor. The number of white certificates is calculate based on the savings:

$$WC = Savings \cdot 0.086 \cdot K \quad (59)$$

Where K is a coefficient that vary in function of the power [30],

- K=1.4 for $P < 1 \text{ MWe}$
- K=1.3 for $1 \text{ MWe} < P < 10 \text{ Mwe}$
- K=1.2 for $10 \text{ MWe} < P < 80 \text{ Mwe}$
- K=1.1 for $80 \text{ MWe} < P < 100 \text{ Mwe}$
- K=1 for $P < 100 \text{ Mwe}$

If the overall first principal yield results less than 75%, there is the necessity to calculate a corrective coefficient as indicated in the guide for high cogeneration efficiency.

The data reported are for a reference year with 10 months of operation with a stop of production in May and October. The annual thermal useful energy has been calculated as:

$$Q_{thermal_useful} = Q_{thermal_load} + \frac{Q_{refrigerant}}{COP} - Q_{surplus} \quad (60)$$

Where:

$$Q_{surplus} = Q_{dissipated} + Q_{avoid_switch_off} \quad (61)$$

Where $Q_{dissipated}$ is the amount of energy wasted into the atmosphere, whereas the second term is the additional, not useful to cover the thermal loads, energy produced to avoid the shutdown of the cells. The fuel cells must operate at a technical minimum.

The COP is the performance coefficient of the absorber, imposed equal to 1.3 in this simulation.

Annual electricity produced	2.585.927 [kWh]
Annual total useful thermal energy produced	1.615.184 [kWh]
Annual thermal energy produced	1.068.597 [kWh]
Annual cooling energy produced	710.562 [kWh_c]
Annual thermal energy wasted to avoid shutdown (for three cells)	310.008 [kWh]
Annual thermal energy wasted (for three cells)	291.395 [kWh]
Fuel consumptions	5.501.973 [kWh]

Table 33 Production in the reference year 2019 for one cell

Electrical efficiency η_{el}	47,0%
Thermal efficiency η_{th}	29,4%
Global first principal η_{sys}	76,4%
EER of the obsorber	1,3
Reference electrical efficiency (PES)	45.4%
Reference thermal efficiency (PES)	92%
Reference electrical efficiency (savings)	39%
Reference thermal efficiency (PES)	90%

Table 34 Calculated and reference efficiencies

Since the global first principle is higher than the threshold of 75%, all the electrical energy produced could be considered cogenerative. This result has been also achieved because the will to insert in the plant the absorber to increase also the number of hours of operation, and consequently the capacity factor.

PES	26,19%
Savings	2.923.258 [kWh]

Table 35 Primary energy saving and total saving for the reference year

The numbers of white certificates results of the simulation are 327 every year.

From the GME site, there is a dedicated section where the value of the certificates is published [31]. In another site, are reported every month the data from the GME [32]. The economic value of each white certificate is around 250€.

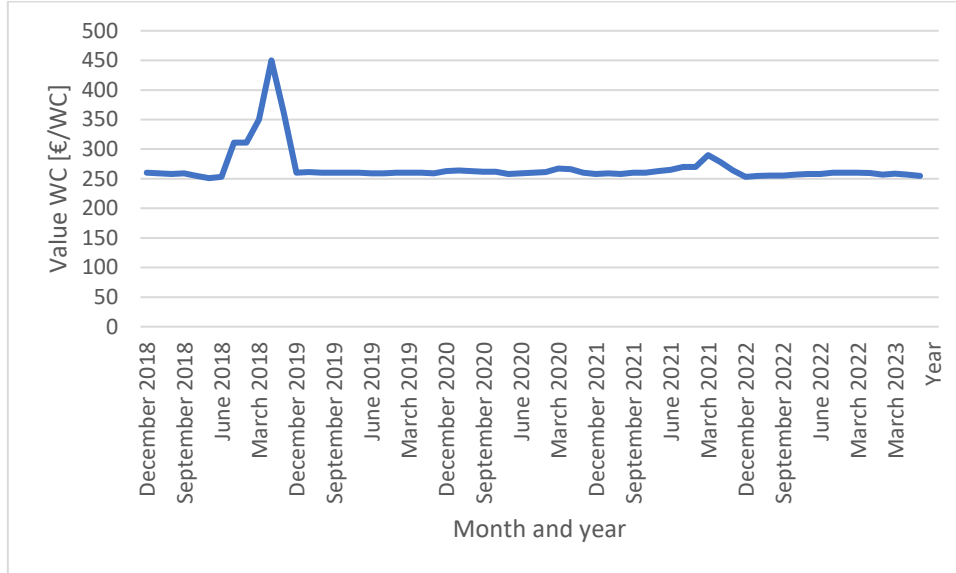


Figure 100 White certificates values during years

With the current prices, the value of the WC is 258.79 €, the historical maximum was 489.90€ in 2018.

1.1 Economical evaluation

The total cost for the electrical energy that SAGAT has to pay is composed of:

- Price of electrical energy bought from the grid [€/MWh]
- Price of electrical energy bought from fuel cells [€/MWh]
- Excise auto-production [€/MWh]
- Annual fixed fee too SNAM [€]

The cost of natural gas can be determined knowing the consumptions:

$$C_{NG}[\text{€}] = \dot{Q}_{NG} \left[\frac{\text{Sm}^3}{\text{y}} \right] \cdot c_{NG} \left[\frac{\text{€}}{\text{Sm}^3} \right] \quad (62)$$

Where C_{NG} is the total cost of natural gas, \dot{Q}_{NG} are the consumptions of natural gas volume flow rate in one, c_{NG} is the specific cost of natural gas. The natural gas consumptions for the year 2019 were 804.335 Sm^3 whereas the future consumptions, considering the quantity to feed the fuel cells, the boilers for the general aviation and to produce heat for AEPAX, will be $2.480.400 \text{ Sm}^3$.

Total future consumptions of natural gas	2.480.400	[Sm3]
Fuel Cells	1.950.000	[Sm3]
General Aviation	80.400	[Sm3]
AEPAX	450.000	[Sm3]

Table 36 Total future fuel consumptions with fuel cells

Total future consumption of electrical energy	16.900	[MWh]
Energy from fuel cells	9.600	[MWh]
Electrical energy saving from absorber	700	[MWh]
Electrical energy bought from the grid	6.600	[MWh]

Table 37 Total future electrical consumptions with fuel cells

The capacity factor of the simulation is 0.913. Initially, the results have been carried out comparing two situations with and without fuel cells. Accordingly to the available data of consumptions in 2019, a reference baseline year has been created to compare the results.

	Reference year	Reference Year with fuel cells
Natural gas price [€/Sm3]	0,608	0,608
Fuel consumptions [Sm3]	800.000	2.480.400
Total Natural gas cost [€]	486.400	1.508.083
Price Electrical energy from the grid [€/MWh]	150	150
Electricity bought from the grid [MWh]	16.900	6.879
Total cost Electrical energy bought from the grid [€]	2.535.000	1.031.850
Price electrical energy bought from fuel cells [€/MWh]	-	Private rate
Electricity bought from fuel cells [MWh]	-	9.600
Excise auto-production [€/MWh]	-	5,2
Annual fixed fee SNAM [€]	-	210.000
Total cost Electrical energy bought from fuel cells [€]	-	701.520
Total cost electrical energy [€]	2.535.000	1.733.370
Total Cost (electricity + gas) [€]	3.021.400	3.241.453

Table 38 Comparison reference year with actual prices and three fuel cells

The natural gas prices and the electricity prices reported in table are the actual price. The cost of the natural gas is the average of the first trimester 2023 [33]. The electricity is the total national Italian price (PUN) [34]. With the actual prices the installation of the fuel cells is not convenient for the SAGAT's bill. The total cost for electricity and natural gas

with fuel cells is 220.053 € higher. This is due to the high cost of natural gas, because in terms of electricity the savings would be 801.630 €.

Is below represented the total savings with respect the natural gas cost, the price of electricity has been kept fixed equal to $138 \left[\frac{\text{€}}{\text{MWh}} \right]$, that was the price in 2019. The savings are positive, when the total cost of electricity and natural gas with fuel cells is lower than the reference year without fuel cells.

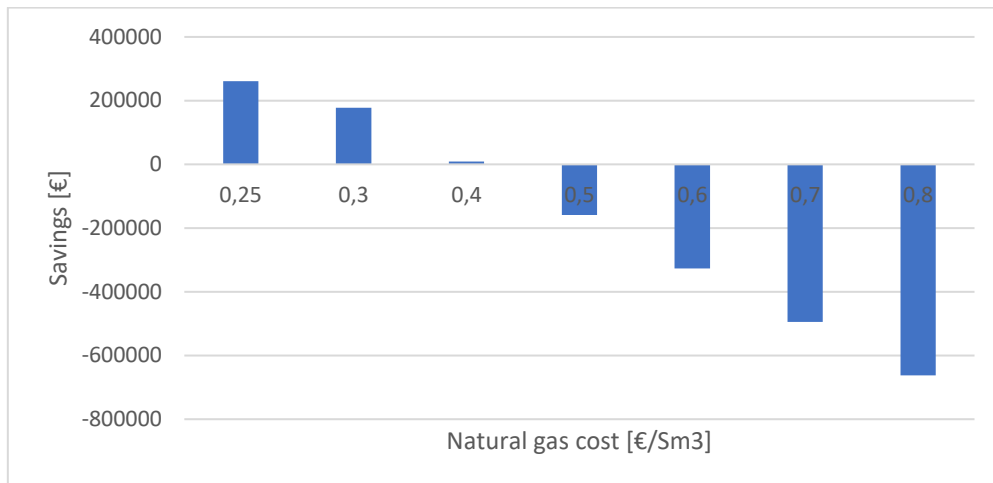


Figure 101 Sensitivity analysis on natural gas price

The natural gas price, affects considerably the bill. Thus, it is difficult forecast with precision the future bills.

The same analysis has been done with respect the price of electricity, the price of natural gas has been kept fixed to $0.2926 \left[\frac{\text{€}}{\text{Sm}^3} \right]$. Both $138 \left[\frac{\text{€}}{\text{MWh}} \right]$ and $0.25 \left[\frac{\text{€}}{\text{Sm}^3} \right]$ have been considered as reference value in the baseline year. The savings are positive.

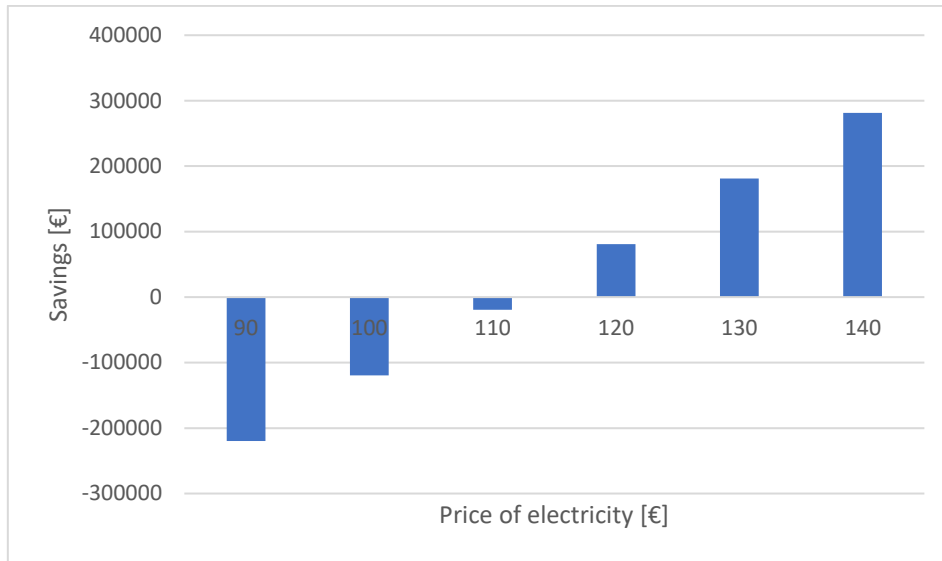


Figure 102 Sensitivity analysis on electricity price

The behavior of the two graphs is opposite. It is better to have a high price of electricity that means that bought the electricity produced from the fuel cell is more convenient than from the network. Instead, it is better to have a low price of natural gas because with the fuel cells, the amount of consumption increases of more than $1.600.000 \text{ Sm}^3$ respect the reference year and so lower prices generate more savings. This explain the fact, that with the actual prices of natural gas, it is not convenient install the fuel cells. A scenario based on the voices of costs presented has been made to estimate the savings after the installation of fuel cells. The reference year, from which the savings have been calculated has a price of electricity of $138 \left[\frac{\text{€}}{\text{Mwh}} \right]$ and $0.2515 \left[\frac{\text{€}}{\text{Sm}^3} \right]$ for the natural gas, to be coherent with the data in 2019. Has been supposed an installation of fuel cells from 2024. Two cases are presented, with three fuel cells, and with two fuel cells.

	Yearly savings with Fuel Cells	Yearly savings without Fuel Cells	$\Delta_{savings}$
2024	229.116,69	- 68.095,19	297.211,88
2025	167.822,53	- 139.995,22	307.817,75
2026	125.437,54	- 188.930,62	314.368,16
2027	48.749,60	- 268.862,11	317.611,71
2028	14.530,22	- 316.697,13	331.227,35
2029	61.255,54	- 283.227,73	344.483,28
2030	55.442,59	- 294.302,15	349.744,74
2031	66.534,24	- 272.534,23	339.068,48

2032	62.391,37	- 290.543,22	352.934,59
2033	39.220,65	- 284.090,40	323.311,05
2034	- 5.034,02	- 282.626,59	277.592,57
2035	- 10.003,22	- 305.244,79	295.241,57
2036	- 22.437,62	- 339.429,20	316.991,58
2037	- 61.872,09	- 352.115,85	290.243,76
2038	- 72.683,76	- 328.415,56	255.731,81
2039	- 67.778,35	- 325.767,55	257.989,20
2040	- 57.545,18	- 326.231,58	268.686,40
2041	- 54.230,02	- 327.106,44	272.876,41
2042	- 56.942,51	- 327.106,44	270.163,92

Table 39 Scenario yearly savings with three fuel cells

The average savings during years are 304.384 €, calculated respect the baseline year.

	Yearly savings with Fuel Cells	Yearly savings without Fuel Cells	$\Delta_{savings}$
2024	68.126,49	- 68.095,19	136.221,68
2025	4.673,86	-139.995,22	144.669,08
2026	- 38.929,85	-188.930,62	150.000,77
2027	-114.814,06	-268.862,11	154.048,05
2028	-152.927,91	-316.697,13	163.769,23
2029	-112.016,26	-283.227,73	171.211,47
2030	-119.521,35	-294.302,15	174.780,80
2031	-108.201,41	-272.534,23	164.332,82
2032	-111.794,53	-275.403,69	163.609,16
2033	-131.572,81	-290.543,22	158.970,42
2034	-175.725,34	-284.090,40	108.365,06
2035	-178.320,52	-282.626,59	104.306,07
2036	-197.223,32	-305.244,79	108.021,47
2037	-233.826,53	-339.429,20	105.602,68
2038	-245.020,40	-352.115,85	107.095,45
2039	-234.433,67	-328.415,56	93.981,90
2040	-226.346,24	-325.767,55	99.421,32
2041	-224.435,74	-326.231,58	101.795,84
2042	-226.437,41	-327.106,44	100.669,03

Table 40 Scenario yearly savings with two fuel cells

The average savings during years with two fuel cells are 132.151 € calculated respect the baseline year.

The value of future electricity and natural gas price used in the simulation are:

	Natural gas	Electricity price
2024	0,28	143,60
2025	0,30	147,13
2026	0,31	149,52
2027	0,33	153,26
2028	0,34	155,75
2029	0,32	154,50
2030	0,32	155,13
2031	0,32	154,52
2032	0,32	154,62
2033	0,33	155,14
2034	0,33	154,83
2035	0,33	154,62
2036	0,33	156,51
2038	0,35	158,58
2039	0,35	157,23
2040	0,34	157,13
2041	0,34	157,23
2042	0,34	157,23

Table 41 Future price and natural gas cost from SAGAT evaluation

The values of electricity and natural gas cost used in this simulation, doesn't take into account the recent geopolitical events, however can be useful compare the results of the investment in a normal scenario.

1.2 Cash flow analysis

The economic evaluation aims at assessing the feasibility of the project. In order to perform it, some data are needed to define the capital expenditure CAPEX and operating expenditure OPEX of the plant and on the financial structure. The possibility to install three, or less, fuel cells must be motivated both from an energetic and an economical perspective. The cash flow analysis has been done from the point of view of the ESCo, that has to pay the initial capital cost of the investment.

In this section are analyzed two cases:

- Installation of three fuel cells, $400 kW_{el}$ and $281 kW_{th}$ each
- Installation of two fuel cells, $400 kW_{el}$ and $281 kW_{th}$ each

For both cases have been considered a stop of two months in May and October with a null production.

The reference voices of costs from the technical report made by STEAM.

Fuel Cell CAPEX [€]	4.300.000
Installation of the cells [€]	300.000
Investment for the plant [€]	900.000
Absorber [€]	400.000

Table 42 CAPEX for three cells

Fuel Cell OPEX [€]	
Maintenance every 7 years [€]	1.433.333
Ordinary maintenance [€/MWh]	0,0012
Ordinary maintenance [€/y]	93.093
Maintenance of the cells [€]	25.000
Fuel consumptions for one year [Sm³]	1.663.903

Table 43 OPEX for three cells

Fuel Cell CAPEX [€]	2.800.000
Installation of the cells [€]	250.000
Investment SAGAT [€]	900.000
Absorber [€]	350.000

Table 44 CAPEX for two cells

Fuel Cell OPEX [€]	118.093
Maintenance every 7 years [€]	933.333
Ordinary maintenance [€/MWh]	0,012
Ordinary maintenance [€/y]	65.100
Maintenance of the cells [€]	20.000
Fuel consumptions for one year [Sm³]	1.163.569

Table 45 OPEX for two cells

The fuel cells capex, 4.300.000 € for three cells and 2.800.000 € for two cells, takes into account the following voices of costs:

- Three (or two for the second case) fuel cells modules $400 kW_{el}$
- Gas cleanup for sulfur removal and others impurities in natural gas input
- Water treatment
- Inverters, one per cell

- Cooling system for the inverter
- Nitrogen used at the start-up and shut-down of the machine
- Compressed air for pneumatical components
- Transport of fuel cells to the site
- Heat recovery section, one heat exchanger per cell for produce hot water 70/90 °C
- Insurance during construction and commissioning
- Construction and installation of the fuel cell and of the HRU section
- Commissioning of the plant, start up and initial test
- Project Management
- Engineering
- Supervisory control of the plant

The extraordinary maintenance, every seven years, it is defined as 1/3 of the fuel cell capex. In that cost is included the maintenance of the fuel cells and of the auxiliaries' components.

The annual opex has been calculated with a specific price per kWh. As comparison the opex has been also estimated starting from literature. The operating expenditure comprehends the maintenance of the cells, the reformer catalyst substitution, the cleaning system maintenance, the savings, every year[35]. The stack substitution depends on the stack lifetime and can vary from 3 to 10 years. The substitutional cost is not equal to the beginning cost of the cell capex, but lower. It accounts for the 35% of the total MCFC module investments. This is in accordance to the proposed estimation, used in the study, of 1/3 of the cell installation capex. The clean-up system cost, it is expressed in [€/kWh]. The labor cost has been evaluated considering one specialized operator, with a salary of 30 [€/h], working 20 hours per week during plant operation. The general maintenance costs are expressed as a percentage of the capex of the plant, generally 3%. Using this information, has been founded a value for the opex of 85.471 €/y that confirmed the assumption made in the study with annual opex of 100.000 €/y.

Some key performance indicators, KPI, can be carried out. To assess the cost effectiveness of the investment, the Net Present Value (NPV) and the Internal Rate of Return (IRR) have been calculated:

$$NPV = C_0 + \sum_{k=1}^N \frac{(R_{WT,k} - C_{O\&m,k})}{(1+r)^k} \quad (63)$$

Where $R_{WT,k}$ are the revenues, $C_{O\&m,k}$ the opex of the plant. The IRR identify the value of the discount rate that makes the discounted cash flows equals to the investment cost.

$$NPV = \sum_{n=0}^N \frac{R_t}{(1+r)^n} = 0 \quad (64)$$

The higher internal rate of return, the more desirable an investment is to undertake. When comparing investment options with other similar characteristics, the investment with the highest IRR would be considered the best. The PBT is expressed as number of years to recover during the lifetime the cost of an investment, representing the moment in which the positive cash flows equals the negative cash flows. This is fundamental parameter because from that moment the investor starts to get positive incomes from the plant.

$$PBT = \frac{p-n}{p} + n_y = 1 + n_y - \frac{n}{p} \quad (65)$$

The n_y describe the number of years after the initial investment and n is the value of the cumulative, both at which the last negative value of cumulative cash flow occurs, p is the value of cash flow at which the first positive value of cumulative cash flow occurs.

The discounting factor is useful to adjust the future cashflow:

$$DF = (1 + WACC)^{-(n-n_0)} \quad (66)$$

The Waighted Avarage Cost of Capital is calculated accordingly to the percentage of equity and dept. Equal to 3.4% in this analysis.

The Levelized Cost of Energy (LCOE), is a useful indicator to compare different technologies has been calculated via the following formula

$$LCOE = \frac{C_0 + \frac{\sum_{k=1}^N C_{O\&m,k}}{(1+r)^k} + \frac{\sum_{k=1}^N C_{f,k}}{(1+r)^k}}{\frac{\sum_{k=1}^N E_{G,k}}{(1+r)^k}} \left[\frac{\text{€}}{MWh} \right] \quad (67)$$

It includes all the costs of the project:

- initial cost of investment (capital expenditures, C_0)
- operation and maintenance expenditures ($C_{O\&m,k}$)

- fuel expenditures ($C_{f,k}$)
- The sum of the generated electricity over the project lifetime (E_G) that is also the output of the power-plant asset

The last two factors in the equation are:

- discount rate (or interest rate) of the project (r);
- lifetime of the system (N), assumed equal to 25.

The results of the simulation, for three cells, operating 10 months. The input value is the one presented in table n.33. The cash flow analysis has been done to estimate the return of the investment for the ESCo. Relying on ESCo, SAGAT doesn't invest with own budget but will give part of its incomes to ESCo in the following years.

Annual electricity production - total	7.758	[MWh]
Annual thermal production - total	3.206	[MWh]
Annual cooling energy production	2.132	[MWhf]
Fuel consumptions	1.663.903	[Sm3]
Natural gas cost	0,21	[€/Sm3]
White certificates	1.047	
Annual Self-consumption electricity	7.758	[kWh]
Annual Sold electricity	-	[kWh]
Self-consumption heating	3.206	[kWh]
Self consumption cooling	2.132	[kWh]
Full load hours h	7272	[h]
DH price thermal	17,1	[€/MWh]
Price of electricity	111	[€/MWh]
Price of cooling energy	23,6	[€/MWhf]
Savings EL	861.114 €	per year
Savings TH	54.819 €	per year
Savings Cooling	50.308 €	per year
Total INCOMES	915.933 €	per year

Table 46 Input Value for the simulation

The cash flow analysis over the years.

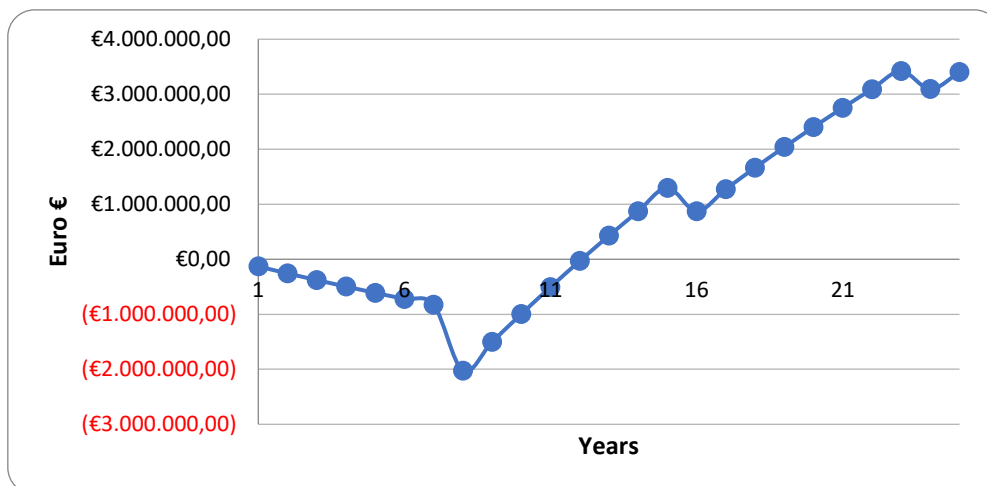


Figure 103 Results cash flow for three cells

A sensitivity analysis has been performed on price of electricity, thermal heat and cooling price.

NPV	3.401.780 €
PBT	12
IRR	17%
LCOE	105,91

Table 47 Results for three cells

The rapid grow in the curve is due to the high electrical incomes, that every year are 861.114 €. As comparison, the quote of the mortgage payment is 842.857 €.

	90 [€/MWh]	111 [€/MWh]	120 [€/MWh]
NPV	687.343	3.401.780	4.565.110
PBT	19	12	10
IRR	5.6	16	25
	5 [€/MWh]	17,1 [€/MWh]	30 [€/MWh]
NPV	2.755.466	3.401.780	4.090.825
PBT	12	12	11
IRR	13	16	21
	5 [€/MWh]	23,6 [€/MWh]	40 [€/MWh]
NPV	2.741.149	3.401.780	3.984.272
PBT	12	12	11
IRR	13	17	20

Table 48 Sensitivity on three fuel cells

The results of the simulations are presented.

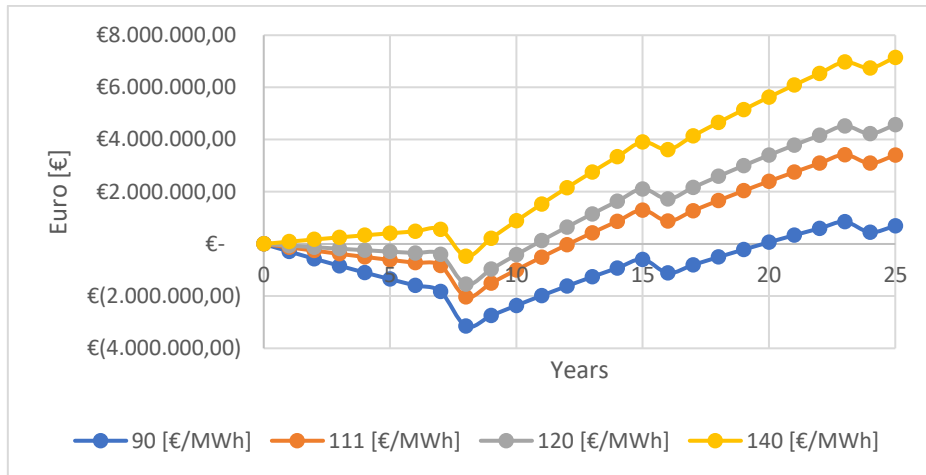


Figure 104 Sensitivity on electricity price

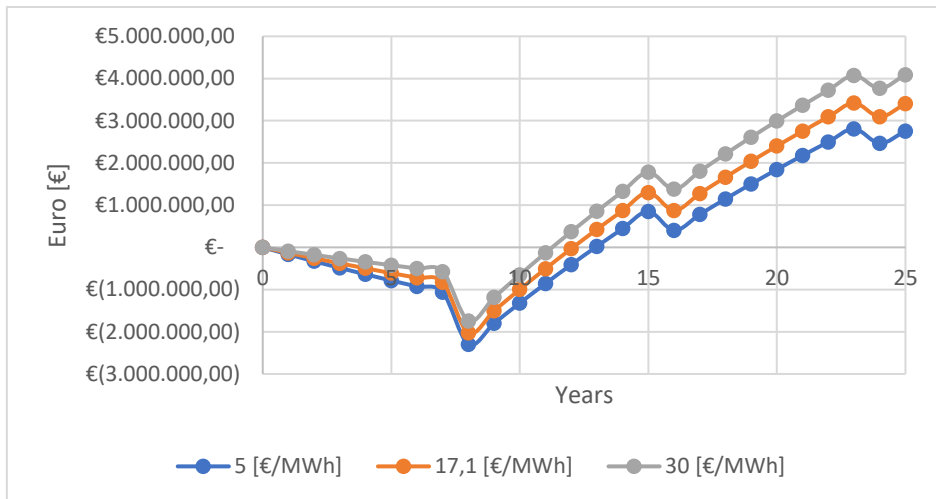


Figure 105 Sensitivity on thermal price

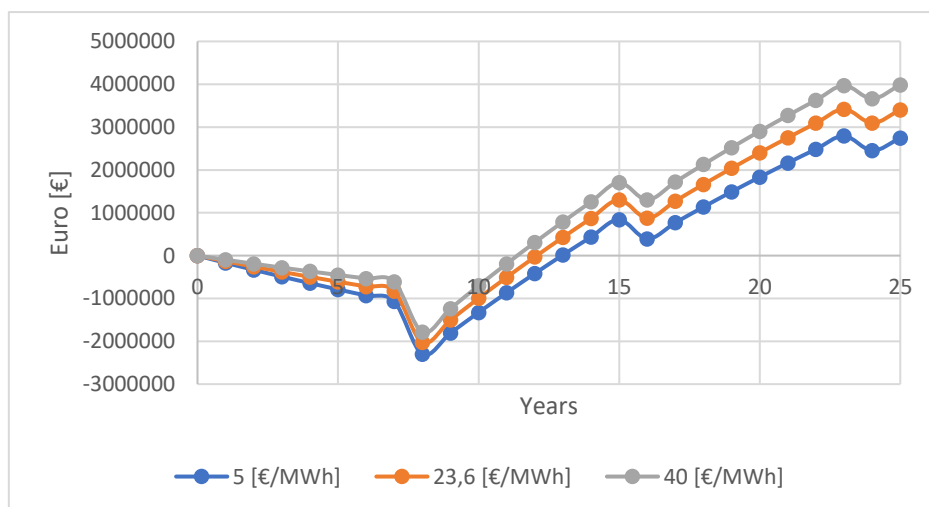


Figure 106 Sensitivity on cooling price

The loan has a duration of 8 years. For this reason, the graph doesn't present a negative capex in the year zero. But every year, for eight years, ESCo pay a quote of the loan that will be summed with the other annual voices.

For two cells, the cash flow analysis is here reported.

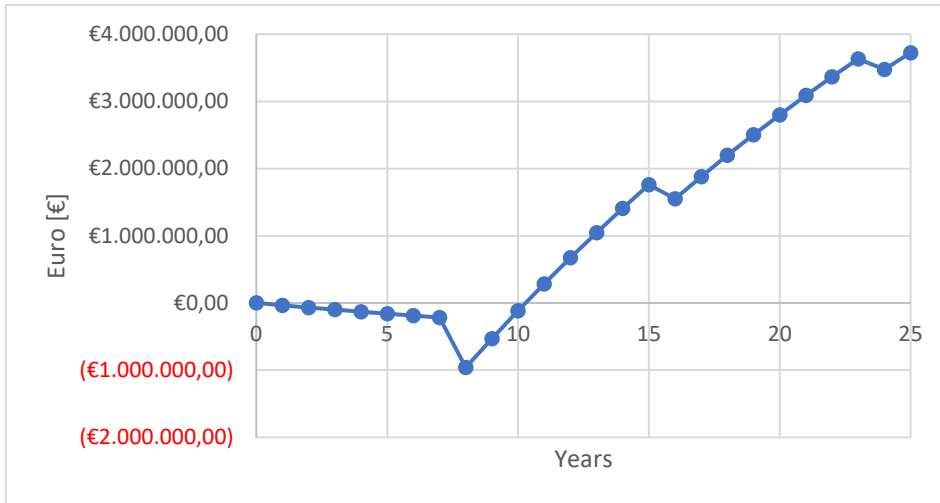


Figure 107 Two fuel cells

NPV	3.336.660 €
PBT	10
IRR	24%
LCOE	107,52

Table 49 Two fuel cells

Electrical	90 [€/MWh]	111 [€/MWh]	120 [€/MWh]
NPV	1.527.035	3.336.660	4.112.213
PBT	15	10	9
IRR	10	24	41
LCOE	107,52	107,52	107,52
Thermal	5 [€/MWh]	17,1 [€/MWh]	30 [€/MWh]
NPV	2.905.784	3.336.660	3.796.023
PBT	11	10	10
IRR	19	24	31
LCOE	107,52	107,52	107,52
Cooling	5 [€/MWh]	23,6 [€/MWh]	40 [€/MWh]
NPV	2.896.239	3.336.660	3.724.988
PBT	11	10	10
IRR	19	24	30
LCOE	107,52	107,52	107,52

Table 50 Sensitivity on two fuel cells

The strategy with three fuel cells, is the best in terms of return of the investment for the ESCo and for the savings in bill for SAGAT. The estimated lifetime of the plant has been assumed equal to 25 years.

12. Conclusions

In this work, the integration of three fuel cells in the airport of Turin have been investigated. An electrochemical model developed in Aspen Plus has been presented. The electrical thermal and cooling loads of the airport have been analyzed to understand the contribution of the fuel cells to cover the demand. Finally, an economical evaluation to assess the investment has been analyzed, showing that the best strategy is the one with three fuel cells. All the electricity produced from the cells is auto-consumed. From an economical point of view, since SAGAT rely on ESCo for the construction of the cells, there is not an initial capital cost but only savings in the bills. Also for the ESCo has been showed a return of the investment in 11 years.

13. Figures

Figure 1 Electrical energy during the years	6	Figure 61 Monthly natural gas consumptions	52
Figure 2 CO ₂ emissions during the years.....	6	Figure 62 Contribution from the fuel cells to the loads	
Figure 3 Fuel consumptions during the years.....	6	CF=0.9	53
Figure 4 World population growth	7	Figure 63 Contribution fuel cells to the load CF=0.8	54
Figure 5 CO ₂ daily and weekly means at Mauna Loa	8	<i>Figure 64 FCE efficiency and power output</i>	57
Figure 6 CO ₂ value at Mauna Loa Observatory	8	Figure 65 Space for PV installations.....	58
Figure 7 Trigeneration Scheme[5]	9	Figure 66 MCFC model Aspen.....	61
Figure 8. MCFC general design.....	12	Figure 67 Air flow rate in function of the $\Delta T_{cathode}$...	66
Figure 9 MCFC operating principle with partial		Figure 68 Net Air Blower work in function of $\Delta T_{cathode}$	
recirculation	13	66
Figure 10. Polarization curves for various fuel cells.....	14	Figure 69 MCFC model for the validation	68
Figure 11 Distribution of molten carbonate electrolyte		Figure 70 Integration of a MCFC in a plant with GT [14]	68
in porous electrodes of MCFC as a result of balance in		Figure 71 Comparison of the curves	69
capillary pressure [9].....	15	Figure 72 Comparison of the two curves.....	70
Figure 12 Connections between anode, cathode,		Figure 73 Distribution of the resistances.....	71
electrolyte	15	Figure 74 MCFC Balance of Plant model.....	72
Figure 13 Schematic of Ni shorting the cell in the		Figure 75 Heat Recovery Unit	73
electrolyte matrix [11]	18	Figure 76 Total area in function of the current Density .	76
Figure 14 Dependences MCFC from pressure Cell		Figure 77 Aspen Model with pressure drops.....	77
voltage and current density	21	Figure 78 Blower's consumptions.....	78
Figure 15 Schematic of MCFC degradation with time at		Figure 79 Efficiency of the system in function of the	
a constant current level.	22	anode pressure drops (the corresponding cathode	
Figure 16 Strategies for the reforming of methane.....	24	pressure drops can be determined from the table)	78
Figure 17 Scheme lithium absorber [13].....	25	Figure 80 Details on pressure drops	79
Figure 18 Absorber technical scheme.....	26	Figure 81 Electrical Efficiency with respect current density	
Figure 19 Torino-Caselle Airport satellite view.....	27	[A/m ²].....	79
Figure 20 Thermal station (red) and connections to the		Figure 82 Electrical Efficiency with respect Steam to	
substations (orange)	28	Carbon Ratio	80
Figure 21 Airport view	28	Figure 83 Electrical Efficiency with respect stack	
Figure 22 Cooling stations (blue) and pipes for cooling		temperature.....	81
water	28	Figure 84 Voltage in function of the cell temperature ...	81
Figure 23 Thermal station.....	29	Figure 85 Voltage in function of the pressure	82
Figure 24 Photo of thermal station and pumping room		Figure 86 Electrical efficiency in function of Fuel	
.....	29	Utilization.....	82
Figure 25 External façade of the thermal station	30	Figure 87 Direct - Indirect MCFC.....	83
Figure 26 Warehouse, space for the installation of the		Figure 88 Net-work air blower in function of the grade	
third cell	30	Internal Reforming.....	84
Figure 27 External space for storage installation and		Figure 89 Electrical stack efficiency in function of the	
auxiliaries	31	grade Internal Reforming.....	85
Figure 28 Warehouse for the third cell (left) and existing		Figure 90 Electrical power in function of the grade	
boilers (right).....	31	Internal Reforming.....	85
Figure 29 Heat Hexchanger S.C.T.....	31	Figure 91 Operating voltage in function of fuel	
Figure 30 Pumping room	32	composition	88
Figure 31 Warehouse for the third cell.....	32	Figure 92 Analysis contribution hydrogen and methane	
Figure 32 AEPAX thermal substation	33	for different compositions	89
Figure 33 AEPAX cooling station, External space for the		Figure 93 Hydrocarbons contribution.....	89
absorber and evaporative tower	33		

Figure 34 Heat Exchangers AEPAX (left) and pumps (right)	33	Figure 94 Volumetric and gravimetric density for different compound[26]	90
Figure 35 Evaporative towers	34	Figure 95 Molecular Weight with respect natural gas composition	91
Figure 36 Collectors BHS (left), heat exchangers BHS (right)	34	Figure 96 Density with respect natural gas composition	91
Figure 37 New underground hot water network (red), subservices (grey)	35	Figure 97 LHV mass [MJ/Kg], LHV volume [MJ/m3] in function of the composition	91
Figure 38 Thermal station and electrical station AEPAX	35	Figure 98 Mass flow rate for different compositions	92
Figure 39 Thermal power installed	36	Figure 99 Economical Scheme Strategy for different contracts	93
Figure 40 Power installed in the heat exchangers in the secondary sub stations	36	Figure 100 White certificates values during years.....	98
Figure 41 Installed power in the cooling stations.....	37	Figure 101 Sensitivity analysis on natural gas price.....	100
Figure 42 Building, in green, served from the trigeneration plants	37	Figure 102 Sensitivity analysis on electricity price	101
Figure 43 Principal thermal station, in red, and the other connections to the substations, in orange.....	38	Figure 103 Results cash flow for three cells	108
Figure 44 Cooling station (blue) and network for cooling water	39	Figure 104 Sensitivity on electricity price	109
Figure 45 Thermal Needs of the Airport	40	Figure 105 Sensitivity on thermal price	109
Figure 46 Refrigeration Needs of the Airport	41	Figure 106 Sensitivity on cooling price	109
Figure 47 Thermal load profile EER=0.7.....	41	Figure 107 Two fuel cells	110
Figure 48 Thermal load profile EER=1.2.....	42		
Figure 49 Electrical Needs with and without absorber.....	43		
Figure 50 Cumulated curve of the thermal load and cooling load transformed in thermal with a double stage absorber	44		
Figure 51 Cumulated curve of the electrical load with absorber	45		
Figure 52 Cumulated curve of thermal load EER=1.3 ...	45		
Figure 53 %Monthly contribution of the cells	47		
Figure 54 Energy in the thermal storage during 2019 ..	48		
Figure 55 Thermal energy dispersed in atmosphere	48		
Figure 56 Cooling energy during discharging phase of the storage	49		
Figure 57 Cooling energy from traditional chillers	49		
Figure 58 State of the storage in summers months	50		
Figure 59 Energy wasted into atmosphere	51		
Figure 60 Electrical energy produced from the fuel cells and bought from the grid.....	51		

14. Tables

Table 1 Fuel cells types.....	11	<i>Table 26 Compositions of hydrogen and natural gas declared by FCE.....</i>	86
Table 2 Fuel cells materials	19	Table 27 Blend composition in accordance with the amount of hydrogen, in volume basis.	87
Table 3 Contaminants and their tolerance limits for MCFCs.....	23	<i>Table 28 Molar and mass flow rate, molecular weight for different compositions of fuels, at fixed volume flow rate 84 Nm³/h</i>	87
Table 4 Energy needs of the Airport	40	<i>Table 29 Results at constant volume flow rate.....</i>	88
Table 5 Contribution of the fuel cells with the storage to the energy needs of the airport.....	46	Table 30 Properties of hydrogen and methane.....	90
Table 6 Contribution from the fuel cells to the loads CF=0.9.....	53	Table 31 Voices of cost SAGAT	94
Table 7 Contribution fuel cells to the load CF=0.8.....	54	Table 32 Taxes to GSE accordingly to the size	94
Table 8 FuelCellEnergy datasheet of the cell	56	Table 33 Production in the reference year 2019 for one cell.....	97
Table 9 Dimensions and weight of the machine	56	Table 34 Calculated and reference efficiencies	97
<i>Table 10 Input data from FCE.....</i>	<i>57</i>	Table 35 Primary energy saving and total saving for the reference year.....	97
<i>Table 11 Molar, mass, volume flow rate FCE simulation.....</i>	<i>58</i>	Table 36 Total future fuel consumptions with fuel cells	99
Table 12 Value of the charge number Z.....	64	Table 37 Total future electrical consumptions with fuel cells	99
Table 13 Working condition of the components in the Aspen Plus Model.....	65	Table 38 Comparison reference year with actual prices and three fuel cells	99
Table 14 Assumption for MCFC simulation [10].....	67	Table 39 Scenario yearly savings with three fuel cells..	102
Table 15 Results from Aspen.....	67	Table 40 Scenario yearly savings with two fuel cells....	102
Table 16 Streams inlet composition.....	69	Table 41 Future price and natural gas cost from SAGAT evaluation	103
Table 17 Reference Input value from the reference paper	70	Table 42 CAPEX for three cells.....	104
Table 18 Volume flow rate in function of pipe diameters	72	Table 43 OPEX for three cells.....	104
Table 19 Mol flow and mole fractions after the burner	73	Table 44 CAPEX for two cells	104
Table 20 Reference Natural Gas composition in the models.....	75	Table 45 OPEX for two cells	104
Table 21 Pressure Drop in the components.....	76	Table 46 Input Value for the simulation	107
Table 22 Net-work fuel and air blowers.....	77	Table 47 Results for three cells.....	108
Table 23 Sensitivity Analysis on pressure drops	77	Table 48 Sensitivity on three fuel cells	108
Table 24 Performance comparison for different reforming options	84	Table 49 Two fuel cells.....	110
<i>Table 25 Working voltage and h₂ fraction in function of grade IR</i>	<i>84</i>	Table 50 Sensitivity on two fuel cells.....	110

Bibliography

- [1] “Repubblica.” https://www.repubblica.it/green-and-blue/2021/12/29/news/aeroporto_di_torino_snam_e_sagat_insieme_per_la_prima_fuel_cell_hydrogen-ready_in_italia-332017174/ (accessed Mar. 13, 2023).
- [2] “Torinotechmap,” Feb. 22, 2023. <https://torinotechmap.it/snam-e-sagat-realizzeranno-a-torino-la-prima-cella-a-idrogeno-italiana/> (accessed Mar. 13, 2023).
- [3] “Hydrogen News,” Feb. 22, 2023. <https://hydronews.it/snam-fornira-allaeroporto-di-torino-un-sistema-di-fuel-cell-alimentato-a-metano-e-h2-per-cogenerazione/> (accessed Mar. 13, 2023).
- [4] “Turin Airport web page,” Feb. 2023, Accessed: Mar. 13, 2023. [Online]. Available: <https://www.aeroportoditorino.it/it/sagat/chi-siamo/azienda/torino-green-airport>
- [5] “Trigeneration,” Mar. 11, 2023. <https://www.edina.eu/power/trigeneration-cchp> (accessed Mar. 13, 2023).
- [6] S. Mekhilef, R. Saidur, and A. Safari, “Comparative study of different fuel cell technologies,” *Renewable and Sustainable Energy Reviews*, vol. 16, no. 1. Elsevier Ltd, pp. 981–989, 2012. doi: 10.1016/j.rser.2011.09.020.
- [7] U. I. Degli Studi di Napoli Federico, R. Dottorando Massimo DENTICE, and A. Ing Gabriele FERRUZZI Profssa Rita MASTRULLO Co-Tutor Ing Francesco CALISE Adolfo PALOMBO Laura VANOLI, “Introduzione-Introduzione alle Celle a Combustibile i ANALISI SPERIMENTALE E NUMERICA DI SISTEMI DI CONVERSIONE DELL’ENERGIA BASATI SU CELLE A COMBUSTIBILE.”
- [8] “Polygeneration and Advanced Energy Systems”, Accessed: Mar. 13, 2023. [Online]. Available: <https://appuntiuniversitari.online/catalogo/teoria/3215-polygeneration-advanced-energy-systems/>
- [9] P. Tomczyk, “MCFC versus other fuel cells-Characteristics, technologies and prospects,” *J Power Sources*, vol. 160, no. 2 SPEC. ISS., pp. 858–862, Oct. 2006, doi: 10.1016/j.jpowsour.2006.04.071.
- [10] U. I. Degli Studi di Napoli Federico, R. Dottorando Massimo DENTICE, and A. Ing Gabriele FERRUZZI Profssa Rita MASTRULLO Co-Tutor Ing Francesco CALISE Adolfo PALOMBO Laura VANOLI, “Introduzione-Introduzione alle Celle a Combustibile i ANALISI SPERIMENTALE E NUMERICA DI SISTEMI DI CONVERSIONE DELL’ENERGIA BASATI SU CELLE A COMBUSTIBILE.”
- [11] S. J. McPhail, P.-H. Hsieh, J. Robert Selman, by San Ping Jiang, and Y. Yan, “Molten Carbonate Fuel Cells.”
- [12] Ing. Giuseppe De Lorenzo, “Modellazione ed Anlisi Energetico-Ambientale di impianti ibridi con celle a combustibile a carbonati fusi,” vol. PhD Thesis.

- [13] "Scheme absorption chiller", Accessed: Mar. 13, 2023. [Online]. Available: <https://www.thermaxglobal.com/how-do-absorption-chillers-work/>
- [14] theengineeringmindset, "theengineeringmindset," Mar. 14, 2023.
- [15] S. Campanari, P. Chiesa, and G. Manzolini, "CO₂ capture from combined cycles integrated with Molten Carbonate Fuel Cells," *International Journal of Greenhouse Gas Control*, vol. 4, no. 3, pp. 441–451, 2010, doi: 10.1016/j.ijggc.2009.11.007.
- [16] L. Duan, L. Yue, T. Feng, H. Lu, and J. Bian, "Study on a novel pressurized MCFC hybrid system with CO₂ capture," *Energy*, vol. 109, pp. 737–750, 2016, doi: 10.1016/j.energy.2016.05.074.
- [17] L. Mastropasqua, M. Spinelli, A. Paganoni, and S. Campanari, "Preliminary design of a MW-class demo system for CO₂ capture with MCFC in a university campus cogeneration plant," in *Energy Procedia*, Sep. 2017, vol. 126, pp. 453–460. doi: 10.1016/j.egypro.2017.08.213.
- [18] H. Hongliang, H. Zhang, S. Weng, and M. Su, "Dynamic numerical simulation of a molten carbonate fuel cell," *J Power Sources*, vol. 161, no. 2, pp. 849–855, Oct. 2006, doi: 10.1016/j.jpowsour.2006.04.109.
- [19] M. Baranak and H. Atakül, "A basic model for analysis of molten carbonate fuel cell behavior," *J Power Sources*, vol. 172, no. 2, pp. 831–839, Oct. 2007, doi: 10.1016/j.jpowsour.2007.05.027.
- [20] J. Brouwer, F. Jabbari, E. M. Leal, and T. Orr, "Analysis of a molten carbonate fuel cell: Numerical modeling and experimental validation," *J Power Sources*, vol. 158, no. 1, pp. 213–224, Jul. 2006, doi: 10.1016/j.jpowsour.2005.07.093.
- [21] J.-H. Koh, H.-K. Seo, Y.-S. Yoo, and H. C. Lim, "Consideration of numerical simulation parameters and heat transfer models for a molten carbonate fuel cell stack," 2002.
- [22] E. Riensche, J. Meusinger, U. Stimming, and G. Unverzagt, "Optimization of a 200 kW SOFC cogeneration power plant. Part II: variation of the flowsheet," 1998.
- [23] M. Mehrpooya, S. Sayyad, and M. J. Zonouz, "Energy, exergy and sensitivity analyses of a hybrid combined cooling, heating and power (CCHP) plant with molten carbonate fuel cell (MCFC) and Stirling engine," *J Clean Prod*, vol. 148, pp. 283–294, Apr. 2017, doi: 10.1016/j.jclepro.2017.01.157.
- [24] J. M. Muñoz De Escalona, D. Sánchez, R. Chacartegui, and T. Sánchez, "A step-by-step methodology to construct a model of performance of molten carbonate fuel cells with internal reforming," *Int J Hydrogen Energy*, vol. 36, no. 24, pp. 15739–15751, Dec. 2011, doi: 10.1016/j.ijhydene.2011.08.094.
- [25] R. J. Braun, S. A. Klein, and D. T. Reindl, "Evaluation of system configurations for solid oxide fuel cell-based micro-combined heat and power generators in

- residential applications,” *J Power Sources*, vol. 158, no. 2 SPEC. ISS., pp. 1290–1305, Aug. 2006, doi: 10.1016/j.jpowsour.2005.10.064.
- [26] D. Pashchenko, “Experimental investigation of synthesis gas production by methane reforming with flue gas over a NiO-Al₂O₃ catalyst: Reforming characteristics and pressure drop,” *Int J Hydrogen Energy*, vol. 44, no. 14, pp. 7073–7082, Mar. 2019, doi: 10.1016/j.ijhydene.2019.01.250.
- [27] “Energy.gov,” Mar. 2023, Accessed: Mar. 13, 2023. [Online]. Available: <https://www.energy.gov/eere/fuelcells/hydrogen-storage>
- [28] “GSE web page,” Mar. 11, 2023. <https://www.gse.it/servizi-per-te/efficienza-energetica/cogenerazione-ad-alto-rendimento/car-e-certificati-bianchi> (accessed Mar. 13, 2023).
- [29] “Guida alla Cogenerazione ad Alto Rendimento CAR.” Accessed: Mar. 13, 2023. [Online]. Available: https://gse.it/documenti_site/Documenti%20GSE/Servizi%20per%20te/COGENERAZIONE%20AD%20ALTO%20RENDIMENTO/Guide/Aggiornamento%20Guida%20CAR%20-%20revisione%202019.pdf
- [30] “GAZZETTA UFFICIALE DELLA REPUBBLICA ITALIANA, 19-9-2011”, Accessed: Mar. 13, 2023. [Online]. Available: https://www.gazzettaufficiale.it/do/atto/serie_generale/caricaPdf?cdimg=11A120470000040110001&dgu=2011-09-19&art.dataPubblicazioneGazzetta=2011-09-19&art.codiceRedazionale=11A12047&art.num=4&art.tiposerie=SG
- [31] “GME web site,” Mar. 2023, Accessed: Mar. 13, 2023. [Online]. Available: <https://www.mercatoelettrico.org/it/>
- [32] “Riesco web site,” Mar. 2023, Accessed: Mar. 13, 2023. [Online]. Available: <https://www.ri-esco.it/aggiornamento-valore-certificati-bianchi-tee/>
- [33] “Price NG,” Mar. 2023, Accessed: Mar. 13, 2023. [Online]. Available: <https://luce-gas.it/guida/tariffe/prezzo-gas-metro-cubo>
- [34] “GME site”, Accessed: Mar. 13, 2023. [Online]. Available: <https://www.mercatoelettrico.org/it/>
- [35] “Argonne National Laboratory, Gas Clean Up for Fuel Cell Application Workshop, (2014) 1 32.”.

Ringraziamenti

Ringrazio tutti coloro che mi sono stati vicini in questi anni di studio. Durante i quali ho approfondito, appassionandomi ed interessandomi con anche preoccupazione alle tematiche energetiche e ai cambiamenti climatici in atto. Il lavoro presentato è stato possibile grazie al supporto della prof.ssa. M.Gandiglio e prof. P.Marocco che ringrazio, e del prof. M. Santarelli. Grazie a loro ho avuto l'opportunità di conoscere ed analizzare un reale caso studio, per me motivo di forte interesse.

Ringrazio i miei amici, ed in particolare Christian per il supporto sempre condiviso durante tutti gli anni di università. In ultimo un sentito ringraziamento alla famiglia, che mi ha permesso di intraprendere il percorso di studi, e che sempre mi è stata vicina, senza il Vostro contributo non sarebbe stato possibile tutto questo.